LARGE STRAIN DEFORMATION OF ALUMINIUM ALLOYS BY CHANNEL-DIE COMPRESSION

LARGE STRAIN DEFORMATION OF ALUMINIUM ALLOYS BY CHANNEL-DIE COMPRESSION

by

ALEXIS DESCHAMPS

A Thesis

Submitted to the School of Graduate Studies

in Partial Fulfilment of the Requirements

for the Degree

Master of Engineering

McMaster University

March 1994

MASTER OF ENGINEERING (1994) McMASTER UNIVERSITY

(Materials Science and Engineering) Hamilton, Ontario

TITLE: Large Strain Deformation of Aluminium Alloys by Channel-Die Compression

AUTHOR: Alexis Deschamps, Ingénieur des Arts et Manufactures (Ecole Centrale Paris, France)

SUPERVISOR: Professor J.D. Embury

NUMBER OF PAGES: xx, 169

ABSTRACT

The mechanical properties of pure Aluminium, Al-0.2%Cu and Al-0.4%Cu at large strains were studied by channel-die compression at three different temperatures: 77K, 200K and 300K. The results were interpreted in terms of work hardening rate versus stress (θ/τ) diagrams. The evolution of the structure was studied on a range of scales from macroscopic to microscopic, by optical study of slip lines, X-ray diffraction for texture measurements, Electron Back-Scattering Kikuchi Patterns for local texture measurements, and by Transmission Electron Microscopy for microstructural information.

Intense shear banding was observed at large strains in all alloys at all temperatures. The texture evolution was shown to be consistent with this change in deformation mode.

At low temperatures, stage III of deformation was shown to be represented by a straight line in the θ/τ diagram. Increasing the temperature lead to a dramatic decrease in work hardening rate and to an increasing concavity of the θ/τ plots. The addition of solutes to pure Aluminium was shown to result in an increase of the work hardening rate, which could be represented by a simple translation of the θ/τ plots on the stress axis. At large strains, all three materials experienced a stage (stage IV) of constant work hardening at low rate. The stage IV work hardening rate decreased with increasing

temperature, and was not influenced by solute content. The stage III-Stage IV transition was very sharp at 77K and smoother at higher testing temperatures.

Phenomenological models were developed for the prediction of the influence of temperature and solute content on work hardening. Moderate strains were modelled taking into account the evolution of the dislocation density into two different populations during the deformation. The influence of solutes on work hardening was modelled by considering how segregation of solute atoms at the dislocation cores influences dynamic recovery. Stage IV work hardening was considered to arise from the accumulation of dislocation debris resulting from the dynamic recovery events.

ACKNOWLEDGEMENTS

I would like to express my grateful thanks to Professor J.D. Embury for his constant guidance and dedication during this work. I hope I will retain some of his insight, knowledge and enthusiasm for Materials Science. I also thank him for making me discover the beautiful canadian wilderness and for the many ski trips we did together!

I sincerely acknowledge the dedicated help that I got for my experimental work, especially from Mrs. Teresa Castillo for the microscopy, Carl Necker from Los Alamos National Lab for the texture, Professor S. Saimoto and Jian Li from Queen's University for the Channelling Patterns work, and Dominique Duly, Michael Gharghouri and Marek Szczerba for the mechanical testing. Many experiments would not have been possible without their help.

A special thank you to Professor Y. Bréchet for his considerable and enthusiastic help for the modelling.

Thank you to Professor Z.S. Basinski for his useful suggestions. An hour of discussion with him is worth a month of work!

Thank you to Pechiney-Centre de Recherches de Voreppe, and especially Joël Courbon for continuous financial and scientific support throughout this study.

I would like to thank all the students of the mechanical properties group for their friendship. Special thanks go to Dominique, Michael and Rosaura for their outstanding

friendship, their continuous support and all the trips we did together. They all made my staying in Canada very enjoyable.

TABLE OF CONTENTS

LIST OF FIGURES

LIST OF TABLES

CHAPTER I

INTRODUCTION

Current applications of aluminium such as packaging and automotive applications require a combination of both high formability and high strength in the final product. Among the different strengthening mechanisms available to the designer, solid solution hardening is one of the most efficient and widely used.

The influence of solid solution on the mechanical properties has to be considered both in terms of the increase of the initial yield stress and of the subsequent work hardening process. The solute atoms, acting as obstacles to dislocations, may dramatically increase the flow stress of pure metals. However they may have greater influence in work hardening and enable high stress levels to be obtained after large strains. For instance, a few percent of magnesium added to aluminium can increase the flow stress after large deformation from around 100 MPa for pure aluminium to over 400 MPa, while the difference in the metal yield stress between the two alloys may be around 50 to 100 MPa.

Therefore, both from the scientific and industrial point of view, it is of great interest to understand how the final state and strength level of dilute alloys deformed to large strains depend on their composition and processing. It would be of value to describe this by relating the final flow stress to the strain, strain rate, temperature, solute

content, mode of deformation, via the provision of a reliable constitutive law. However, in addition to the hardening mechanisms consideration has to be given to competing processes such as strain localization, damage and eventual fracture. These occur when the work hardening rate of the material becomes too low to accommodate geometric changes. The deformation then localizes, leading to failure. It is of interest to relate the generation of such instabilities to factors as the strain path, presence of atoms in solid solution, and evolution of the microstructure.

One of the purposes of the current investigation was to study the influence of low copper additions on the properties of aluminium. Al-Cu alloys have only been investigated for relatively high contents ($>1\%$), where hardening mechanisms due to second phase particles play a predominant role. However, the influence of low addition of copper in solid solution in Aluminium are of interest from an industrial viewpoint (e.g. beverage packaging applications). This study concentrates on three alloys : pure aluminium, and aluminium added with respectively 0.2 and 0.4Wt% of Copper.

In choosing an experimental method to study high strain deformation it is of value to avoid limitations due to ductility, the presence of large internal strain gradients and to simplify the preparation of samples for structural analysis. The deformation technique chosen here was channel-die compression. Although it has seldom been used for the quantitative study of large strains, it has some important advantages: the deformation

mode is plane strain compression, similar to many industrial processes, the deformation curves obtained are real-time continuous curves, and the temperature control is easy and precise. Finally, there is existing literature on the analysis and simulation of texture evolution for this deformation path which can be applied to the present study.

The aims of this study are threefold :

a) to show the utility of channel die compression as a tool for the study of large strain behaviour of metals.

b) to obtain reliable data for large strain behaviour in dilute solid solutions.

c) to attempt to understand, as completely as possible, the deformation of a system, including small and large strain behaviour, strain localization, texture development, solute content and testing temperature and to summarize this in simple constitutive laws.

The essential approach in this study has been to develop a test procedure and to use a series of methods of structural analysis capable of giving an overview of the structural evolution from the macroscopic to the microscopic level. The main chapters of the thesis are: literature review, experimental results, including mechanical testing, microstructural studies and texture evolution, modelling of the work hardening, and discussion of the results.

CHAPTER 2

LITERATURE REVIEW

2.1 INTRODUCTION

Large strain deformation is one important aspect of work hardening in f.c.c. metals. This subject is of great importance both for the understanding of plasticity both from the scientific point of view and for the understanding and control of industrial forming processes such as cold rolling, sheet forming or wire drawing. The experimental investigation of the large strains behaviour of metals raises difficult problems, as it has to encompass factors such as friction, plastic instabilities and damage accumulation. Thus we will first discuss the choice made in this study to use channel die compression as the deformation procedure.

In considering the existing literature it is clear that deformations at moderate strains (up to 30 to 50%) has been extensively reviewed. Therefore, we will briefly review the mechanisms of hardening and dynamic recovery at these strain levels.

At large strains and low temperatures work hardening has been observed to persist at a low and nearly constant level up to very large strains. This is usually termed stage IV hardening. Since the first observations of this stage of work hardening (among them Langford and Cohen, 1969), much experimental data have been collected which show

that this stage is very general. Many models have recently been developed to explain various features of this stage of hardening. However, there is at present no consensus about the governing mechanisms. Modelling of stage IV is essentially limited by the lack of definitive experimental evidence for the mechanisms involved, and it is appropriate to discuss how the models compare to the existing experimental evidence.

In studying the behaviour of materials at large strains, it is useful to consider the influence of the addition of solutes on work hardening. The next section will discuss this issue.

Some of the other factors which influence the behaviour of materials at large strain deformations are the occurrence of strain localization and texture development. We will review the occurrence and characteristics of strain localization as a form of instability at large strains and its influence on the behaviour of the material and discuss texture evolution at large strains and how it influences the mechanical properties.

2.2/ CHANNEL-DIE COMPRESSION AS A MECHANICAL TESTING PROCEDURE

The choice of the deformation procedure for this investigation had to meet several criteria: achievement of large strains without failure of the specimen, provision of data for the reliable interpretation of the stress-strain curves, the possibility of deforming at different temperatures, and simple methods of obtaining samples for structural studies. Different techniques may be used to investigate the mechanical behaviour at large strains,

which can be summarized as:

a) Wire-drawing followed by tensile tests: this method, which enables very large strains to be reached, has been used successfully in iron alloys for instance (Embury and Fisher, 1966; Langford and Cohen, 1969; Rack and Cohen, 1970; Leslie, 1972). However, this technique presents three major drawbacks:

- it is a discontinuous test, i.e. the flow curve will be an envelope of the yield points of discrete tensile tests;
- recovery may take place between the drawing operations and the subsequent tensile test, restricting its use at low temperatures;
- the deformation path is not the same during drawing and the subsequent tensile test.

b) Torsion tests: this method allows one to reach von Mises strains of the order of 2 with the absence of friction and limits the occurrence of plastic instabilities. It has been successfully used in Aluminium alloys (Rollett, 1988) and Nickel-Cobalt alloys (Hughes, 1986) for instance. This method produces severe strain gradients unless tubular samples are used. However, this experimental facility was not available at McMaster University.

c) Plane strain compression tests: in this context, channel-die compression seemed the most suitable testing method to undergo this investigation. The advantages and drawbacks of this procedure can be summarized as follows :

- advantages: plane strain compression (is comparable to many industrial processes), continuous stress-strain curve obtained, large sample dimensions are possible (useful

when the grain size is difficult to control), it has the facility to operate at different temperatures, ease of subsequent structural studies.

- drawbacks: the low strain behaviour is not reliable, many interrupted tests needed to obtain large deformations, problem of the testing machine loading capacity with large samples, problems of recovery during remachining (especially when testing at low temperatures), no satisfactory model for the influence of friction is available, the deformation mode favours the occurrence of localized deformation (shear bands).

The choice of this technique did present experimental difficulties: it is often considered that friction biases the results so much that it is impossible to derive any quantitative stress-strain data. Indeed, there is no analytical expression for the friction in a channel-die, because friction occurs on four faces of the sample. Because the pressure on the lateral faces is about half the pressure on the top and bottom faces of the sample, friction on theses faces is often neglected (Nourbakhsh and Song, 1989). However, this approximation is no longer true when the height of the sample becomes of the same order than its thickness. For these reasons the use of channel-die has been mainly restricted to structural investigations (see for instance Chandra, 1979, Harren *et al.*, 1988; Dève *et al.*, 1989; Butler and Hu, 1989; Orlans-Joliet *et al.*, 1990; Becker, 1991; Becker and Lalli, 1991; Bronkhorst *et al.*, 1991; Maurice and Driver, 1993), while the examples of its use for deriving stress-strain curves are infrequent (Nourbakhsh *et al.*, 1986; Bronkhorst *et al.*, 1991; Poole, 1993).

2.3 THE WORK HARDENING OF F.C.C. METALS AT LARGE STRAINS

2.3.1/ The stages of work hardening

The stress-strain curve of f.c.c. single crystals is generally divided into four different stages (Fig. 2.1). These stages can be represented by a plot of work hardening rate versus stress in which in the ideal case they can be represented as straight lines (Fig. 2.2). Additional stages have been proposed for further deformation to very large strains, but their existence and physical meaning is not assessed with certainty and they are not of interest here. The characteristics of the different stages are the following :

Stage I, or easy glide: this stage is only present in single crystals. The work hardening rate is very low but finite (of the order of magnitude of 10^{-4} G, where G is the shear modulus) and constant. The mode of deformation is glide on a single activated slip plane and the work hardening occurs by storage of stable dislocation dipoles.

Stage II, or athermal hardening : after some deformation has occurred, secondary slip occurs and the secondary dislocations interact with primary dislocations by forest hardening. No significant annihilation of the stored dislocations occurs. The strain hardening rate in this stage is of the order of G/200, and is constant, independent of temperature and strain rate.

Stage III, or thermally activated hardening : In this stage new mechanisms become dominant, including cross-slip of screw dislocations, formation of edge dislocation

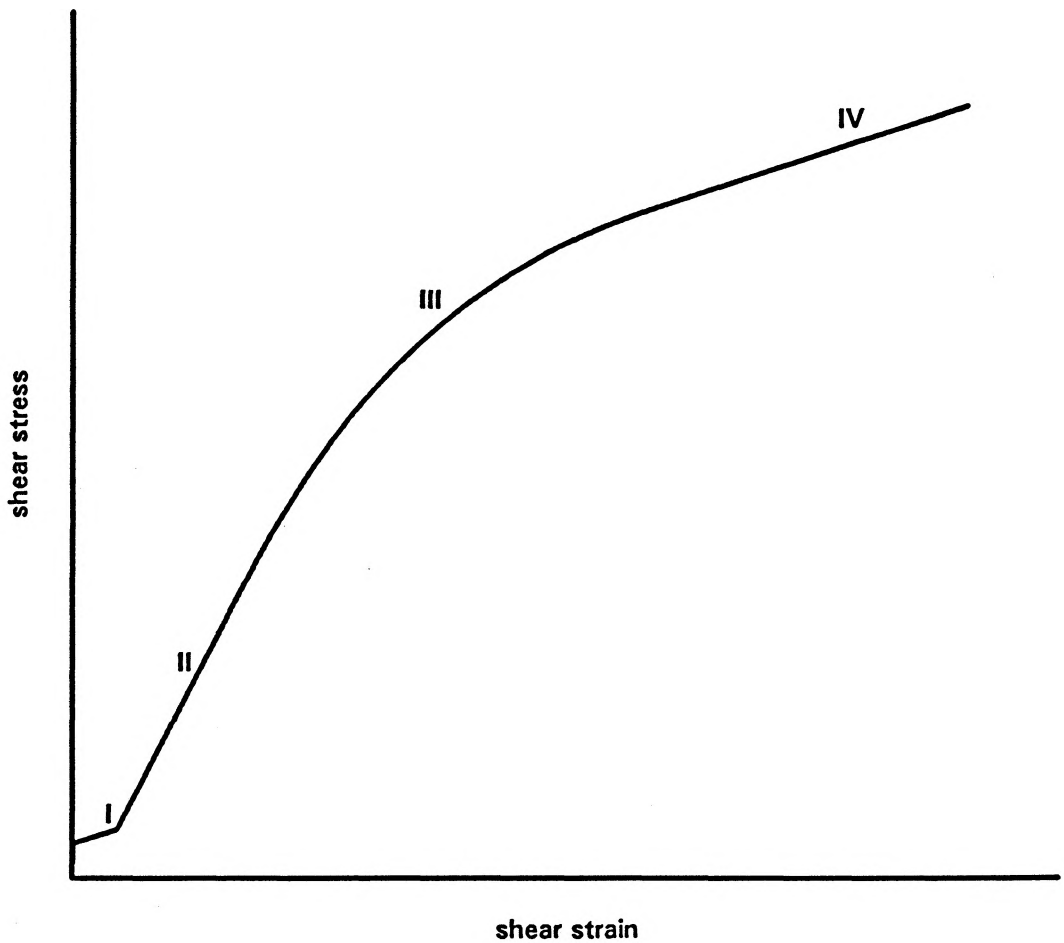

Figure 2.1/ Schematic stress-strain curve representing the four stages of work hardening

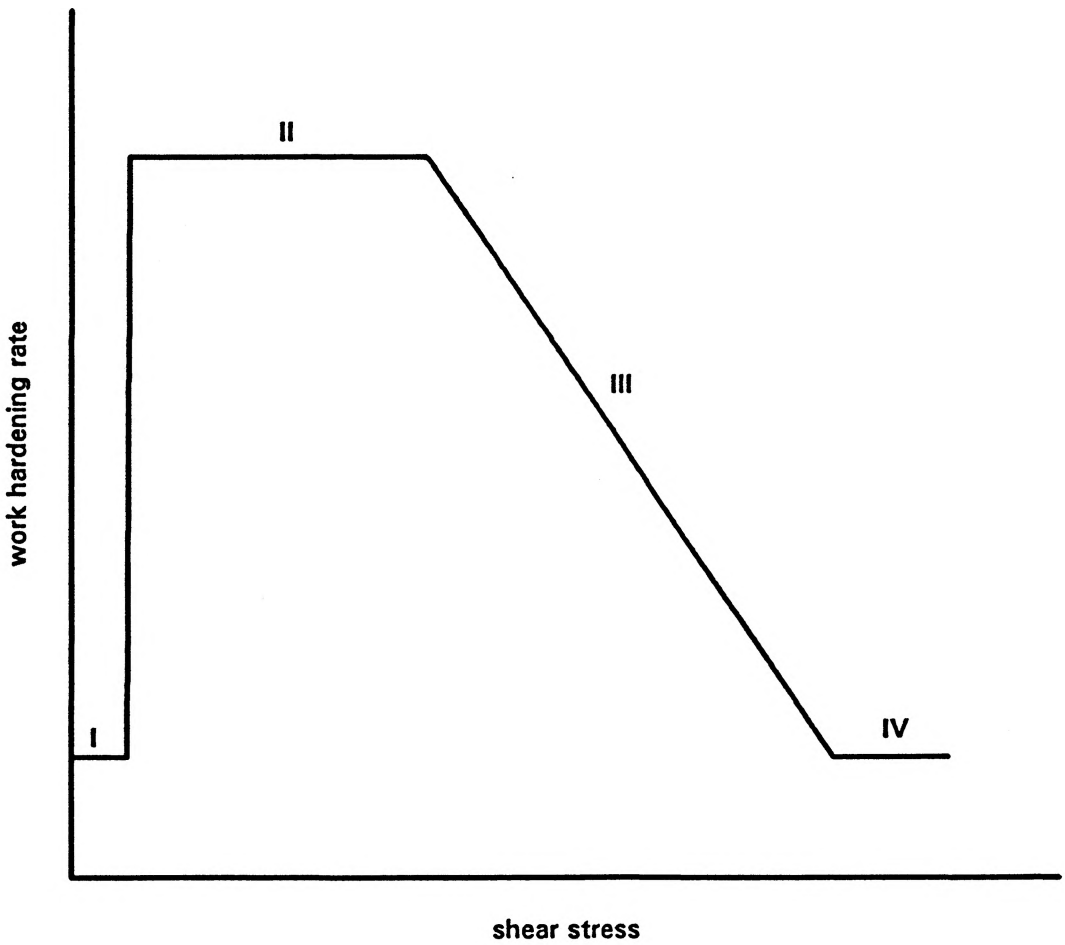

Figure 2.2/ Schematic work hardening rate vs. stress curve representing the four stages of work hardening

dipoles and, if the temperature is high enough, climb of edge dislocations. This results in a continuously diminishing strain hardening rate corresponding to the competition between the dislocation storage rate and increasing dislocation annihilation. This stage is strongly temperature and strain rate dependant. A number of works have proposed that materials reach an apparent saturation stress at large deformations. This stage is fundamentally concerned with dynamic recovery.

The behaviour of polycrystals is different. The relation between the macroscopic stress and the shear stress is given by the Taylor factor M, which averages the stresses with orientation. Polycrystals do not present stage I of work hardening: the compatibility conditions between the different grains makes a single slip throughout the sample impossible. Stage II of work hardening will be observed only at low temperatures: in many cases the dynamic recovery processes become effective immediately after yield. Two fundamental mechanisms govern the large strains behaviour of polycrystals: dynamic recovery, and so-called stage IV of work hardening, with a low but constant work hardening rate. Indeed, at large strains and low homologous temperature, the saturation expected from stage III is not observed, but a constant low work hardening rate is reached, of the same order of magnitude that the stage I strain hardening rate. The underlying causes are still unclear and this constant work hardening has been associated with various mechanisms (presence of dislocations debris resulting from the annihilation events of stage III, evolution of the dislocation substructure, presence of internal stresses).

Low and moderate strain work hardening mechanisms will not be reviewed further here. Reviews can be found in Basinski and Basinski (1974), Kocks (1964, 1966, 1976), Kuhlmann-Wilsdorf (1985), Mecking and Kocks (1981), Nabarro *et al.* (1964), Nabarro (1967, 1989).

2.3.2/ Dynamic recovery

Dynamic recovery is the process by which the dislocations that have been created during the deformation annihilate during straining, resulting in a global decrease in work hardening rate. This process has been associated to several mechanisms, depending on the temperature and strain rate at which the mechanical testing is done, and of the alloy itself, being of f.c.c., b.c.c. or h.c.p. structure (the present review is restricted to f.c.c. metals), having a high or a low stacking-fault energy, etc...

The mechanisms that will interest us here are :

- annihilation of screw dislocations of opposite sign by cross-slip
- formation of edge dislocation dipoles
- annihilation of narrow edge dislocation dipoles

2.3.2.1/ Annihilation of screw dislocations by cross-slip

The way by which two screw dislocations of opposite sign annihilate each other

is intimately related to the mechanism of cross-slip. Cross-slip occurs in a crystal when the local stresses push a dislocation into a plane which is different from the original gliding plane, and therefore enables two screw dislocations on parallel slip planes to annihilate each other.

2.3.2.1a/ Mechanism of cross-slip

Cross-slip was evidenced a long time ago by the observation of slip line traces at the sample surface. The outlines of the first realistic models were derived by Friedel (1956), and by Schoeck and Seeger (1955). Later, cross-slip was identified as one controlling mechanism for creep at intermediate temperatures, which led some authors to link the corresponding activation energies to cross-slip (e.g. Friedel, 1959, 1964). Cross-slip was also suggested to be the key process at the transition between stage II and stage III of work hardening (Schoeck and Seeger, 1955 ; Friedel, 1956 ; Haasen, 1967). Alternative mechanisms have also been suggested for the stage II-stage III transition (Bonneville *et al.*, 1988).

The theoretical aspects of cross-slip have been studied by Escaig (1968), following Friedel's view. In this model, cross-slip starts by the constriction of two partial screw dislocations on the primary plane. Under the influence of the applied stress and the thermal activation, the two halves of the dislocation are separated, and, as suggested by Friedel (1956, 1957), the dislocation segment between them splits in the secondary cross-slip plane.

Escaig has shown that the process depends mainly on the ratio of the width of splitting under stress on the primary and secondary planes. Moreover, he has also shown that the redissociation can occur in the cross-slip plane without any applied stress, with only thermal activation, if the energy of the dislocation in the new plane is lower than on the primary plane.

This model has been generally preferred to the model of Schoeck and Seeger (1955), which states that the dislocation must recombine over a certain length, and that this recombined dislocation must cross-slip on a critical configuration in the secondary plane before cross-slip becomes a stable configuration.

2.3.2.1b/ Critical conditions for the annihilation of screw dislocations by cross-slip

In the absence of external stresses, two screw dislocations of opposite sign, separated by a distance y, experience an attractive shear stress $Gb/2\pi y$, where G is the shear modulus and b is the magnitude of the Burgers vector. In a very crude picture, two screw dislocations will annihilate mutually if this stress exceeds the stress τ required for dislocation glide on the secondary plane. The energy necessary to bring together the two partial dislocations would then be brought by thermal activation. The critical spacing has been given in this case by Essmann and Mughrabi (1979) :

$$y_s \simeq \frac{Gb}{2\pi\tau} \qquad (2.1)$$

However, the critical spacings obtained by this method are usually too high in

comparison to the experimental data, which shows some much smaller critical spacings to be stable.

Nabarro (1967) developed an other model taking into account the difference in the stress needed to move a screw dislocation on its original plane and the stress to move it on the cross-slip plane, and derived a diagram showing the critical conditions for cross-slip.

2.3.2.1c/ The role of cross-slip

Many authors associate dynamic recovery with cross-slip, specifically with the elimination of screw dislocations from the microstructure by thermally activated cross-slip. However there is still no clear understanding of the detailed mechanisms that are involved in recovery by cross-slip, and which mechanisms really control dynamic recovery and the onset of stage III.

As pointed up in the review by Jackson (1985), the onset of stage III has been extensively thought to correspond to the onset of dynamic recovery and to be due to the cross-slip in large numbers of primary dislocations. These ideas predict correctly the temperature dependence of τ_{III}, since this cross-slip of primary dislocations is a thermally activated process.

However, the association of dynamic recovery with the anihilation of screw dislocations is inconsistent with some microstructural observations, as pointed out by Basinski and Basinski (1966) and stressed by Kuhlmann-Wilsdorf (1968) : it has been

observed in Copper that cross-slip of screw dislocations begins long before the onset of stage III, even at 4.2K during stage I of the deformation, which could be due to the easy nucleation of cross-slip at existing jogs or forest dislocations, for example. Cross-slip traces have been observed during stage I and II of deformation. Moreover, screw dislocations are conspicuously absent from the microstructure, from stage I onwards.

Hence it is clear that to reconcile microstructural observations with cross-slip models of stage III, distinctions must be made between different kinds of cross-slip, or cross-slip in different circumstances. Some suggestions have been made (see Jackson, 1985) that the screw dislocation anihilation processe which occur in stage I (and leads to the formation of cells) become inhibited in stage II, where it is observed that the screw dislocations are trapped in networks of secondary dislocations. Then cross-slip would resume when the stress is high enough to cause cross-slip in the tangled structure. One other possibility is that the dislocations are trapped in pile-ups, and that the cross-slip from a pile-up is intrinsically more difficult than cross-slip induced by localized obstacles, and therefore requires a larger stress.

2.3.2.2/ Creation of dislocation dipoles

An important recovery event is the formation of an edge dislocation dipole. This occurs when one edge dislocation gliding on a plane comes near a trapped edge dislocation of opposite sign lying in an adjacent plane. If the spacing between the two slip planes is small enough, the two edge dislocations will form a stable dipole. The

stress field of such a dipole is of shorter range than the stress field of a single dislocation: while the stress field of a single dislocation diminishes with 1/r, if r is the distance from the dislocation, in the case of a dislocation dipole, the stress field decreases with $1/r^2$. Therefore, the interaction between a dipole and a passing dislocation is much weaker than the interaction between two single dislocations, and the formation of a dipole is hence a recovery event.

The critical spacing of the slip planes under which two passing dislocations will align in a stable dipole has been derived by Gilman (1964):

$$h = \frac{Gb}{8\pi(1-\nu)\tau} \qquad (2.2)$$

2.3.2.3/ Annihilation of edge dislocations

Two edge dislocations cannot annihilate mutually by glide, except if they are on the same slip plane. Mutual annihilation is possible either by collapse of very narrow dipoles (at low temperature) or by dislocation climb (mostly at high temperatures).

2.3.2.3a/ Collapse of dipoles

Theoretical arguments (Friedel, 1964) and some indirect experimental evidence (Essmann and Rapp, 1973) suggest that very narrow edge dislocation dipoles are unstable and can disintegrate spontaneously. In this process, defects will be created, of vacancy or interstitial type, depending on the type of the dipole, which have been observed.

According to an estimate by Friedel (1964), spontaneous annihilation will occur when the elastic forces between the two dislocations will exceed the climb resistance. This yields the following critical spacing :

$$\frac{y_e}{b} = \frac{Gb^3}{2\pi(1-\nu)\,U_f} \qquad (2.3)$$

where U_f is the energy of formation of the atomic defects formed and ν is Poisson's ratio. In some circumstances y_e can be a few atomic distances.

Cotterill (1977) indicates that under a critical spacing the dislocation configuration is not stable any more, which brings the configuration to an amorphous state, which cannot be described in terms of dislocations (in the case of edge dislocations, this amorphous state would be a row of interstitials or vacancies). This leads to a critical spacing given by :

$$\frac{Gb(y_e-2r_c)}{4\pi} = E_c \qquad (2.4)$$

where r_c is the core radius and E_c is the core energy. This critical spacing could be of a few nanometres.

If such a recovery event occurs, it will leave behind an important number of dislocation debris, which have been held responsible for the presence of stage IV of work hardening.

2.3.2.3b/ Climb of edge dislocations

As the process of climb is very stress and temperature dependant it will occur either at high temperature and low stresses, as observed in creep, or at low temperatures and very high stresses, possibly aided by point defects brought by plastic deformation, especially in the cell walls, where it can be an important feature of dynamic recovery.

2.3.2.4/ A model for dynamic recovery

Intermediate strains have often been represented by power law of the Hollomon type (see for instance Rao *et al.*, 1982):

$$\sigma - \sigma_0 = K \epsilon^n \qquad (2.5)$$

where σ_0 is the initial yield point. Very simple, this type of empirical relationship is very useful to the industrialist. However, it has two major drawbacks: it does not describe the behaviour of most metals at low temperatures (especially at large strains), and it lacks any physical input.

Voce (1948) proposed an alternative exponential law that shows an asymptotic saturation stress. It can be expressed in differential form as:

$$\theta = \theta_0 \left[1 - \frac{\sigma}{\sigma_s}\right] \qquad (2.6)$$

where θ is the work hardening rate, θ_0 the initial work hardening rate, σ the flow stress and σ_0 the saturation stress. This type of relationship has been shown to be useful in a

wide range of materials and testing procedures (Kocks, 1976; Mecking *et al.*, 1986; Rollett, 1988), although a further description is needed when the material reaches large strains (stage IV). The validity for this type of relation for Aluminium is shown in Fig. 2.3.

A physical basis for the Voce relation was provided by Kocks (1976), on the principle of the juxtaposition of a dislocation storage rate and a dislocation recovery rate. In this picture the rate of dislocation storage in stage III is the same as the storage rate in stage II, or forest hardening rate:

$$\frac{d\rho^{+}}{d\gamma} = k\sqrt{\rho} \qquad (2.7)$$

Meanwhile, the amount of dislocation line length lost per unit strain by dynamic recovery is assumed to be proportional to the current dislocation density:

$$\frac{d\rho^{-}}{d\gamma} = -L\rho \qquad (2.8)$$

Combining this with the relationship between the shear stress and the dislocation density

$$\tau = \alpha\mu b\sqrt{\rho} \qquad (2.9)$$

gives an equivalent of the Voce relation in shear hardening rate and shear stress. The variation of the saturation stress is, by analogy with stress-assisted, thermally activated motion of dislocations :

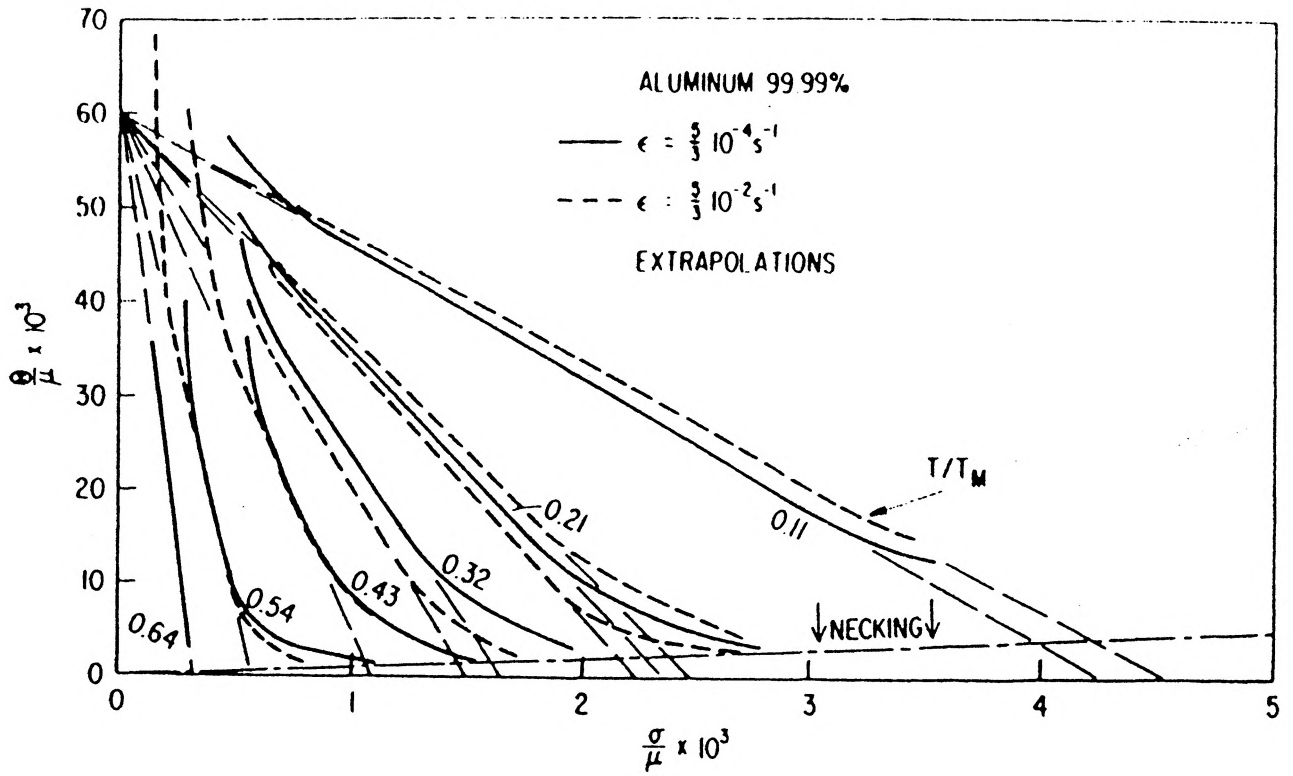

Figure 2.3/ Work hardening rate vs. stress curves for polycrystalline Aluminium at various temperatures and 2 strain rates (from Kocks, 1976)

$$\ln\left[\frac{\tau_s}{\tau_{s0}}\right] = -\frac{kT}{A}\ln\left[\frac{\dot{\epsilon}_0}{\dot{\epsilon}}\right] \qquad (2.10)$$

where $\dot{\epsilon}_0$ is a reference strain rate and A represents an activation energy. The value of this activation energy for Aluminium is approximately 0.4 eV.

2.3.2.5/ Mechanisms for dynamic recovery

To summarize, we can indicate which mechanisms can be held responsible for dynamic recovery and the onset of stage III of work hardening, according to Nabarro's treatment (1989). The most likely temperature-dependant mechanisms that can be present in plastic deformation are given to be :

(i) cross-slip of dislocations at pre-existing constrictions

(ii) cross-slip of dislocations at general points (with no need for an existing jog or constriction)

(iii) climb of dislocations induced by point defects produced by plastic deformation

(iv) thermally assisted cutting of repulsive forest dislocations

- Process (i) is the cross-slip present in stage I and at very low temperatures

- Process (ii), which is thermally activated but can occur even at low temperatures where point defects are immobile if the stress is high enough, is thought to control stage III.

- Process (iii) is stress assisted, but fundamentally thermally-controlled. It controls dynamic recovery when the temperature is high enough.

- Processes (i) and (iv) are thermally activated but stress-controlled.

2.3.3/ Work hardening at large strains

The modelling of large strain deformation has received much attention in the last decade, with the development of many different models to account for the stage IV of work hardening. In this section we will first review the experimental characteristics of this stage. We will then review some of the models which have been developed to describe stage IV. We will finally conclude by the difficulties encountered by these models to represent successfully the experimental observations.

2.3.3.1/ Stage IV : experimental characteristics

From the considerable data available on stage IV of work hardening, the following definition can be proposed : stage IV is a stage of the stress strain curve where the material experiences very low and nearly constant or slowly decreasing work hardening rate, retarding the occurrence of a saturation in flow stress to very high strains.

This stage has been shown to be present in a wide variety of metals experiencing many different strain paths. Often cited examples include :

- for f.c.c. metals : bulge testing of Al-Ni alloys (Lloyd *et al.*, 1977); testing of aluminium alloys under various deformation procedures (Lloyd and Kenny, 1982); torsion of aluminium alloys (Rollett, 1988); torsion of Nickel alloys (Hughes and Nix,

1988, 1989); wire drawing of Cu alloys (Fargette *et al.*, 1968); torsion of copper (Alberdi, 1984);

- for b.c.c. metals : wire drawing of iron and its alloys (Langford and Cohen, 1969; Rack and Cohen, 1970; Leslie, 1972);

- for h.c.p metals : wire drawing of Titanium (Gil Sevillano *et al.*, 1981)

Several characteristics of stage IV can be deduced from the available experimental data:

- The work hardening rate (resolved on a single slip plane and reduced by the shear modulus) is material independent : its value is generally between 10^{-4} and 10^{-3} G (Gil Sevillano *et al.*, 1981; Rollett, 1988).

- The ratio between the work hardening rate and the stress at the beginning of stage IV is approximately constant around 0.2 (Hodierne, 1962; Lloyd et al., 1980; Rollett, 1988; Krokha et al., 1991).

- The work hardening rate generally decreases slightly with temperature (Rollett, 1988; Hughes and Nix, 1989).

- The work hardening rate has been shown to be independent of strain rate (Rollett, 1988) and, for alloys, of solute content (Rack and Cohen, 1970; Rollett, 1988; Hughes and Nix, 1989).

2.3.3.2/ Stage IV : microstructure

Stage IV microstructures are generally very well defined cell structures. These microstructures consist of sharp walls of very high dislocation densities and cells which are almost without dislocations. In the early stages of the deformation these cells are known to be roughly equiaxed. The shape of these dislocation cells, however, might become much more elongated as the deformation proceeds to large strains, as Hughes and Nix showed for Nickel alloys (1989). However, in Aluminium alloys the cells stay roughly equiaxed to large strains, or become slightly elongated with low aspect ratios (Rollett, 1988), with the exception of region experiencing intense shear banding (Korbel and Martin, 1986; Harren *et al.*, 1988). In case of the presence of elongated cells, the elongation takes place in the direction of macroscopic deformation. However, one should point out that this cell-type of behaviour is not general in stage IV deformation: when high contents of solute atoms are present, a tangled dislocation structure can be retained until large strains, well into stage IV. This is important when considering whether the cell structure is in fact responsible for stage IV work hardening.

The microstructure evolves with increasing strain. The walls sharpen, the size of the cells decreases. It has been proposed that the microstructure obeys the principle of similitude (Gil Sevillano *et al.*, 1981), even though it is difficult to assess because of the change in cell geometry and the extremely small cell wall thickness. The misorientation between the cells increases (Gil Sevillano *et al.*, 1981; Rollett, 1988), which may result in increasing internal stresses in the metal, at least according to the X-ray experiments

conducted by Mughrabi and co-workers and explained by Argon and Haasen (1993) in their description of stage IV.

2.3.3.3/ Existing models for stage IV

In the past decade many models have been developed to account for the characteristics of stage IV. However, no consensus has been reached so far regarding its causes. We will describe in the following three different categories of models. First, two models based on a composite cell walls/cell interiors structure; second, a model based on internal stresses; third, a model based on dislocations debris.

2.3.3.3a/ The Prinz and Argon model (1984)

This model is based on a well-defined cell structure which obeys the principle of similitude, that is the microstructures at different strains are equivalent to the exception of their scale. This model considers the different storage and anihilation processes that occur when the structure evolves during deformation.

The work hardening behaviour in the cell interiors is simply assumed to follow the Kocks-Mecking behaviour: the rate of dislocation density increase is proportional to the square root of the current dislocation density inside the cells (stage II-type of dislocation storage), and the rate of dislocation decrease is the resultant of the cancellation of stored dislocation loops by gliding dislocation, resulting in a rate of decrease proportional to the current dislocation density inside the cells.

In the cell walls, the increase of dislocation density occurs by trapping the dipoles and loops which have been created in the cell interiors, and then driven inside the cell walls by other gliding dislocations, where they get pinned by the cell wall debris. The dislocation density decrease in the cell walls occurs by diffusion-controlled dislocation climb.

The overall behaviour is then deduced on a basis of a rule of mixtures between the plastic resistances of the cell interiors and the cell walls. The model was compared to the experimental data of Lloyd *et al.* (1977) for Al-Ni alloys (Fig. 2.4). It should be pointed out that this material is a two-phase alloy, which is not taken into account in the model, although it is well-known that the large-strain behaviour of multi-phase alloys can be very different from the single phase behaviour (Embury and Fisher, 1966).

Although this model includes many useful ideas about modelling of large strains behaviour, it presents several limitations. First of all, it does not predict a low continuing work hardening rate up to large strains, but instead predicts a continuously decreasing work hardening rate until saturation of the stress. Moreover, at low homologous temperatures diffusion controlled climb of dislocations cannot occur and the model can therefore not account for recovery in the cell walls, which clearly is not a reasonable assumption. Finally, as stated before, stage IV is known to occur in a similar way in the absence of a well-defined cell structure, as in Al-5Wt% Mg alloys. These materials are not accounted for by this model.

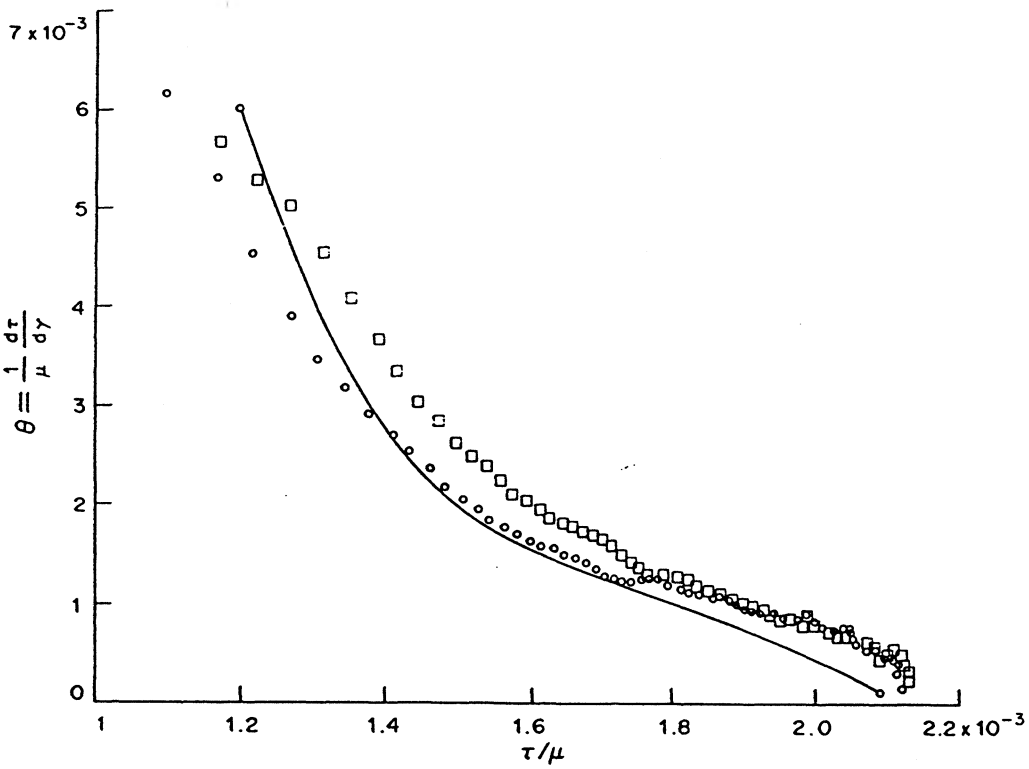

Figure 2.4/ Work hardening rate vs. stress curve calculated according to Prinz and Argon's model as compared to experimental data from Lloyd et al. (1977) for Al-6%Ni (from Prinz and Argon, 1984)

2.3.3.3b/ The Nix, Gibeling and Hughes model (1985)

This model is also based on a composite microstructure. In this case, however, the cell walls are assumed to be infinite slabs of constant thickness (its value being set quite arbitrarily at 100 nm), and the spacing between the dislocation walls is supposed to be 10 times the average dislocation spacing (on the consideration that greater spacings would lead to the formation of new walls and that smaller spacings would make the bowing of dislocations in the cell interiors to difficult in comparison to the stress levels).

The model assumes that edge dislocation segments deposit in the cell walls when extending in the cell interiors under the effect of the stress. The dislocation storage rates both in the cell wall and in the cell interiors are modeled on the geometric basis of stage II of work hardening (forest hardening behaviour). The rate of dislocation recovery in the cell interiors is modeled by the cross-slip of screw dislocations, whereas the recovery in the cell walls is governed by diffusion-controlled climb of edge dislocations.

The resultant behaviour is again obtained by a rule of mixtures between the cell walls and the cell interiors. As can be seen in Fig. 2.5, the computed work hardening rate versus stress curves for Nickel have some of the features of stage IV, namely a continued low level work hardening rate until very high strains, and an decreasing stage IV work hardening rate with temperature.

However, this model has severe limitations. First, the fundamental assumptions about the microstructure geometry are very limited : a constant cell wall thickness is not in agreement with the experimental data. Second, the model fails to show the sharp

a)

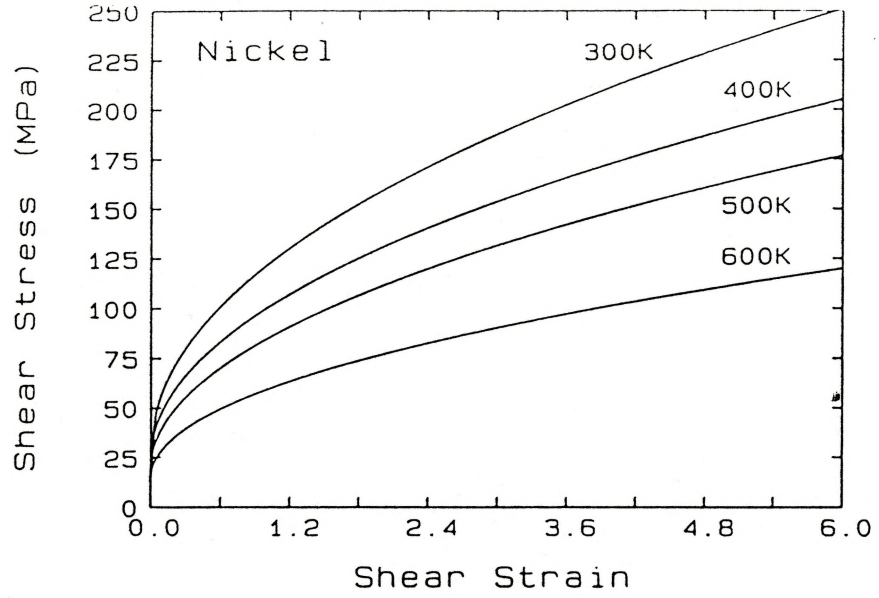

b)

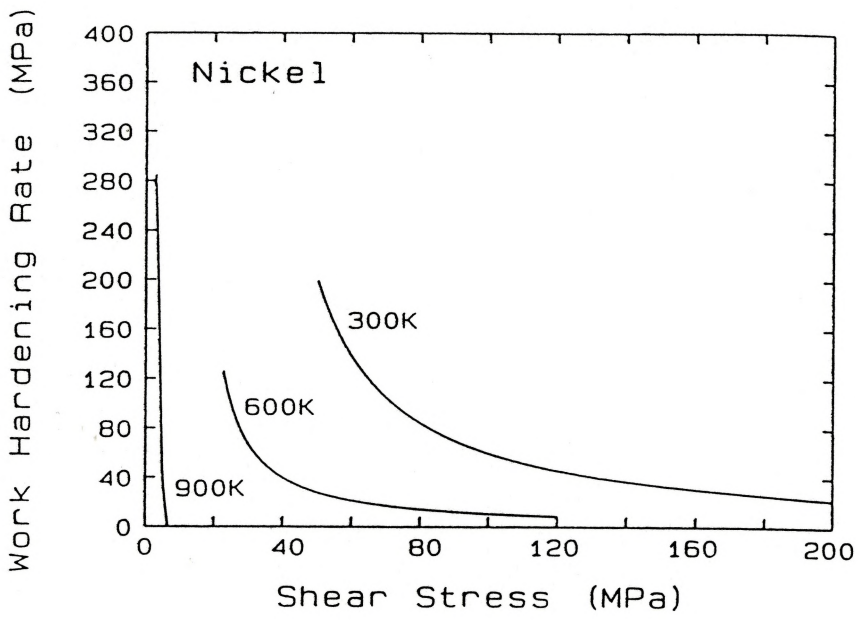

Figure 2.5/ Stress-strain curves and work hardening rate vs. stress curves calculated according to Nix et al.'s model for pure Nickel at various temperatures (from Nix et al., 1985)

transition that occurs in a wide variety of cases between stage III and stage IV, and, as with the previous model, the climb controlled recovery will not be possible at low homologous temperatures. In conclusion, this model gives a good representation of the behaviour at relatively high homologous temperatures, but cannot successfully represent low temperature large strain deformation.

2.3.3.3c/ The Argon and Haasen model (1993)

This model is based on the existence of internal stresses and the increase of the misorientation between cells in metals deformed up to large strains. The microstructure geometry considered here is a well defined equiaxed cell structure obeying the principle of similitude throughout the deformation (from stage II to stage IV). One basic assumption in this model is that the dislocation density in the cell interiors is negligible as compared to the dislocation density in the cell walls. The structure is treated like a composite, the overall behaviour being obtained by an Eshelby model of constraint.

The storage of dislocations in the cell walls consists of retaining a fixed fraction of the coming dislocation flux. The dislocation annihilation can occur by different processes : annihilation of edge dislocations when two edge dislocations of opposite sign meet each other on the same plane. This is considered to become significative when $\rho_{wall} > 10^{16}$ m^{-2}; cross-slip induced annihilation of two screw dislocations present on both sides of the walls (this process can be triggered by the first process if the considered edge dislocations were the obstacles separating these screw dislocations); and dislocation

core controlled climb.

The behaviour in the cell interiors is this time very different : the cell interiors are assumed not to harden by a dislocation density related mechanism. Indeed, the dislocation density in the cell interiors is supposed to be negligible. The hardening mechanism considered here is the building up of an increasing misorientation between the cells, inducing increasing internal stresses. These internal stresses are associated with the presence of the geometrically necessary (or non-redundant) fraction of the cell walls dislocation density, which accounts for the misorientation between the cells.

During the early stages of deformation, the work hardening behaviour is governed by the dislocation walls. Indeed, the hardening rising from the internal stresses is very small and negligible as compared to the hardening in the walls. However, as the deformation proceeds, the walls experience saturation and the overall work hardening rate corresponds to the increasing internal stresses in the cells.

We can see in Fig. 2.6 the evolution of stage IV work hardening rate with increasing flow stress level, as calculated by this model. Stage IV work hardening rate is represented to increase proportionally to the square root of the flow stress. This is in contradiction with every experimental data available. However, this model is of interest since it shows a useful approach to take into account the relation between large strains and microstructures and refocuses attention on the question of internal stresses in dislocated structures.

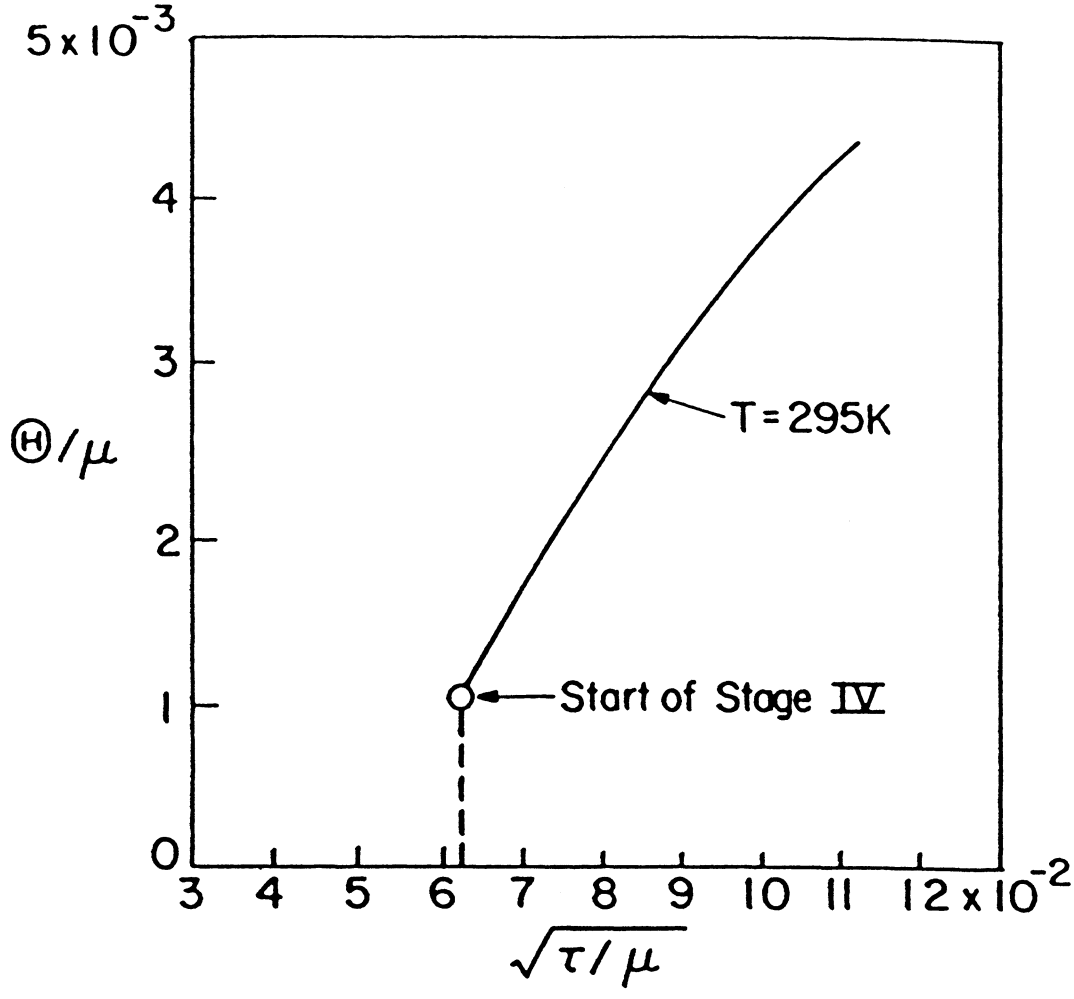

Figure 2.6/ Computed dependence of the stage IV work hardening rate on plastic resistance according to Argon and Haasen's model (from Argon and Haasen, 1993)

2.3.3.3d/ The Rollett model (1988)

One recent quite successful approach has consisted in modelling stage IV in terms of dislocation interactions and anihilation events rather than in terms of microstructure. In other words, although the microstructure is also taken into account in this model, it is considered more as a consequence of the hardening mechanisms and the dislocation interactions than the cause of the macroscopic behaviour. The evolution of the microstructure will hence not be the prominent feature in this type of modelling.

The model is based on the rate of accumulation of dislocation debris as a result of the dynamic recovery events. These recovery events can be of different nature :

- Screw dislocations can annihilate totally by cross-slip.
- Two nearby edge dislocations can form a dipole if their slip planes spacing is small enough (see section 2.3.2.2). These dislocation dipoles can break down into loops, which become additional obstacles to the gliding dislocations. These are the so-called dislocation debris, which have a rate of storage proportional to the current dislocation density.

During the early stages of deformation, debris, which contribution to the flow stress is very weak, have no influence on the work hardening rate. However, when the work hardening rate becomes very low and approaches saturation, it becomes determined by the rate of accumulation of debris. This is the stage IV of deformation. The microstructure evolution is accounted for by stating that the volume available for debris storage is the cell wall volume, which is decreasing with strain.

As we can see in Fig. 2.7, this model leads to the experimentally observed sharp

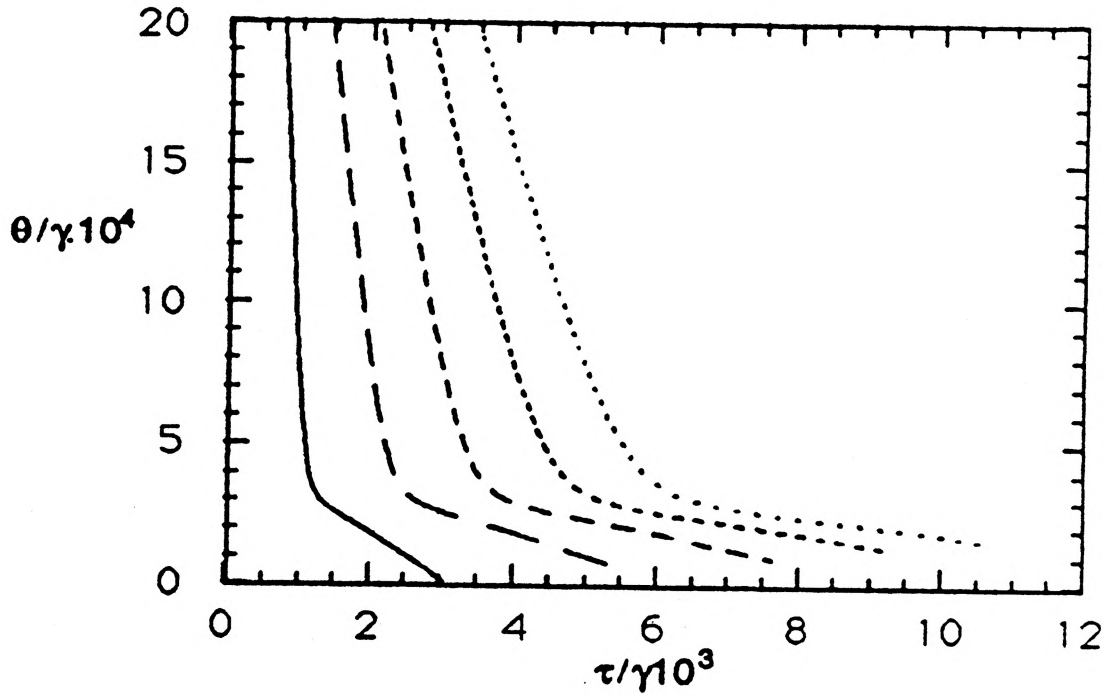

Figure 2.7/ Work hardening rate vs. stress curve calculated according to Rollett's model for Aluminium at various temperatures (from Rollett, 1988)

transition between stage III and stage IV, and afterwards to a slowly decreasing work hardening rate that stays of the order of magnitude of 10^{-4} G. The predictions are in very good agreement with the experimental data for low homologous temperature. However, at higher temperatures the model will not account for the occurrence of dislocation climb and will predict transitions between stage III and IV which are too sharp and levels of stage IV work hardening which are too high.

2.3.3.4/ Models compared to experiments

It is clear from this overview that there is no consensus regarding the mechanisms responsible for stage IV of work hardening. The diversity of the models presented here is striking: some view the deformed metal as a composite which properties are governed by the existing internal stresses, some view stage IV as a debris accumulation process. This diversity stresses the main difficulty in developing these models: the great complexity of the state of metals at large strains limits the ability to distinguish clearly between the different potential governing mechanisms.

Therefore, one has to be very careful before setting the structural basis of a stage IV model. The question to address is: what is the experimental evidence behind these models?

- The development of the microstructure is very variable from one metal to another: some metals will more readily form a cellular structure than others, the structures will be either equiaxed or elongated, etc. However, the stage IV behaviour has proven to be

independent from these structure variations. It seems hence dubious that stage IV behaviour could be fully described by these structures.

- The presence of internal stresses and their evolution with strain has been measured by X-ray methods summarized in Argon and Haasen (1993). However, it appears that the range of materials and conditions over which these measurements have been carried out is too limited to prove either that they are general or that they are responsible for stage IV. Moreover, there is no evidence that the presence of internal stresses can be a cause for material hardening.

- Stage IV models based on debris accumulation state that debris (i.e. dipoles and loops) become the dominant microstructural feature in large strains. However, there is no evidence that the presence of dislocation dipoles and loops is even significant in the microstructure at large strains. It has been observed in fatigue (Basinski and Basinski, 1992) that a saturation stress is actually reached, in a regime of dipole accumulation. However, in consideration of the very high dislocation densities reached in stage IV, it is very difficult to undergo the characterisation of dislocation structures, and hence evidence the presence of dipoles and loops in the microstructure.

Finally, stage IV modelling experiences other severe limitations: the additional complexity arising from the strain localization and the constant change in the relation between the behaviour on a slip system and the overall response due to the evolution of texture. These two issues will be discussed below.

2.4/ THE INFLUENCE OF SOLUTES ON WORK HARDENING

The influence of solid solution on the mechanical properties has to be considered both in terms of the increase of the initial yield stress and of the subsequent work hardening process. The solute atoms, acting as obstacles to dislocations, may dramatically increase the flow stress of pure metals. However they may have greater influence in work hardening and enable high stress levels to be obtained after large strains. Although much data is available on the work hardening of solid solutions, it has been mostly interpreted qualitatively. Most of the modelling of large strains behaviour, for instance, has been for pure metals, and the reviews on solid solution strengthening concentrate on yield point effects.

Neuhauser and Schwink (1993) propose that solute strengthening on the yield point and work hardening add linearly, but this is clearly in contradiction with the experimental data (e.g. Rollett, 1988; Hughes and Nix, 1989). Gleiter (1988) and Nix et *al.* (1985) propose that the increase in the stage III work hardening rate with increasing solute content is due to the change in the initiation of cross-slip induced by the change in stacking-fault energy. However, it is known that in Aluminium alloys the SFE does not change significantly with solute content.

Lloyd and Kenny (1982) interpret qualitatively the influence of solute atoms on work hardening as a decrease in dynamic recovery rate, and hence a change in the microstructure evolution. The work hardening rate was observed to be much higher at

moderate strains in concentrated Aluminium alloys than in more dilute alloys. Stage IV of work hardening, however, was observed to be concentration-independent, as in the works of Rollett (1988) and Hughes and Nix (1989). The same type of behaviour was observed for b.c.c. metals in the works on Iron alloys of Rack and Cohen (1970) and Leslie (1972).

2.5/ THE LOCALIZATION OF DEFORMATION: SHEAR BAND FORMATION

Localized plastic deformation is a natural outcome of large strain plasticity. It affects a wide range of materials properties: localized plastic flow influences constitutive behaviour, texture development, and serves as a direct precursor to failure, thus limiting ductility. Two types of instabilities can be observed. The first type is representative of the tension modes of deformation. This instability arises when the ratio between the work hardening rate and the stress reaches 1; at this point the strain hardening of the material is not able to spread the deformation in the entire sample, and necking occurs. This is known as Considiere's criterion. This type of instabilities is avoided in compressive or torsional modes of deformation. Shear localization, or shear banding, is there the most common type of non uniform deformation, and occurs extensively in some deformation processes like cold rolling or plane strain compression. These shear bands can be defined as sheet-like regions of concentrated plastic shear strain having a characteristic orientation with respect to the directions of principal strain. Here we will first review the

different characteristics of shear bands in metals, and then review the attempts that have been made to explain the mechanisms of their formation.

2.5.1/ Shear bands : characteristics

The shear localization taking place by the formation of shear bands can be separated in two distinct stages: the formation of microbands or Grain-scale Shear Bands (GSBs), the extension of which is restricted to a single grain, and the extension of these GSBs into Macroscopic Shear Bands (MSBs), also called sample-scale shear bands, which cross a number of grains and possibly the entire sample.

The critical strain at which shear bands appear is dependent on several parameters:

- it is very strain-path dependent: in the case of the tensile test or plane strain extension, for instance, they occur as early as 20% of strain as necking initiates (Bird *et al.*, 1987); in compressive strain paths their appearance is postponed to larger strains: GSBs form at strains of about 30% (Dève and Asaro, 1989), and MSB form at strains of about 60% (Dève and Asaro, 1989) to 100% (Korbel *et al.*, 1983, Korbel and Richert, 1985).
- it is dependent on the work hardening rate versus stress ratio (θ/σ): in the case of the tensile test, this corresponds to Considière's criterion, and necking occurs when $\theta/\sigma \simeq 1$. In compressive tests, shear band formation has been shown to corresponds to θ/σ ratios of about 0.1 (Harren *et al.*, 1988).
- the onset of shear bands is delayed by a lower grain size (Nourbakhsh and Vujic,

1986), and the first GSBs are observed in the larger grains of the grain size distribution;

- it is temperature dependant: in pure aluminium single crystals deformed by rolling, shear bands were observed at 77K but not at room temperature. This was ascribed to the lack of a lamellar dislocation structure at this temperature (Morii and Nakayama, 1985). The same phenomenon was observed in Al-3%Mg: shear bands were observed when the deformation was carried out at room temperature, but not at 473K, where the recovery was considered to be too extensive (Nakayama and Morii, 1987);

- in the case of single crystals, the occurrence of shear bands is very orientation dependant: extensive studies of rolling and plane strain compression of single crystals have shown that the occurrence of shear bands was critically dependant of the initial crystal orientation (Morii and Nakayama, 1985; Morii *et al.*, 1986; Harren *et al.*, 1988; Dève and Asaro, 1989; Kamijo *et al.*, 1991). As an example, shear bands were reported in pure aluminium single crystals of initial orientation {211} <111> deformed by rolling at room temperature, but not in the orientation {011} <100>;

- shear banding is dependent on the addition of solutes: this can be illustrated by the example of aluminium at room temperature: Morii and Nakayama (1985), reported that shear bands did not form in pure Al at room temperature (it should be noted that Kamijo *et al.* (1991) found the opposite result), while their formation is very easy in the presence of Mg, where negative strain rate sensitivity may occur (Korbel and Martin, 1986; Bird *et al.*, 1987; Nakayama and Morii, 1987);

- it is dependent on the presence of second phase particles: this is illustrated by studies

of Al-Cu alloys both in the age-hardened state and in the homogenized state (Morii *et al.*, 1986; Harren *et al.*, 1988; Dève and Asaro, 1989; Lee and Chan, 1991). If the shear bands formation is not affected by the presence of second phase particles, it appears earlier than in solid solutions due to the high level of flow stress and the decreased work hardening rate (hence the low level of the ratio θ/σ).

Shear bands have well-defined characteristics. They are essentially planar throughout the sample, although they may be S-shaped towards the extremities of the sample (Harren *et al.*, 1988). Several families of shear bands are usually present simultaneously, but in the case of high Stacking Fault Energy (SFE) f.c.c. metals two sets develop in a given grain (Hatherly and Malin, 1984). Although it was long thought that the MSB had no particular crystallographic habit plane (Brown, 1972), it is now believed that they propagate in each grain along crystallographic directions, and that they propagate from grain to grain by local bending of the shear band plane (Korbel and Martin, 1986; Chang *et al.*, 1989; Dève and Asaro, 1989; Lee and Chan, 1991). The lattice inside the MSB has been observed to be rotated by angles from 2 to 5° with respect to the lattice outside the MSB, the axis of rotation being normal to the lateral surface in plane strain compression (Harren *et al.*, 1988; Dève and Asaro, 1989). This is not always true however, and angles of the order of 10° have been observed (Hatherly and Malin, 1984). The MSBs make usually very characteristic angles with the macroscopic flow direction. These angles range usually from 15 to 50°, 35° being by far the most commonly observed value, together with angles of the order of 20°

(Nourbakhsh and Vujic, 1986; Yeung, 1987; Yeung and Duggan, 1987; Harren *et al.*, 1988; Nourbakhsh and Song, 1989; Lee and Chan, 1991; Shen, 1993). See Table 2.1 for a summary of these results.

2.5.2/ Shear bands: mechanism of formation

Two types of models have been developed to account for the formation of the shear bands and the angles they make with the general flow direction. The first approach views the initiation of localized shear bands as a bifurcation phenomenon in continuum mechanics. This was for instance described using a constitutive law exhibiting pressure-sensitivity, dilatancy and non-coaxiality by Anand and Spitzig (1982). The second approach has received more attention recently and seems more successful. It considers shear band formation to be due to geometrical (or texture) softening and will be outlined here. This approach can be separated in two steps: why do shear bands initiate and develop at some characteristic angles, and how do shear bands grow from microscopic to sample-scale.

Plastic instability can be caused by a number of factors, made apparent by recognizing that σ is a function of many variables, including strain, strain rate, temperature, and even surface energy (Backofen, 1972):

$$\sigma = \sigma(\epsilon, \dot{\epsilon}, T, \Gamma, \ldots) \qquad (2.11)$$

Therefore the net rate of the material strain hardening is:

Reference	Material	Mode	Angles (degrees)
Hatherly and Malin	various	rolling	35
Nourbakhsh and Vujic (1986)	Brass	channel-die	27 to 40
Yeung (1987)	Al alloy	rolling	35
Yeung and Duggan (1987)	f.c.c. metals	rolling	20 and 30-35
Harren et al. (1988)	Al-Cu	channel-die	30-40
Deve and Asaro (1989)	Al-Cu	channel-die	45
Nourbakhsh and Song (1989)	Brass	rolling	40 to 45
Lee and Chan (1991)	Al-Cu	rolling	19 and 35

Table 2.1/ Angles between shear bands and direction of deformation in previous studies

$$\frac{d\sigma}{d\epsilon} = \left(\frac{\partial\sigma}{\partial\epsilon}\right) + \left(\frac{\partial\sigma}{\partial\dot{\epsilon}}\right)\left(\frac{d\dot{\epsilon}}{d\epsilon}\right) + \left(\frac{\partial\sigma}{\partial T}\right)\left(\frac{dT}{d\epsilon}\right) + \left(\frac{\partial\sigma}{\partial\Gamma}\right)\left(\frac{d\Gamma}{d\epsilon}\right) + \ldots \quad (2.12)$$

Any one of the terms on the right could be responsible for the initiation of instability if it become sufficiently negative. In high rate deformation, for instance, the heat generated by plastic deformation may cause adiabatic shear banding to occur. We will limit our investigation to the first term, the other terms being assumed negligible for the deformation procedures used in this study.

The principle of geometrical softening is the following: the global deformation involves rotation of the grains: their orientation is no longer random, and texture develops. Locally, this leads to a modification of the angle between the slip planes and the direction of deformation, so that the Taylor factor M that relates stress and strain from crystallographic to macroscopic axes is modified. Even though the shear hardening rate on a particular slip system may still be positive, the true work hardening rate may become locally negative, introducing an instability. Several criterions for geometrical softening have been proposed. The simplest was presented by Canova *et al.* (1984): shear bands appear when there is a net softening,

$$\frac{d\sigma}{d\epsilon} = M^2 \frac{d\tau}{d\gamma} + \tau \frac{dM}{d\epsilon} < 0 \quad (2.13)$$

Lee and Chan (1991) developed a criterion to predict the angle at which shear bands develop. This criterion is based on three factors: the variation with angle of the Taylor factor, the texture softening factor and the number of slip systems activated to

enable the deformation on this direction. First the effective Taylor factor M' is minimized (where $M' = M/\cos 2\alpha$, α being the angle of deviation from the shear band to 45°). If a range of shear angles all possess the same minimum M' then the shear angle with both the minimum M' and the smallest number of slip systems will be selected. If still no unique angle is found, the softening factor is minimized. This criterion predicts the dominance of 35° and 19° angles found in the literature.

A mechanism for the growth and propagation of shear bands was proposed by Harren *et al.* (1988):

- in the early stages of deformation, the grains tend to rotate towards the ideal texture orientation; the global anisotropy of the crystal increases, and the grains become more aligned with each other;
- meanwhile, some grains gain a favourable orientation for texture orientation. This, combined with the compatibility conditions between the grains, leads to the formation of grain-scale shear bands. The lattice in this grain rotates so that it is aligned with the direction of shearing;
- when the GSB impinges on the grain boundary, compatibility conditions force localized shear on the nearby grain. This shearing rotates the lattice in the second grain towards the ideal texture orientation. The shear band can then propagate further and in the entire sample.

These models predict that shear bands should generally initiate in zones of large local deformation. In channel die compression, this corresponds to the corners of the

sample. This prediction is also in agreement with the experiments (e.g. Nourbakhsh and Vujic, 1986).

In conclusion, macroscopic shear bands can form even if the macroscopic work hardening rate is still positive. Recent experiments on Copper, Silver and Aluminium at low temperatures (Szczerba, private communication) have shown that necking in tension can occur when the ratio between work hardening and flow stress is as high as 3, when the material still has high dislocation storage capabilities. These instabilities may be caused by a sudden change in the dominant slip system.

2.6/ TEXTURE EVOLUTION AT LARGE STRAINS

We will give here a brief overview of the texture evolution at large strains in f.c.c. metals and how it relates to the mechanical properties.

Texture evolution is well known to be highly path dependant, and is responsible for a large part of the differences that are encountered when one is testing the same material at large strains under different deformation conditions (Kocks *et al.*, 1988; Bronkhorst *et al.*, 1991). Takeshita and co-workers (1989) strained polycrystalline cubic aluminium specimens along complex strain paths bringing them back to their initial shape. Although no net strain had occurred, the texture had changed from the initial recrystallized texture to a texture exhibiting cubic symmetry. This experiment demonstrates the importance of strain path on texture development, and hence on the

mechanical properties and plastic anisotropy of metals.

Texture evolution in channel die compression has been mostly studied for single crystals (Butler and Hu, 1989; Becker, 1991; Maurice and Driver, 1993) and bicrystals (Blicharski *et al.*, 1993). Studies of the texture evolution of aluminium polycrystals in plane strain compression include the work by Franciosi *et al.* (1987), Becker and Lalli (1991), Bronkhorst *et al.* (1991) and Panchanadeeswaranan and Doherty (1993). The texture development is essentially similar to the texture development in rolling. For most f.c.c. metals, the most common resultant orientations obtained by this type of deformation path are the Copper orientation $\{112\}<111>$ and the Brass orientation $\{110\}<112>$. Pure plane strain compression, with no influence of twinning, is represented by the Copper texture. This type of texture occurs mostly in high-Stacking Fault Energy (SFE) metals. Brass texture represents the influence of intense shear banding and massive presence of twins in the microstructure. This type of texture is characteristic of high SFE metals.

The occurrence of shear banding in a number of deformation procedures has an important influence on the texture evolution. In channel-die, for instance, the texture will evolve from a plane strain compression texture towards a shear texture. Aernoudt (1978) investigated the influence of shear superimposed on plane strain compression (Fig. 2.8). Berveiller *et al.* (1988) investigated this influence of shear on texture for rolling, and related the texture type to the mode of deformation occurring in the material. In the case of rolling of aluminium, Truszkowski *et al.* (1982) and Major (1992) studied the

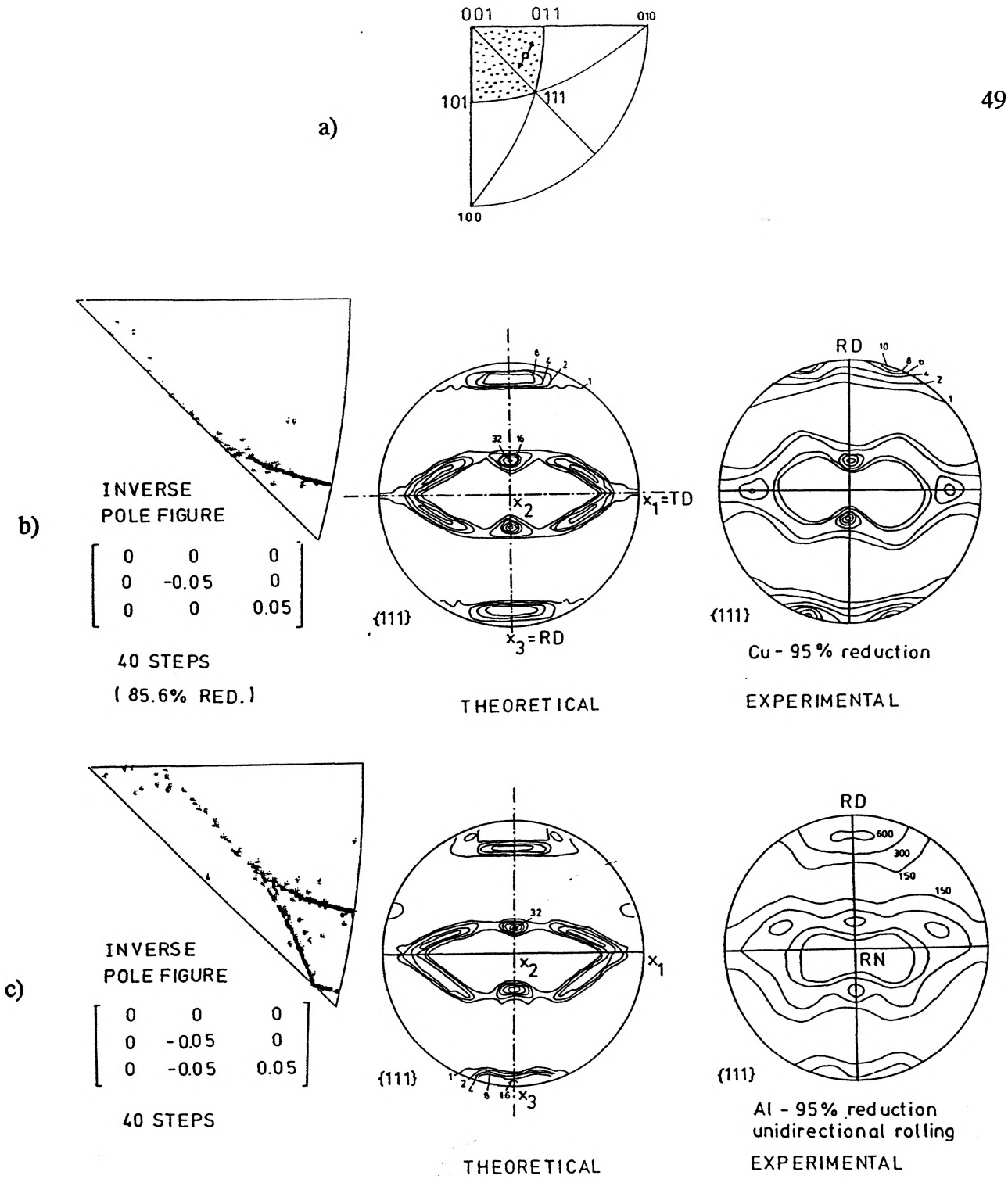

Figure 2.8/ a) Inverse pole figure configuration; b) Inverse pole figure and theoretical and experimental {111} pole figures for pure plane strain compression; c) Inverse pole figure and theoretical and experimental {111} pole figures for pure plane strain compression with superimposed shear (from Aernoudt, 1978)

evolution of texture as a function of the distance from the surface of the rolled sheet, and correlated it to the presence of a heavily sheared layer close to the rolling surface. Fig. 2.9 shows the presence of shear texture at the surface and rolling texture at the centre of a cold-rolled aluminium sheet.

There is a wide recognition that one needs to consider both the texture evolution and the microstructural evolution in order to complete a clear view of the deformation process. Some attempts have been done to correlate the evolution of texture with the evolution of the microstructure (Hirsch, 1990; Leffers and Juul Jensen, 1991). Nowadays, much of the texture evolution can be quite accurately predicted by polycrystalline codes (e.g. the Los Alamos Lapp code). However, these codes still lack microstructural input. For instance, most predicted textures are much sharper than observed textures. This may be caused by the development of a cell block structure in the material, which will scatter the orientation around the preferred pole. Other factors that need to be taken into account are the elongation of the dislocation substructure at large strains and the occurrence of shear banding. However, including these elements in texture evolution predictions requires both a more clear and more quantitative knowledge of structural evolution and very large computing capabilities.

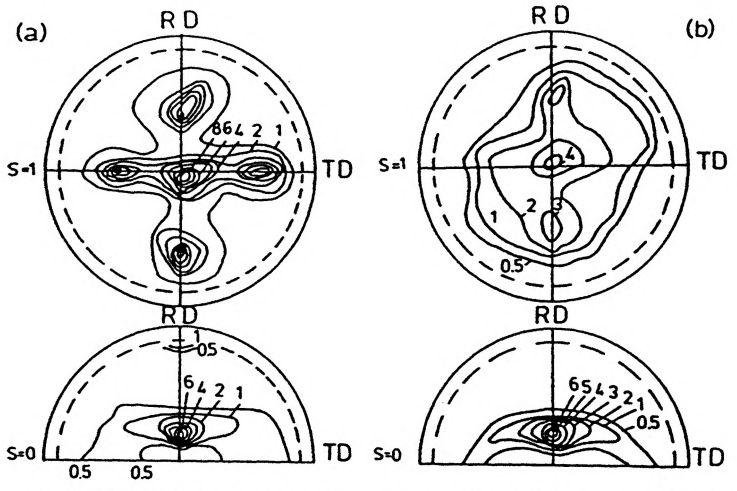

a 73·1% reduction ($l/h = 7{\cdot}5$), surface ($S = 1$), centre ($S = 0$);
b 67·1% reduction ($l/h = 6{\cdot}85$), surface ($S = 1$), centre ($S = 0$)
RD rolling direction; TD transverse direction

Figure 2.9/ {111} pole figures for a) Aluminium b) Copper after cold rolling, showing shear texture in surface and rolling texture in centre (from Major, 1992)

CHAPTER 3

EXPERIMENTAL INVESTIGATION

3.1 PROCESSING OF THE ALLOYS

3.1.1 Alloys choice and composition

Aluminium alloys are very suitable for the study of solid solution strengthening and large strain behaviour. The addition of solute elements does not change appreciably their stacking fault energy (Kritzinger et al., 1969), they do not twin except under extreme conditions of shock loading, and they do not undergo dynamic recrystallization even at elevated temperatures. The hardening processes in these alloys are due to the presence of dislocations and their interactions with solute atoms and second phase particles which results in solution and precipitation hardening; in addition solutes can influence the net work hardening rate and produce other phenomena such as the Portevin-le-Châtelier effect and strain localization.

The alloys chosen for this study were Aluminium-Copper alloys, the Copper concentrations ranging from 0 to 0.4 weight percent (or 0.23 at%). These concentrations were used in order to avoid the precipitation of Al_2Cu and its intermediate phases during processing and testing of the alloys. According to the Al-Cu phase diagram, at concentrations below 0.5 Wt% all the Copper will be in solution (Fig. 3.1). It was

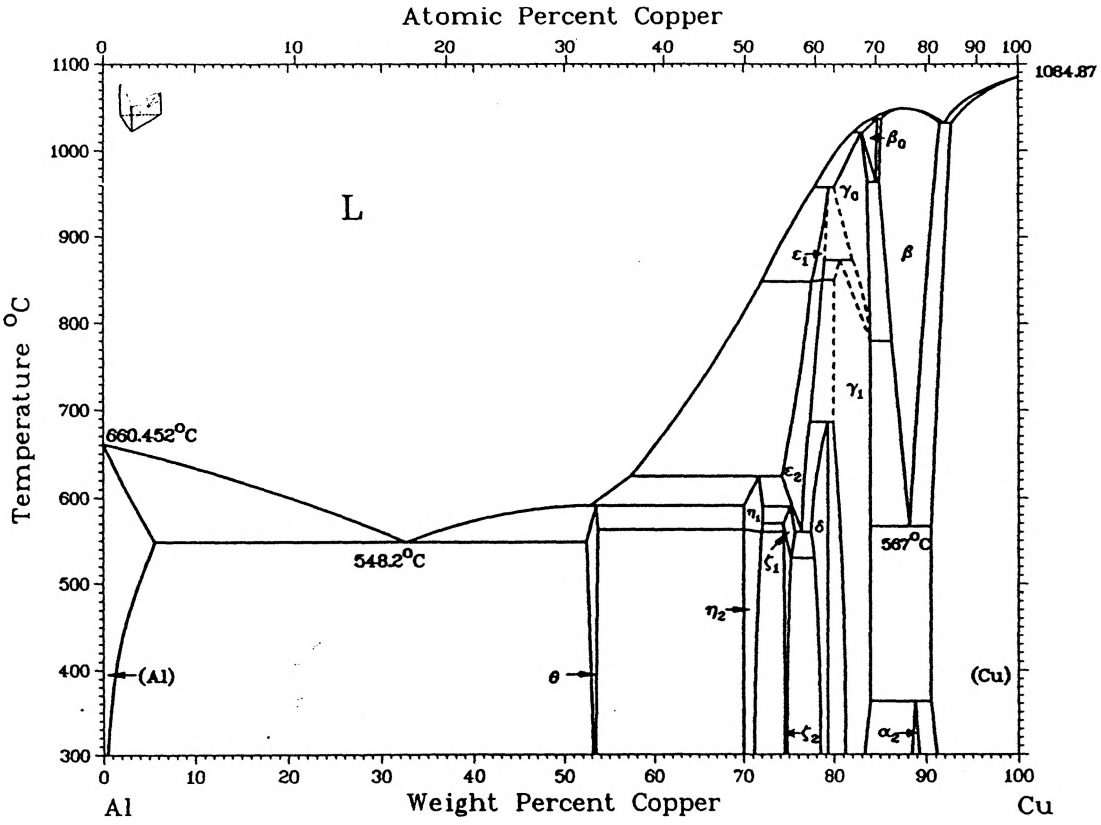

Figure 3.1/ Al-Cu phase diagram (from Binary Alloy Phase Diagrams, V. 1 (1986), ed. in chief: Masalski,TB, The American Society for Metals, Metals Park, Ohio

therefore possible with the chosen concentrations to study the effects of the solid solution on the mechanical properties.

The alloys were supplied by the Voreppe Research Centre (CRV, France) and based on 99.99% pure Aluminium. The chemical composition was determined by a chemical analysis in solution which was carried out at CRV by Inducted Plasma Emission Spectroscopy and is given in the table below :

Table 3.1 : composition of the alloys

	Al (Wt %)	Cu (Wt %)	Fe (ppm)	Others (ppm)
Alloy 1	99.99	0.0057 ±0.0002	17 ±3	<20 each
Alloy 2	99.7	0.218 ±0.007	20 ±3	<20 each
Alloy 3	99.5	0.413 ±0.012	20 ±3	<20 each

3.1.2 Thermomechanical processing

The alloy was received from Pechiney in the form of as-cast slabs of dimensions 25 x 250 x 150 mm^3. In order to determine the homogenization temperature, Differential Thermal Analysis was carried out on the three alloys. The melting started at temperatures of 656°C for pure Al, 658°C for Al-0.2%Cu and 655°C for Al-0.4%Cu, which is consistent with the phase diagram (Fig. 3.1).

The homogenizing treatment was 12 hours at 620°C, after which all the Copper was assumed to be in solution.

The slabs were subsequently cold rolled to a thickness of about 12 mm and machined to

the dimensions of 9.5 x 35 x 50 mm^3, which were the dimensions for the channel die compression tests. Lastly, the samples were individually recrystallized in a salt bath for the following times and temperatures :

- pure Aluminium, 15 minutes at 330°C
- Al-0.2% Cu and Al-0.4% Cu, 120s at 400°C

The temperature of 400°C was chosen in order to avoid the possible precipitation of Al_2Cu, which is fastest at 350°C.

The grain sizes resulting from these treatments were measured by anodizing and optical metallography to be of the order of 150 μm (Fig. 3.2; see Appendix A for the conditions).

3.2 MECHANICAL TESTING

3.2.1 Testing method

The method chosen for the study of the mechanical properties at large strains was channel-die compression (see section (2.2) in the literature review for the details).

3.2.1.1 Testing machine

The channel die apparatus (Fig. 3.3b) was placed in a stainless steel container (Fig. 3.4a) in order to perform tests at low temperatures. The apparatus was then attached to the grips of an MTS testing machine (Fig. 3.4b). The load was measured using a 100 kN load cell and the strain was calculated from the displacement of the

a)

b)

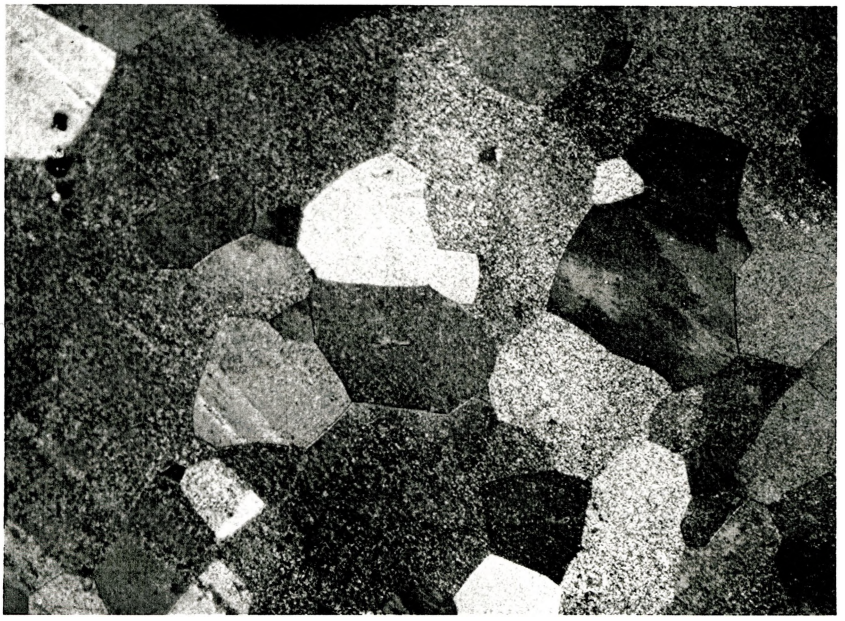

Figure 3.2/ Optical micrographs after recrystallization and anodization for a) Pure Al b) Al-0.2%Cu showing the grain sizes; magnification X102

a)

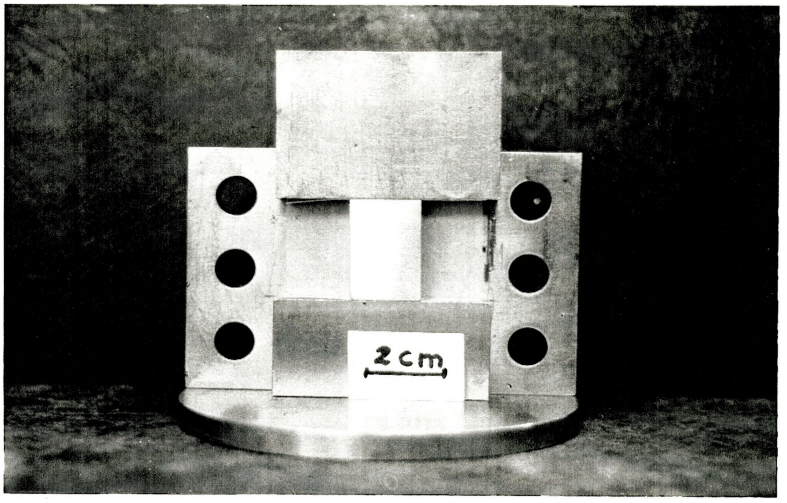

b)

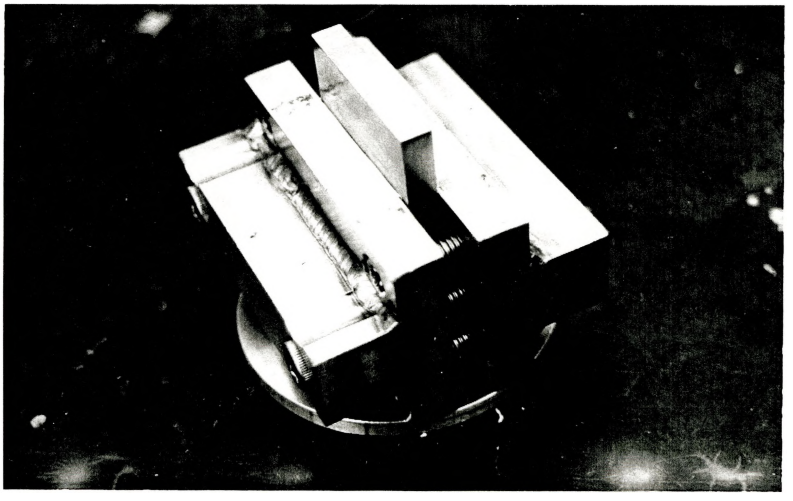

Figure 3.3/ Channel-die apparatus a) position of the teflon sheets b) mounted

a)

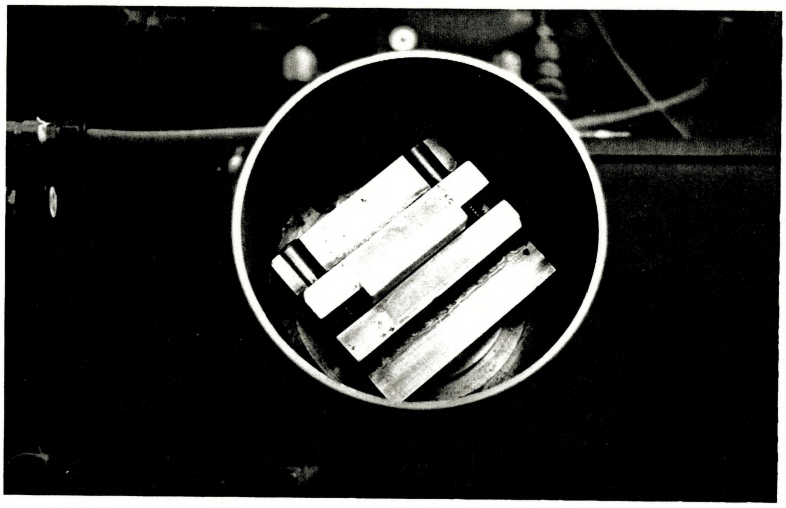

b)

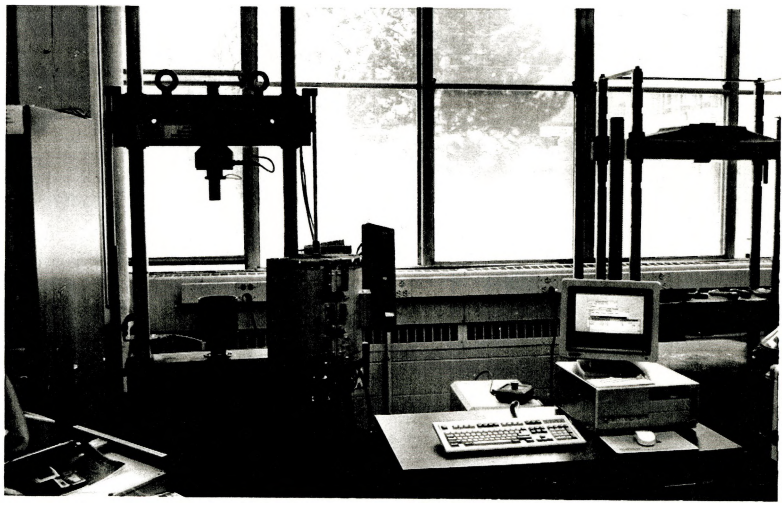

Figure 3.4/ a) Channel-die apparatus in the stainless steel container b) The MTS testing machine

cross-head as measured by an LVDT. The load cell measurements were precise to ± 20 N, and the LVDT measurements to ± 0.005 mm.

3.2.1.2 Temperatures and strain rate

The tests were carried out at three different temperatures : ambient temperature, 200K (dry ice) and 77K (liquid Nitrogen). For the tests at 200K, cooling was achieved by immersing the compression device in methanol cooled by pieces of solid CO_2 (dry ice). The temperature was measured by a thermometer immersed in the bath. For the tests at 77K, cooling was achieved by immersing the device in liquid Nitrogen and allowing it to equilibrate. The test was started when the boiling of the liquid had dramatically decreased.

The strain rate used for all the tests was 10^{-3} s^{-1} (in true strain). This strain rate is low enough so that a slight change in strain rate has little effect on the stress level, and high enough to limit the testing times to a reasonable duration. Moreover, at such strain rates, the temperature rise caused by the dissipation of the energy of plastic deformation is negligible.

3.2.1.3 Lubrication

Since the contact surface between the specimen and the die is very large, lubrication is an important consideration in channel-die compression. At room temperature the lubrication was achieved by placing 0.003 inch thick teflon tape on every surface in contact with the die : two teflon sheets were glued on the channel die walls (Fig. 3.3a, 3.3b), one teflon sheet laid between the bottom of the device and the sample,

and another sheet laid between the sample and the punch. At the two other temperatures, a molybdenum disulfide-based high pressure grease was spread on the faces in addition to the teflon tape because of the brittleness of the tape at cryogenic temperatures.

3.2.1.4 Recording of the displacement

Displacements δh_{rec} were directly recorded using the LVDT of the hydraulic machine. The direct LVDT measurement has a major drawback : the displacement measured by the LVDT corresponds to the cumulative compression of the sample, the teflon tape and both of the crossheads. The deformation of the steel parts (crossheads, channel-die device) can be neglected; however the deformation of the teflon tape is certainly significant, especially at the beginning of the test. This has two consequences on the interpretation of the results :

- First, the slope of the elastic region of the stress-strain curves obtained would be expected to vary between E (this corresponding to free compression, if the sample is not fully constrained in the die) and $E/(1-\nu^2)$ (plane strain compression). At room temperature it should therefore be around 70 GPa. However, it was measured to be around 10 GPa. Harren, Dève and Asaro (1988) have shown that this discrepancy is mostly due to the teflon tape.

- Second, the final recorded displacement $\delta h_{rec,tot}$ was usually higher by about 5% than the final reduction in height $\delta h_{real,tot}$ measured directly on the sample. It was assumed that during the test the real reduction in height δh_{real} was :

$$\delta h_{real} = \delta h_{rec} \cdot \delta h_{real,tot} / \delta h_{rec,tot}$$

As a result of these difficulties, the first few percent of the stress-strain curves are unreliable. However, as one gets to higher strain, these effects are much less important. Since the present study is mainly concerned with large strain behaviour, this was considered to be acceptable.

3.2.1.5 Testing procedure

It is not possible to achieve high strains in channel-die compression in one continuous straining operation. Indeed, after some deformation has been carried out, the lubricating teflon tape is damaged and the resultant friction increases, making interpretation of the data very difficult. Moreover, as the deformation proceeds, the load increases, due to work hardening and to the increase in the cross-sectional area of the specimen, so that the capacity of the testing machine would eventually be exceeded. Therefore large strains were achieved by unloading, remachining and then reloading the sample. Although this caused some static recovery to occur when the samples tested at low temperatures were warmed up to room temperature, this was the best compromise available. An important point is that it is necessary to install the sample always the same side up. Indeed, due to the effect of friction, the top part of the sample undergoes more deformation and is therefore harder. If the sample is installed upside down for the next deformation step, the bottom part will deform significantly less both because it experiences a smaller pressure and because of the hardening gradient present at the

beginning of the step. On the contrary, if the sample is always positioned the same way, the positive work hardening rate will help spreading the deformation through the sample and make the deformation more homogeneous.

The choice of the sample dimensions is important: if large strains are to be reached, the initial sample dimensions need to be large. Indeed, as the deformation proceeds, the thickness of the sample becomes significant as compared to its height, increasing the role of the friction due to the bottom and top faces of the sample, making the results difficult to interpret. Moreover, as the sample dimensions diminish, the displacement control and measurement become more imprecise, making the results less reliable. Hence the larger the initial dimensions, the larger the final attainable strain. One limitation occurs, however, due to the load cell capacity, which limits the maximum specimen length that can be used. A second choice to make is the height to length ratio: if this ratio is too high, the sample may buckle during the test. On the other hand, a low ratio increases the load required for deformation and increases the total friction.

On the basis of the load cell capacity (100 kN) and the experience of previous work on Copper-based composites (Poole, 1993), the initial sample dimensions were chosen to be 50mm (height), 35mm (length) and 9.5mm (thickness) for room temperature and 35mm (height), 25mm (length) and 9.5mm (thickness) for the lower temperatures. The height to length ratio was therefore approximately 1.4, which prevented buckling and minimized the friction.

The samples were deformed by steps ranging from 30 to 50%, and then cut and

remachined to new dimensions, the height and thickness of the sample staying constant, and the length being diminished to achieve again a ratio of 1.4. The samples were finally polished with a 1200 SiC paper and placed again in the compression device for further deformation.

3.2.2 Definition of stresses and strains

The results are presented in the form of load-displacement curves. There are several ways to draw the resultant stress-strain curve, depending on the definitions of stress and strain that are used. In this context, three different approaches can be used:

- true stress / true strain

These are the stresses and strains directly related to the deformation procedure. They can be expressed as follows :

$$\epsilon_{true} = \ln\left[\frac{h_0}{h}\right] \qquad (3.1)$$

$$\sigma_{true} = \frac{F}{S} = \frac{F}{l w_0} = \frac{F h}{w_0 h_0 l_0} \qquad (3.2)$$

where w is the thickness of the sample, l its length and h its height, F is the recorded load and the subscript 0 indicates the dimensions at the beginning of the test. This is obtained considering that w does not change and that the specimen stays a rectangle, that is the product l.h is constant.

- Von Mises equivalent stress and strain

If comparisons are to be drawn between the results of different testing procedures involving different deformation modes (e.g. plane strain compression, tension and torsion), one has to convert these true stresses and true strains, specific to the studied deformation path, into their Von Mises equivalents. In the case of plane strain compression, the two are related in the following way (Hosford and Caddell, 1993) :

$$\epsilon_{von\ Mises} = \frac{2}{\sqrt{3}} \epsilon_{true} \qquad (3.3)$$

$$\sigma_{von\ Mises} = \frac{\sqrt{3}}{2} \sigma_{true} \qquad (3.4)$$

- Shear stress and strain

These are the stresses and strains resolved on a single slip system. In the case of a randomly oriented crystal, they are related to the true stress and true strain by the average orientation factor, or Taylor factor M (Taylor, 1938) :

$$\tau = \frac{\sigma_{true}}{M} = \frac{\sigma_{true}}{3.07} \qquad (3.5)$$

$$\gamma = M \epsilon_{true} = 3.07 \epsilon_{true} \qquad (3.6)$$

Unless stated otherwise, σ and ϵ will in the following always refer to Von Mises stresses and strains, and τ and γ to shear stresses and strains. The work hardening rates will be written as follows : $\theta_{VM} = d\sigma/d\epsilon$; $\theta_T = d\sigma_{True}/d\epsilon_{True}$; $\theta = d\tau/d\gamma$.

3.2.3 Study of friction

There exist no analytical solution to the problem of friction in a channel die and there appears to have been no attempt to simulate it numerically. As pointed out by Nourbakhsh and Song (1989), an approximation can be found by comparison with the free compression test. Indeed, in channel die compression the lateral faces of the specimen (faces in contact with the die walls) are subject to only about half of the pressure applied on the punch. It is therefore often assumed that the friction on the lateral faces is negligible and that the friction problem can be solved by considering the friction on the top and bottom faces only. The stress applied by the punch on the sample, σ_a, and the flow stress of the material (true stress) are then related as follows :

$$\sigma_a = \frac{\sigma_f}{\mu l / w} \left[\exp\left(\mu \frac{l}{w}\right) - 1 \right] \qquad (3.7)$$

where μ is the coefficient of friction, l the length of the specimen and w its thickness.

To assess the influence of friction in our case, several samples of a 6061 Aluminium alloy were deformed at room temperature in the channel die. The height to length ratios varied between 0.5 and 2, and different dimensions were kept constant from sample to sample (see Table 3.2 for the dimensions and ratios of the different samples, and Fig. 3.5 for the results of the compression tests). After the first few percent of deformation all the samples show the same work hardening rate, regardless of their initial dimensions. The curves stay separated in two groups separated by a slight shift in stress. This shift can be explained by texture effects: the samples were cut in two different

Sample	Height (h)	Length (l)	Width (w)	h/l
1	19.97	39.20	9.56	0.51
2	11.35	20.18	9.49	0.56
3	19.94	28.68	9.55	0.70
4	19.92	20.47	9.47	0.97
5	25.00	20.49	9.50	1.22
6	20.04	13.76	9.55	1.46
7	20.02	11.32	9.47	1.77

Table 3.2/ Initial dimensions of the samples used for the friction study in Fig. 3.5

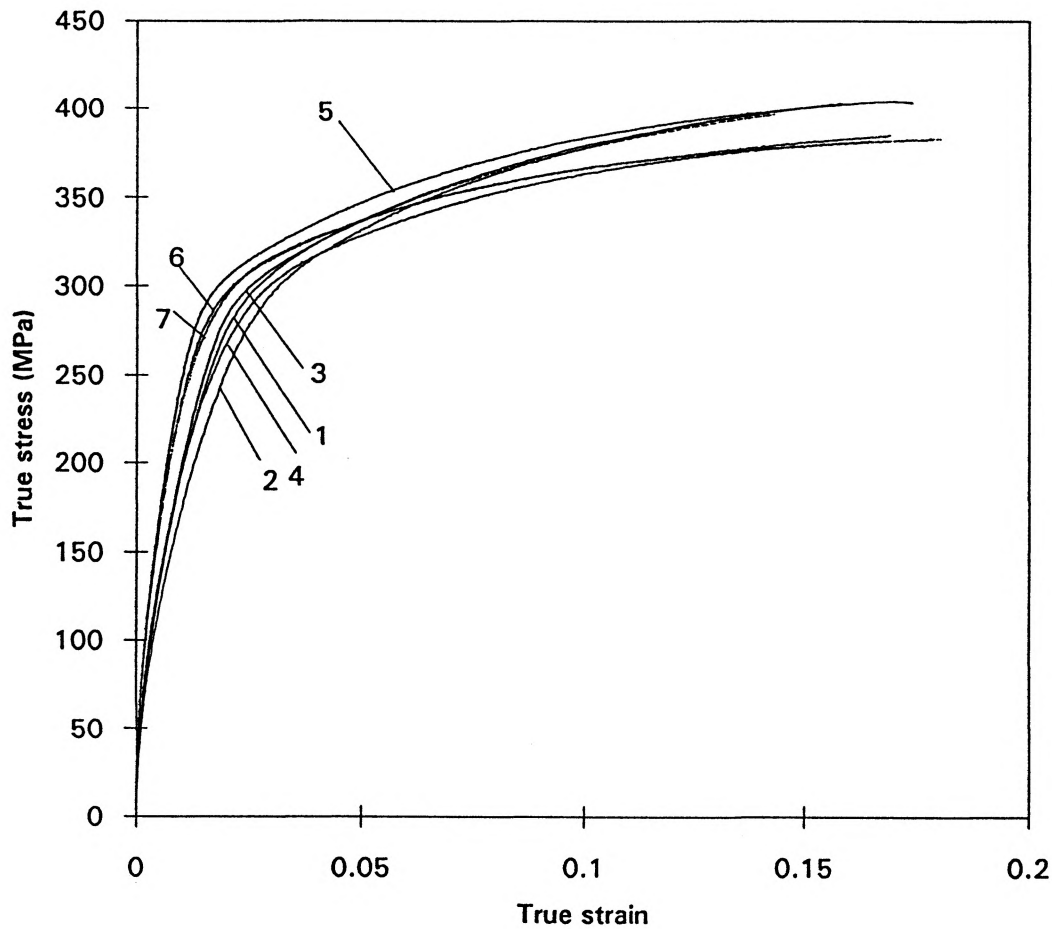

Figure 3.5/ Channel-die compression stress-strain curves for 6061 samples of different aspect ratios (reference numbers correspond to Table 3.2)

directions from the initial 6061 slab. This slab may have retained some anisotropy from its former processing. From consideration of these results, it can be concluded that the friction has a negligible effect on the measurement of the flow stress under these testing conditions.

However, it appears that friction effects cannot be neglected when the height of the sample becomes lower than its thickness. Indeed, when this stage is reached, a substantial increase of the level of stress can be consistently observed (see as a typical examples Fig. 3.6 for pure Aluminium deformed at 200K). To assess the relationship between this increase in flow stress and the critical height of the sample, Duly (1993) carried out the following experiment (on the same channel die compression device) : two samples of Al - Mg - Mn alloy were deformed at room temperature with the same strain rate of 10^{-3} s^{-1} up to 60% of true strain. Both the height to length ratio (1.4) and the thickness were identical for the two samples, but their initial height was different, namely 35mm and 10.5mm. As can be seen in Fig. 3.7, both samples experience the same stress levels at the beginning of the test. However, as the height of the smaller sample becomes less than its thickness, the two curves diverge significantly, being finally different by more than 30 MPa after 60% of true deformation. It is believed that this is due to the effect of friction : the area of the top and bottom surfaces is w.d, and the area of the lateral surfaces is h.d. As the height diminishes, the contact surfaces between the sample and the punch, where the pressure (hence the friction) is the largest, become dominant in comparison to the lateral surfaces, and the fraction of the load due to friction cannot

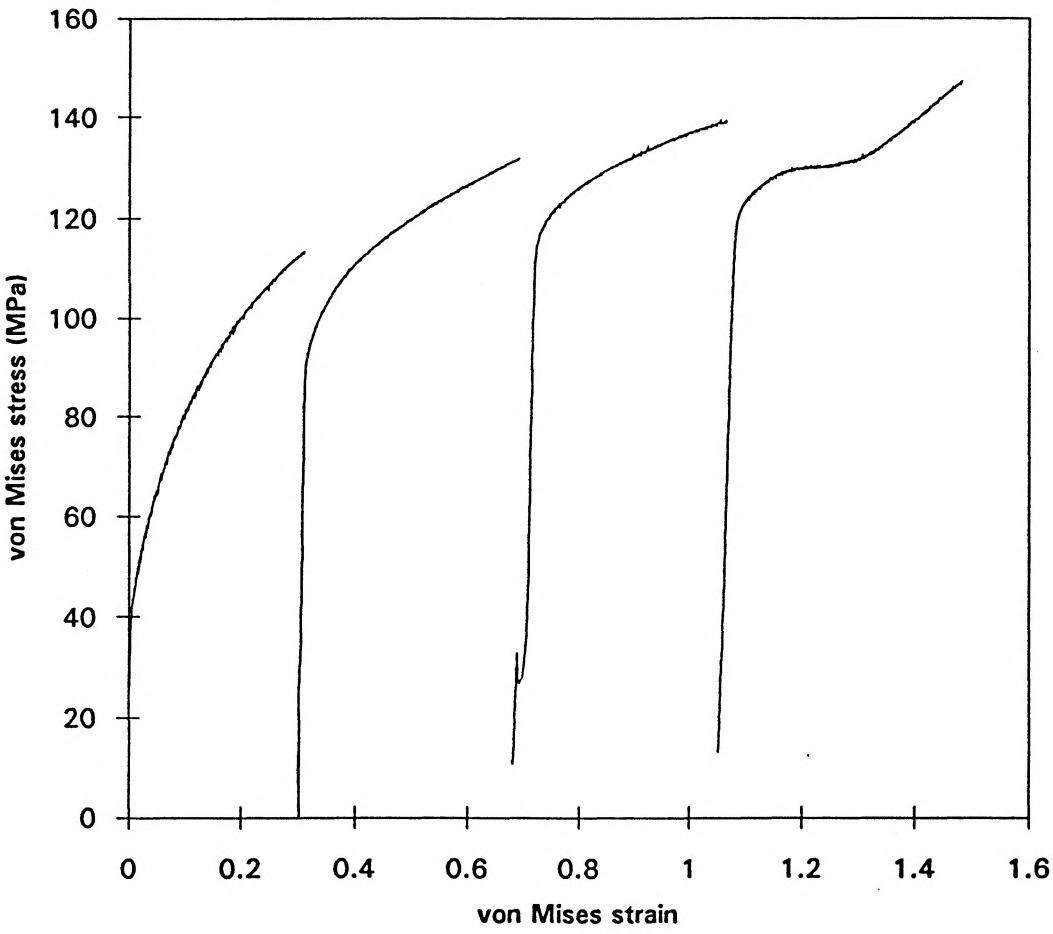

Figure 3.6/ Channel-die compression stress-strain curves for pure Al deformed at 200K showing the dramatic increase in friction at large strains

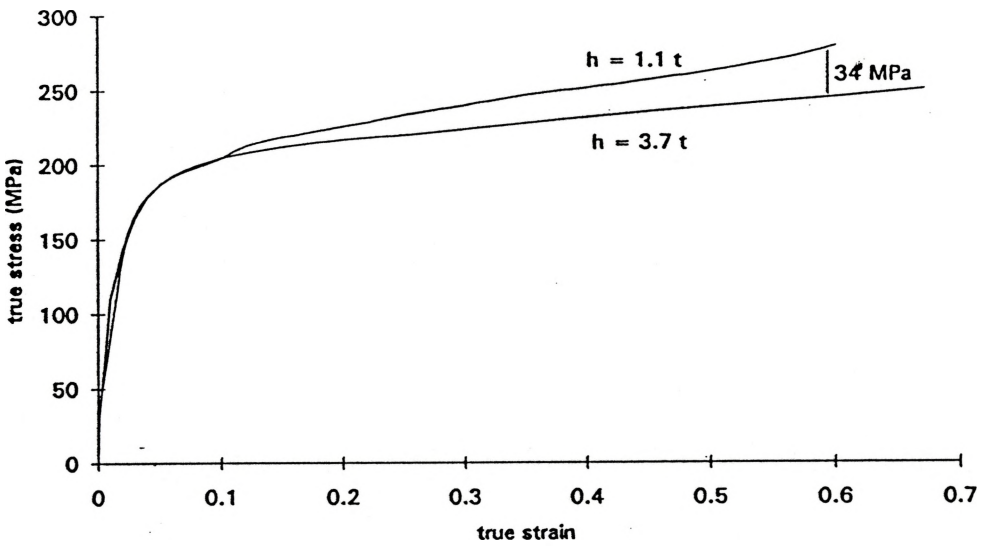

Figure 3.7/ Channel-die compression stress-strain curves for two Al-Mg-Mn samples of same initial aspect ratio but of different initial height (from Duly, 1993)

be neglected.

In conclusion, the friction was shown to be negligible when the height of a sample was larger than its thickness. However in other geometries the friction may become dominant and the curve cannot be interpreted in terms of the stress-strain relationship of the material.

3.2.4 Construction of the curves

All the large strain tests were carried out in several passes. In order to identify the different characteristics of the deformation, it is necessary to derive an envelope to link the sequence of stress-strain curves obtained.

The first step consists in eliminating the fluctuations in the results by smoothing of the curves for the different passes. Some load fluctuations were obtained which varied between ± 0.2 MPa and ± 1 MPa around the average value (Fig. 3.8). The latter were observed both in the alloys and in the pure aluminium and at all temperatures. Thus they are unlikely to come from the Portevin-Le-Châtelier effect. However the fluctuations were not a reproducible effect and may reflect some local stick slip in the teflon tape. As the magnitude of the fluctuations was small and they did not influence the overall stress levels or hardening rates their origin was not investigated further.

After smoothing the curves, the next step was to derive the overall envelope. At room temperature, the successive curves connect with each other quite well (Fig. 3.9a). However, this is no longer true at lower temperatures. After a given test at low

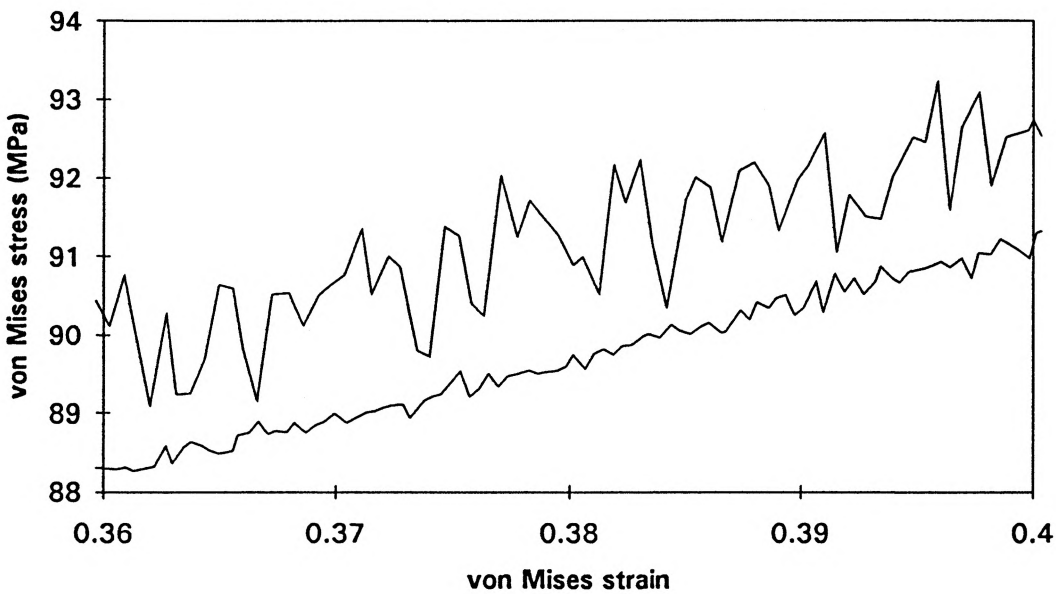

Figure 3.8/ Random fluctuations in the channel-die compression stress-strain curves for two tests of Al-0.2%Cu at room temperature

a)

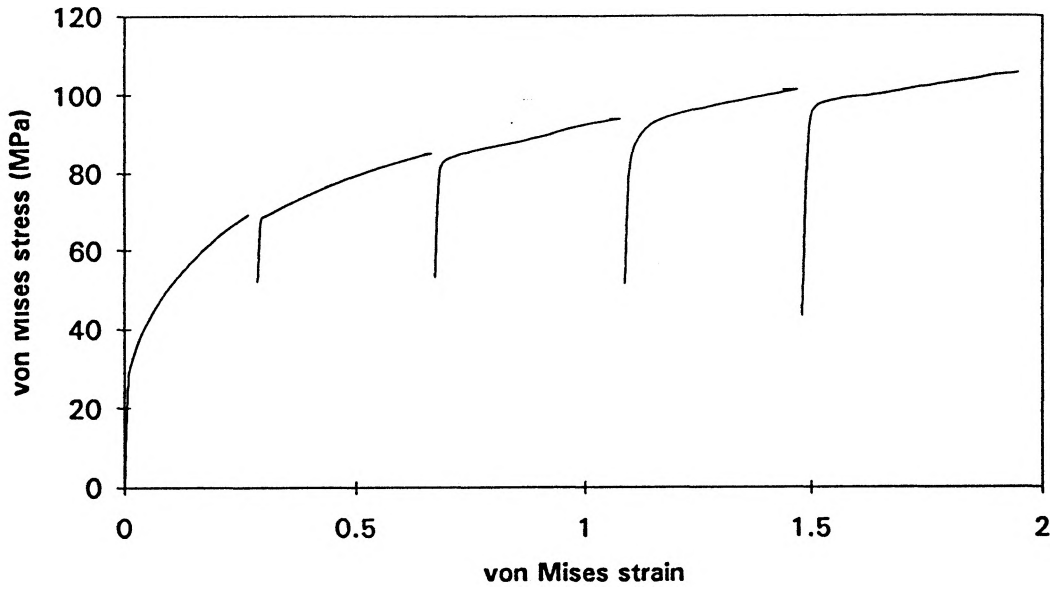

b)

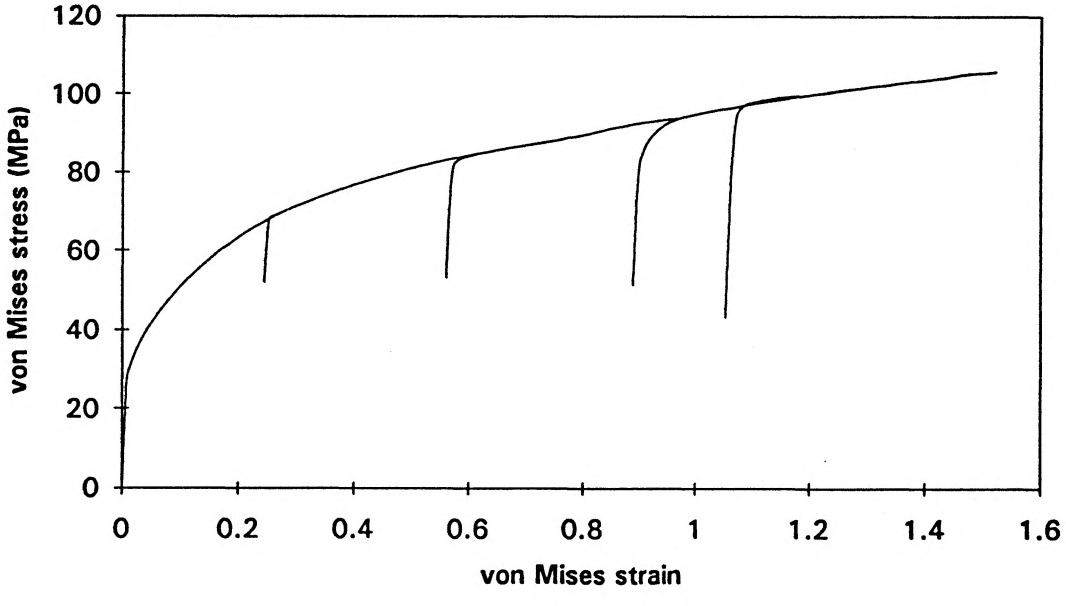

Figure 3.9/ Channel-die compression stress-strain curves for Al-0.4%Cu at room temperature a) initial b) after shifting in strain

temperature, the sample has to be warmed up to room temperature for cutting and polishing. During this time (approximately 30 min) static recovery occurs and the flow stress diminishes (Fig. 3.10a). However, it was observed that the work hardening rate versus stress curves (or θ-σ curves) were continuous (Fig. 3.10b), except for a short transition period. Mathematically this means that the stress-strain curve can become continuous by a simple shift of strain. The physical reason behind this is that the recovery process corresponds to a loss of dislocation density in the material without a major change in its substructure. The replacement of this loss of dislocation density requires an additional straining. Thus the sample then starts the next deformation step at a lower equivalent strain, but undergoes a work hardening rate consistent with the former curve (at same equivalent strain), with the exception of the transition period. We can see in Fig. 3.9b, 3.11a and 3.11b that this technique enables us to construct an envelope for the stress strain curve in each case.

This phenomenon has an important consequence : it limits the maximum strain attainable by the sample. Indeed, at low temperatures, after a certain level of stress is reached, the loss of dislocation density by static recovery during two deformation steps becomes equivalent to the gain of strain during one of these sequences. At these point, no more efficient deformation can be achieved, with the additional limitation that the height of the sample becomes rapidly lower than its thickness (see section 3.2.3).

a)

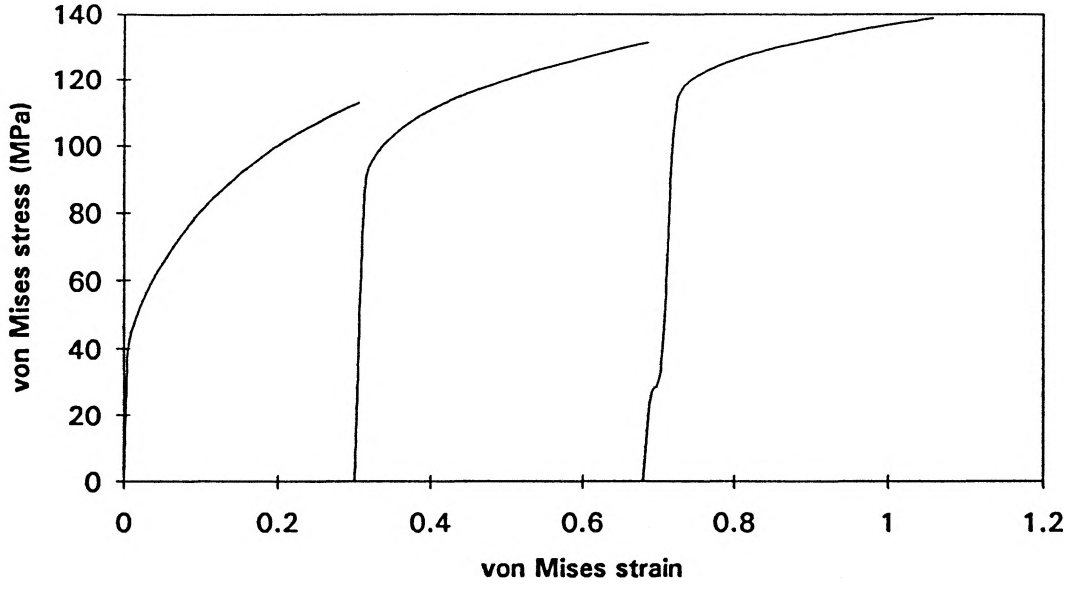

b)

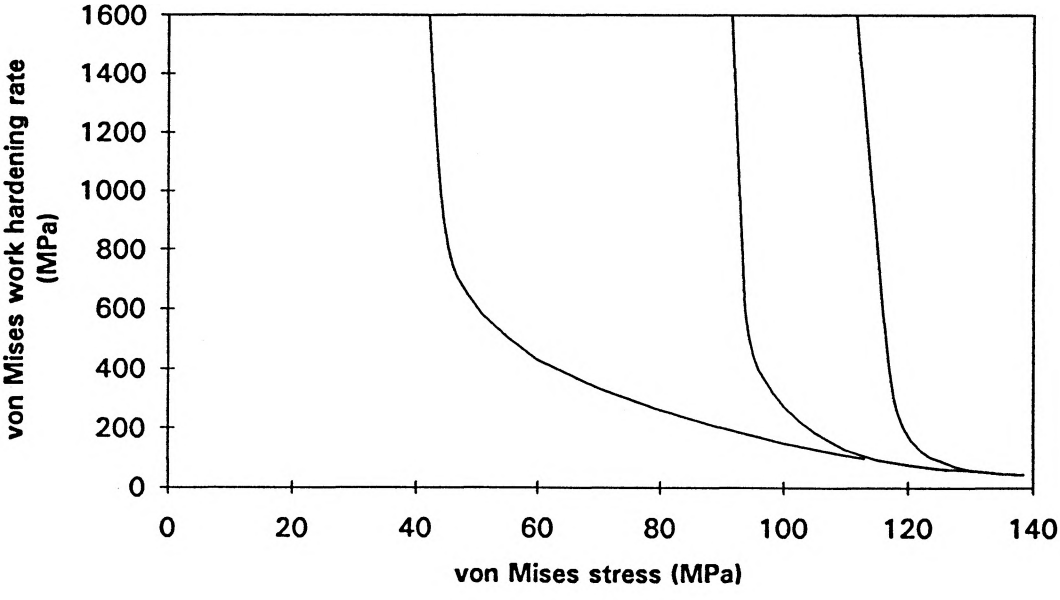

Figure 3.10/ a) Channel-die compression stress-strain curves for pure Al at 200K b) θ/σ curve calculated from a)

a)

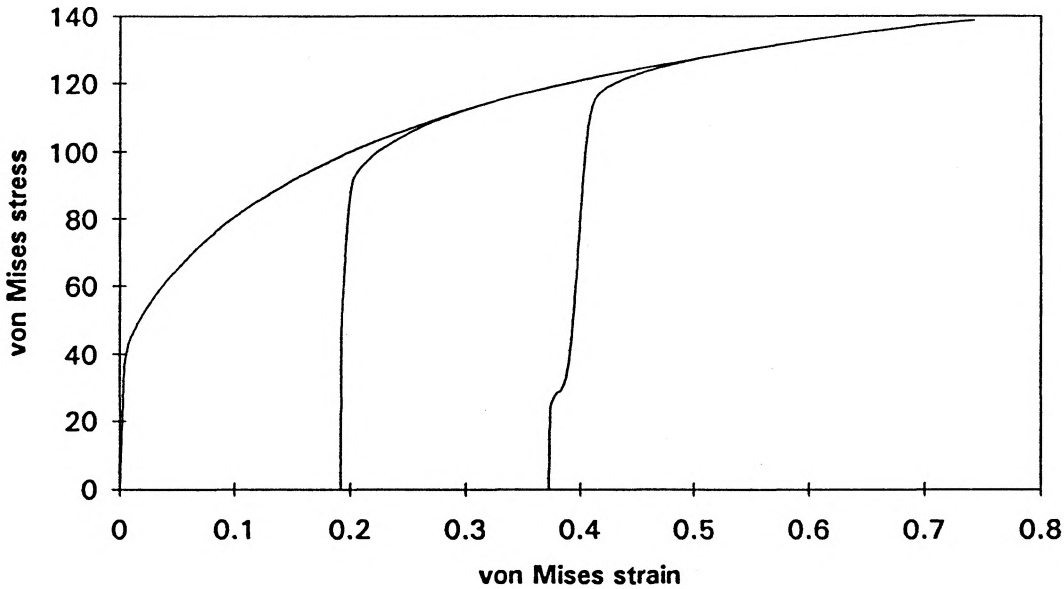

b)

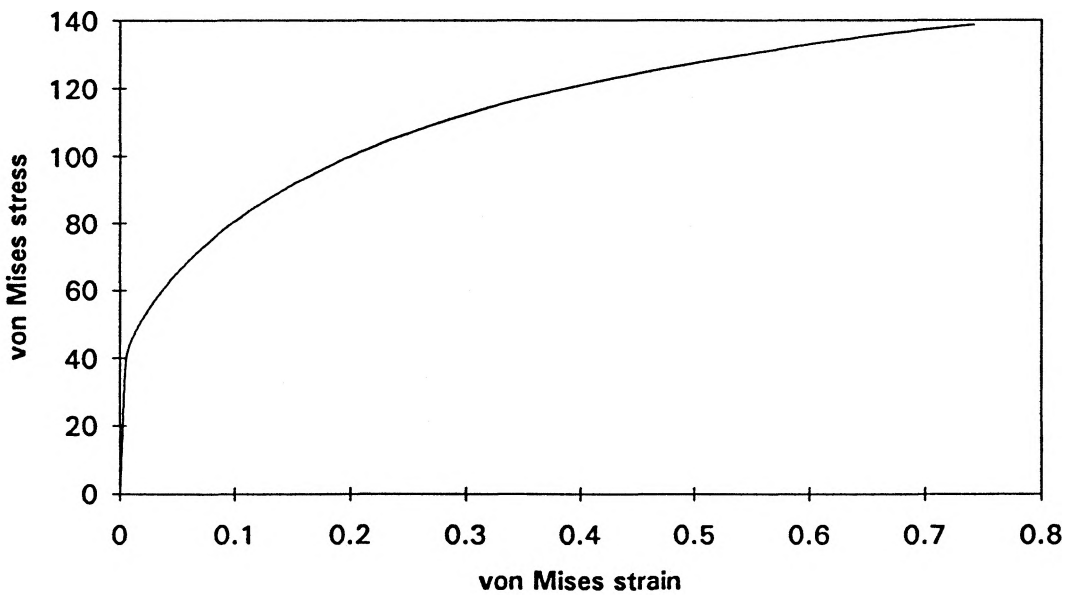

Figure 3.11/ a) Channel-die compression stress-strain curves for pure Al at 200K after shifting in strain b) the final envelope

3.2.5 Reproducibility of the results

At minimum two, and when possible, three or more samples were tested for each of the different conditions of alloying and temperature. Several examples show that the reproducibility of the results was very good both at room temperature and at lower temperatures (Fig. 3.12). This means that the careful positioning of the teflon sheets and of the grease enabled a consistent and reproducible mechanical testing procedure to be developed. Taken together with the results of the friction study, this indicates the value of the channel-die compression test as a viable procedure for the study of mechanical properties at large plastic strains.

3.2.6 Tensile tests

Tensile tests were carried out at room temperature on the three alloys for two purposes : first, to assess the mechanical properties of the alloys at low strains, which is difficult with channel die compression because of the unreliability of the data at the first few percent of strain; second, to give an additional proof of the reliability of our channel die compression results by comparison at intermediate strains (10-20%).

The grip configuration is shown in Fig. 3.13. The gauge section was 4.75 mm in diameter and the gauge length was 13 mm. The tensile tests were carried out on the same hydraulic machine that was used for channel die compression, at a strain rate of 10^{-3} s^{-1}. The load was measured by the same 100kN load cell (this time the 10 kN range was used) and the strain was measured via an extensometer. In the case of the tensile

a)

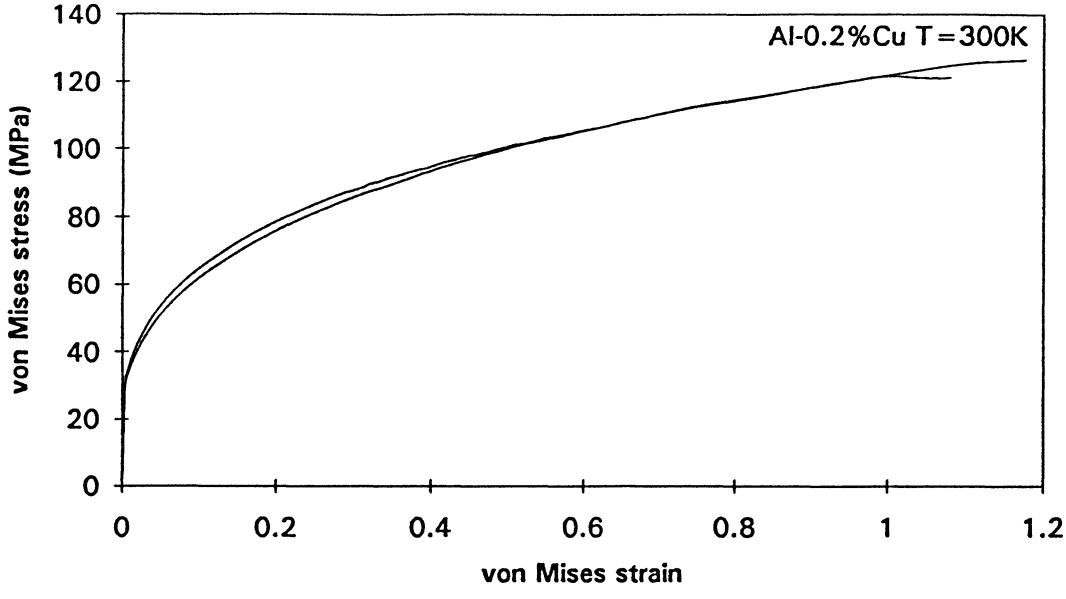

b)

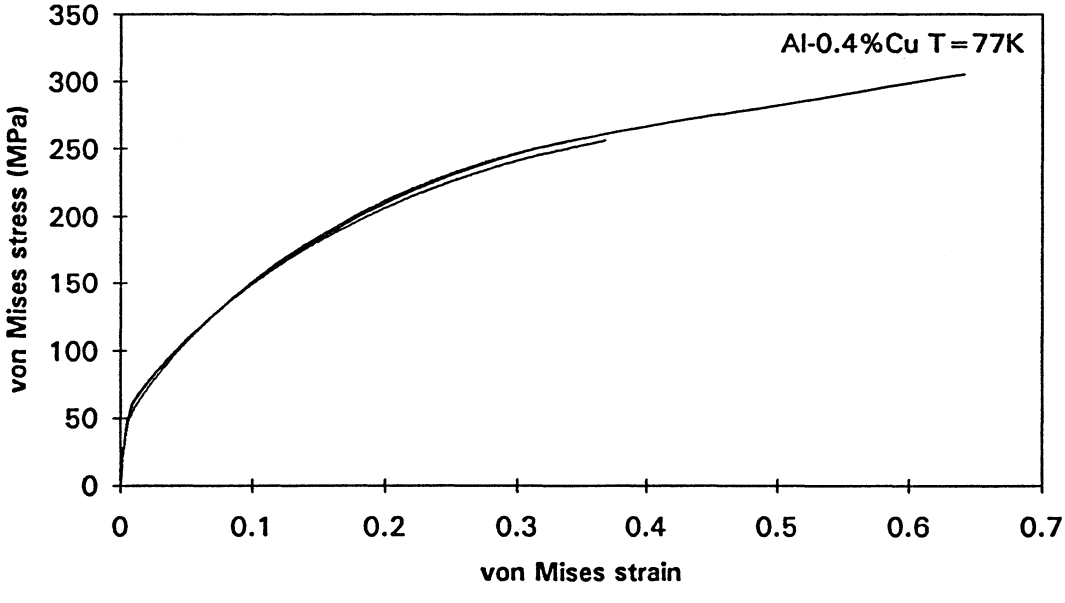

Figure 3.12/ a) Channel-die compression stress-strain curves for Al-0.2%Cu at room temperature showing good reproducibility b) Channel-die compression stress-strain curves for Al-0.4%Cu at 77K showing good reproducibility

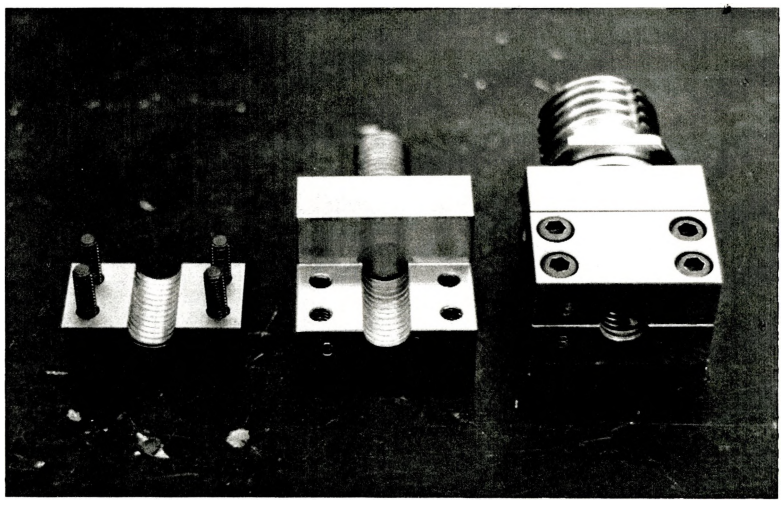

Figure 3.13/ Grip configuration for the MTS tensile tests

test, true stress/true strain and von Mises stress/von Mises strain are equivalent.

The comparison between the tensile and channel die compression von Mises stress-strain curves can be seen in Fig. 3.14 (pure Aluminium), Fig. 3.15 (Al-0.2%Cu) and Fig. 3.16 (Al-0.4%Cu). As expected, the curves are significantly different at low strains : in channel die compression the samples undergo a long elastic-plastic transition which is not present in the tensile case. After this transition period, the two curves are remarkably similar, both in terms of work hardening rate and level of stress. Such similarities of behaviour between channel die compression and tensile tests have previously been observed in Aluminium alloys (Kocks et al., 1988).

A second series of tensile tests was carried out on an other apparatus which enabled tensile testing to be conducted at low temperatures. The gauge section for these tests was 2.5 mm and the gauge length 16 mm. Tensile tests were carried out on the pure Aluminium used in this study, at ambient temperature and liquid Nitrogen temperature. The deformation was measured by the displacement of the cross-head and the load by a high precision load cell. Fig. 3.14 and 3.17 show the comparison between the von Mises stress-strain curves obtained by channel-die compression tests and these tensile tests, at ambient temperature and liquid Nitrogen temperature respectively. The tensile test stress levels are clearly much lower. This is an interesting observation and is related to the number of grains in the specimen cross-section as outlined in the discussion section.

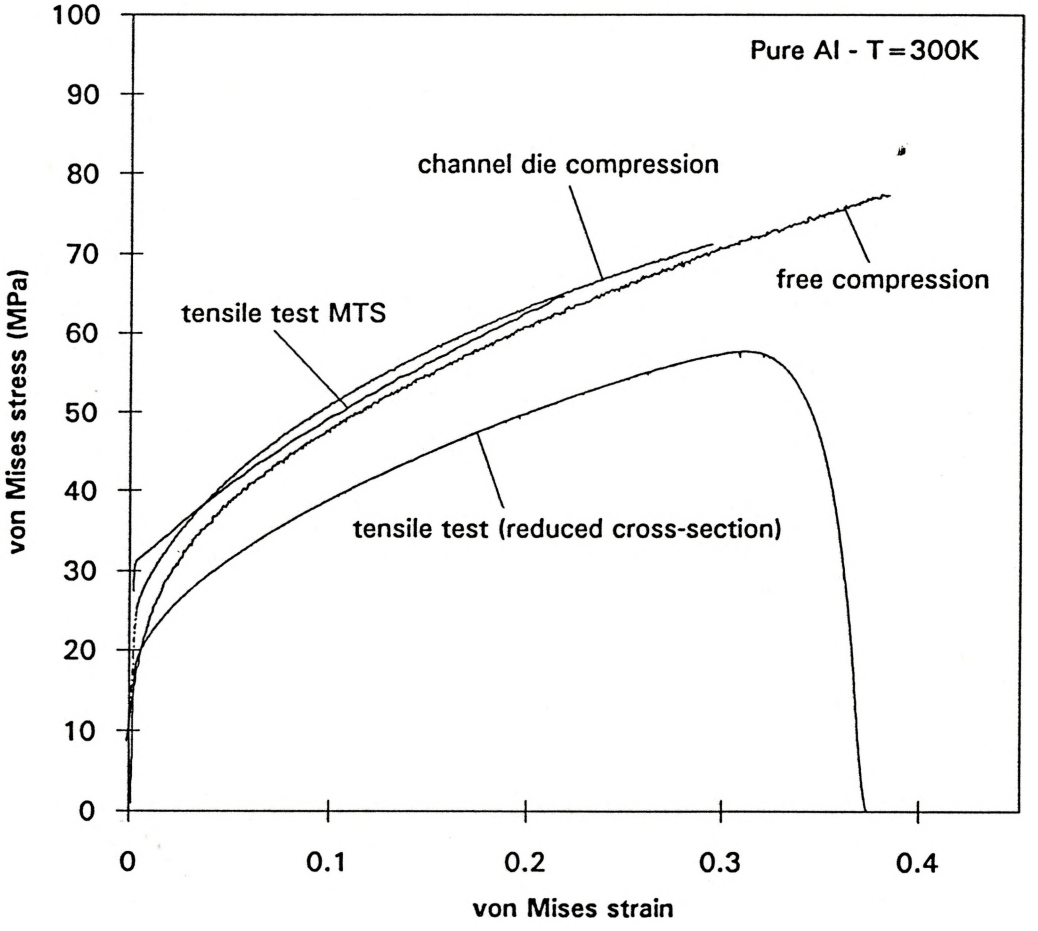

Figure 3.14/ Comparison between a channel-die compression test, a tensile test on the MTS testing machine, a tensile test with reduced cross-section and a free compression test for pure Al at room temperature

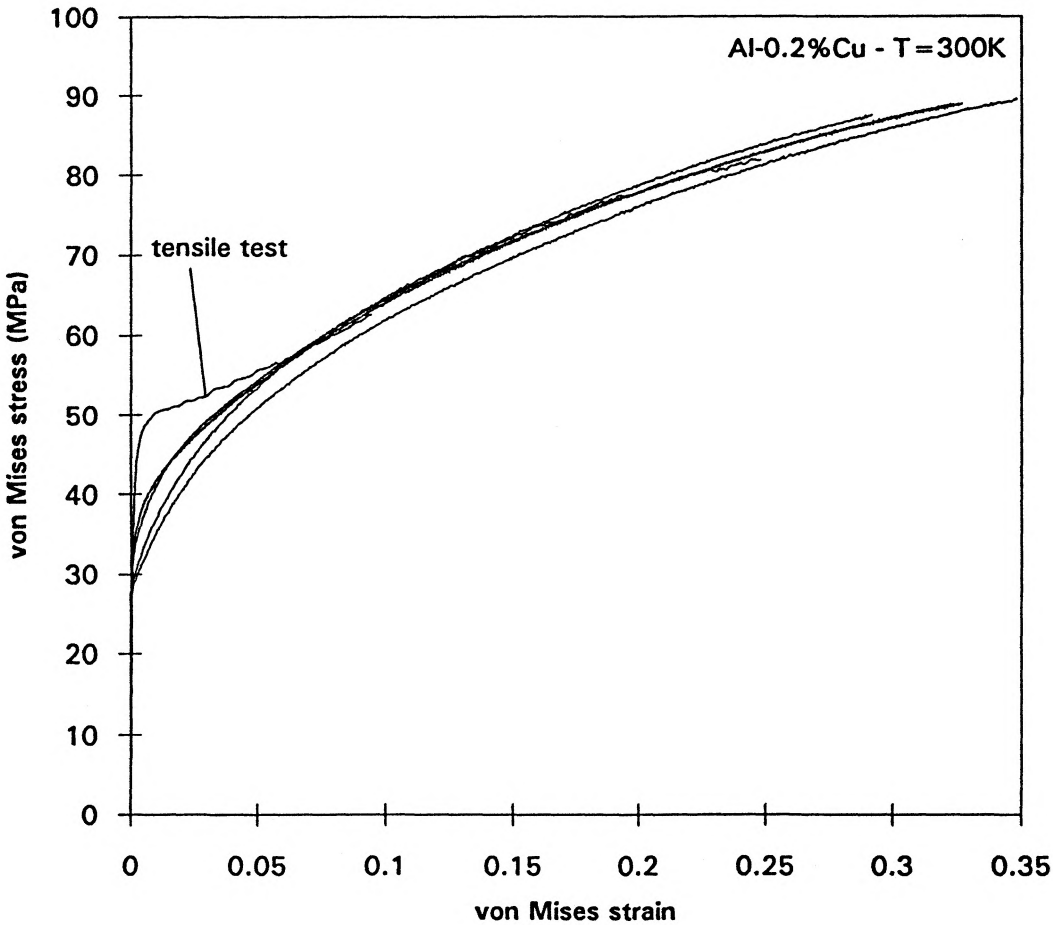

Figure 3.15/ Comparison between several channel-die compression tests and a tensile test on the MTS testing machine for Al-0.2%Cu at room temperature

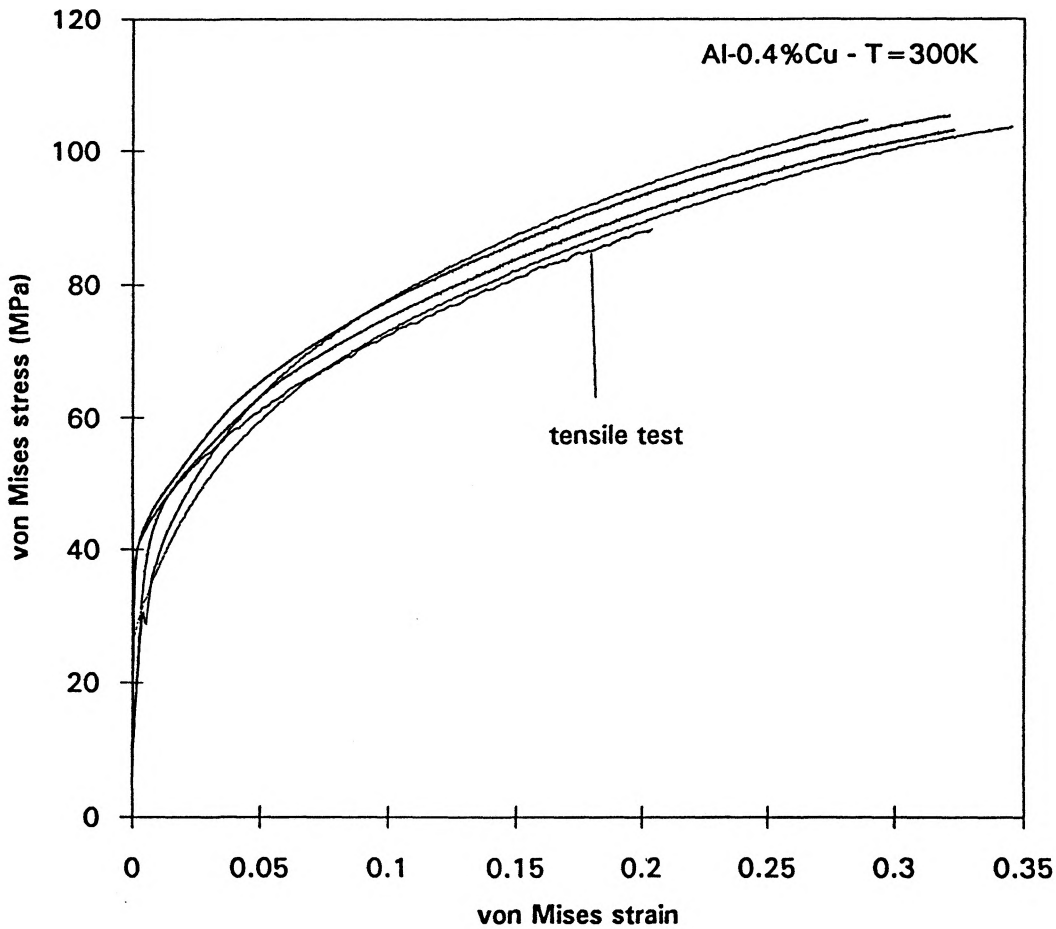

Figure 3.16/ Comparison between several channel-die compression tests and a tensile test on the MTS testing machine for Al-0.4%Cu at room temperature

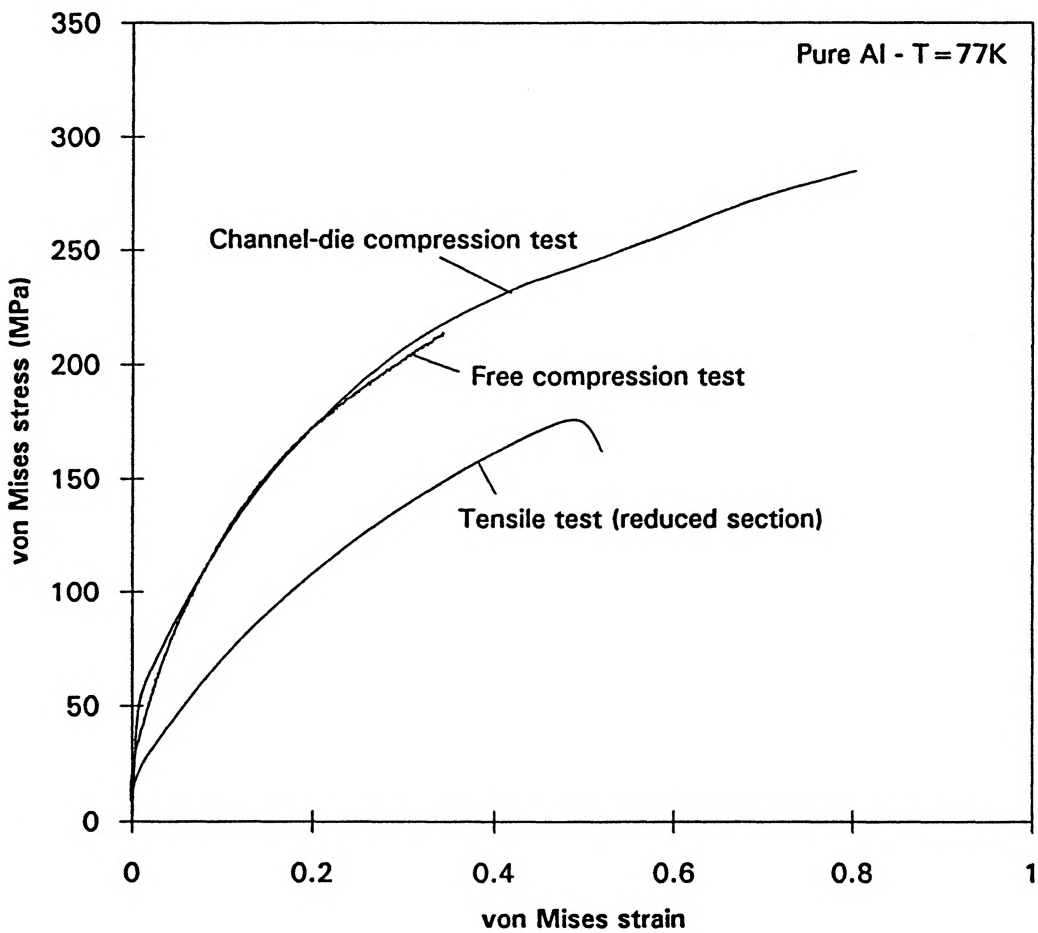

Figure 3.17/ Comparison between a channel-die compression test, a free compression test and a tensile test with reduced cross-section for pure Al at 77K

3.2.7/ Free compression tests

Free compression tests were carried out as a further assessment of the validity of the channel-die results at room temperature and liquid nitrogen temperature. Teflon tape spread with molybdenum disulfide grease was placed on the bottom and top surfaces of the sample for lubrication. Fig. 3.14 and 3.17 show the stress-strain curves obtained by channel-die compression and free compression of pure Aluminium at 300K and 77K. We can see that the agreement is very good, apart from the initial portion of the curve.

3.2.8/ Stress-strain curves for large strain deformation by channel-die compression

3.2.8.1/ Influence of alloying at constant temperature

Fig. 3.18, 3.19 and 3.20 show for each alloy the stress-strain curves at the different testing temperatures.

For all three temperatures the influence of solid solution is very important. The final flow stress differences are most important at room temperature, and can reach 50 MPa. This is quite considerable when considered that the maximum addition of Copper is 0.4wt%. Even though the low strains part of the curve is unreliable, it can be noticed that the increase in yield stress due to the solute atoms is very small in comparison to the final increase in flow stress. In other words, the major component of the flow stress increase is due to a change in the work hardening behaviour with solute content rather than solution hardening at the yield point. This final increase in flow stress with solute

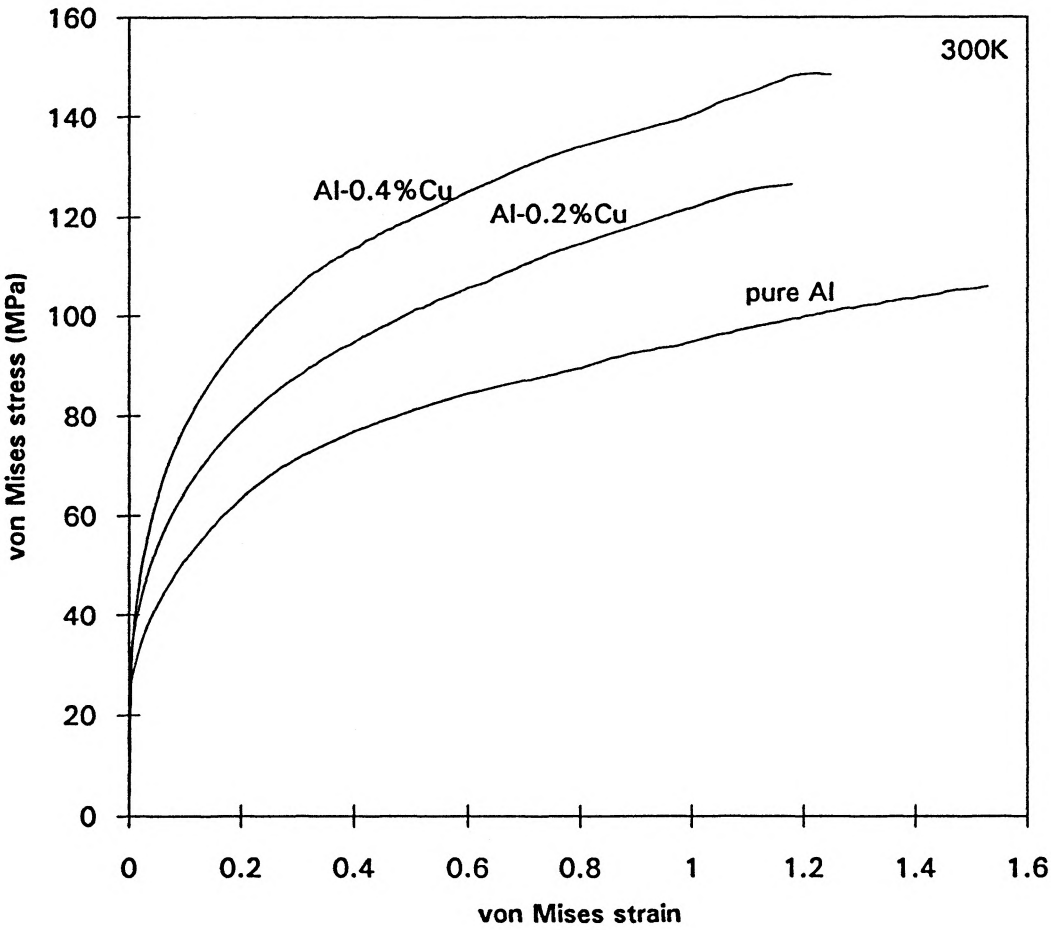

Figure 3.18/ Channel-die compression stress-strain curves for pure Al, Al-0.2%Cu and Al-0.4%Cu at room temperature

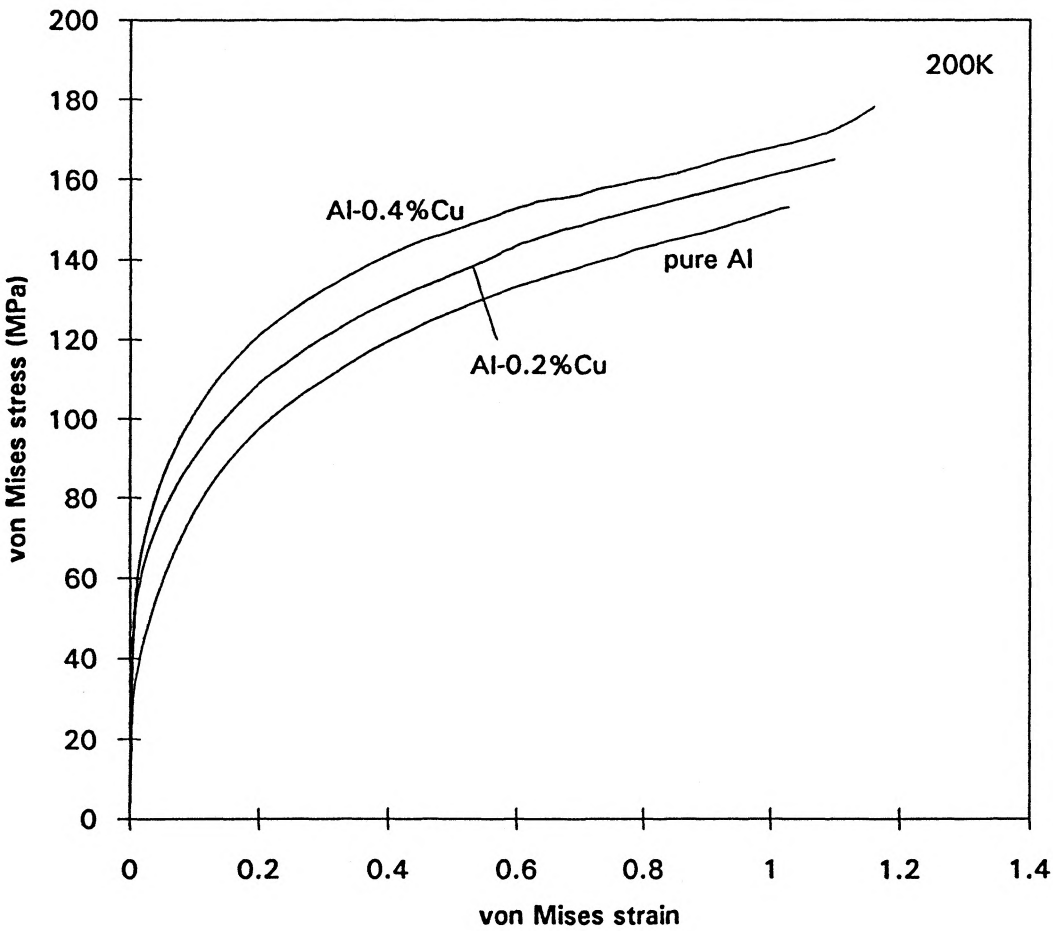

Figure 3.19/ Channel-die compression stress-strain curves for pure Al, Al-0.2%Cu and Al-0.4%Cu at 200K

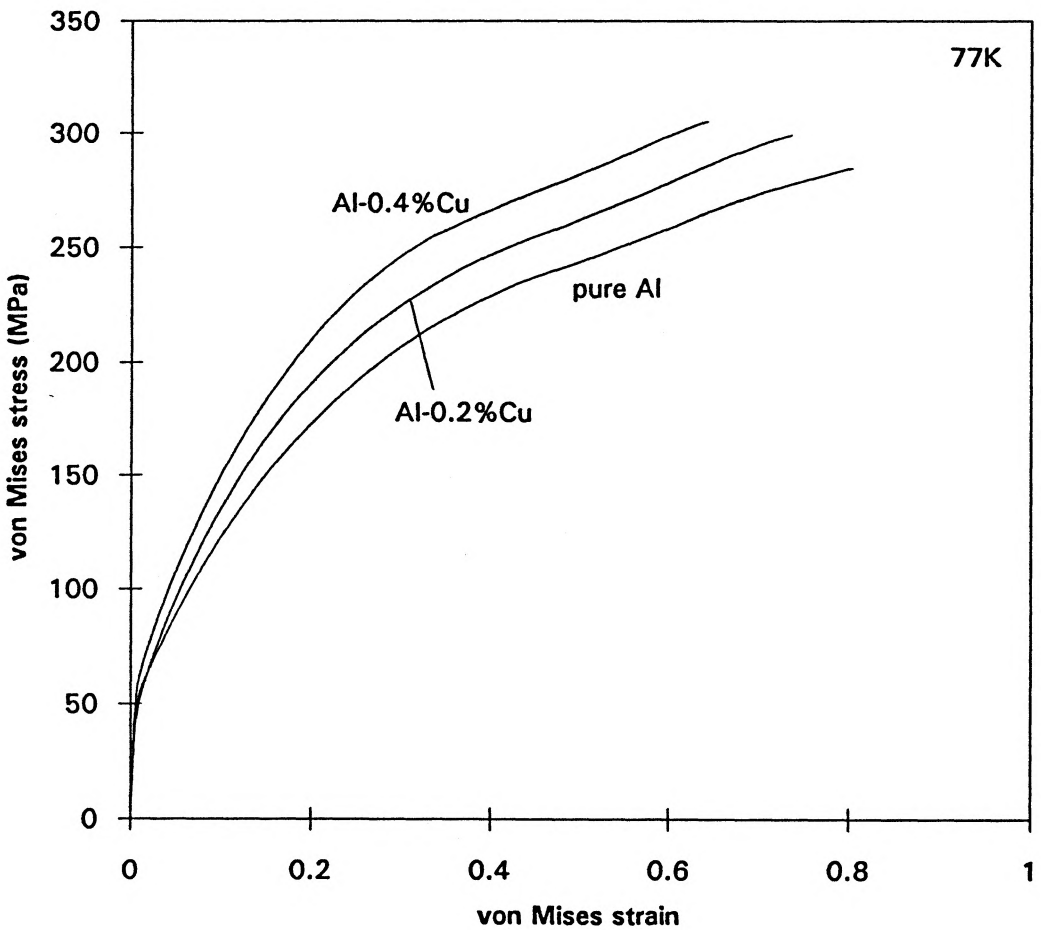

Figure 3.20/ Channel-die compression stress-strain curves for pure Al, Al-0.2%Cu and Al-0.4%Cu at 77K

content is clearly different at each temperature : as the temperature decreases, so does the increase in stress.

Stage IV of work hardening can be consistently observed at every temperature and every solute content: when the deformation reaches large strains, the stress-strain curves experience a stage of sustained low-level work hardening until the highest level of strain. At each temperature this work hardening level is the same for each of the alloys.

3.2.8.2/ Influence of temperature at constant alloying

Fig. 3.21, 3.22 and 3.23 show for each testing temperature the stress-strain curves of the three alloys.

It can be seen that temperature influences both the initial yield stress and the hardening rate: the level of flow stress obtained after strains over 1 is of the order of magnitude of 100 MPa at room temperature, and reaches 300 MPa at liquid Nitrogen temperature. Most of this difference, again, arises from the deformation. In the case of room temperature, the work hardening rate rapidly decays with increasing strain, whereas at liquid Nitrogen the work hardening rate is substantial until relatively high strains.

3.2.9/ Work hardening rate vs. stress diagrams

The work hardening rate vs. stress diagrams were obtained from the initial stress-strain curves: the initial stress-strain curves included approximately 2 to 3000 points, and

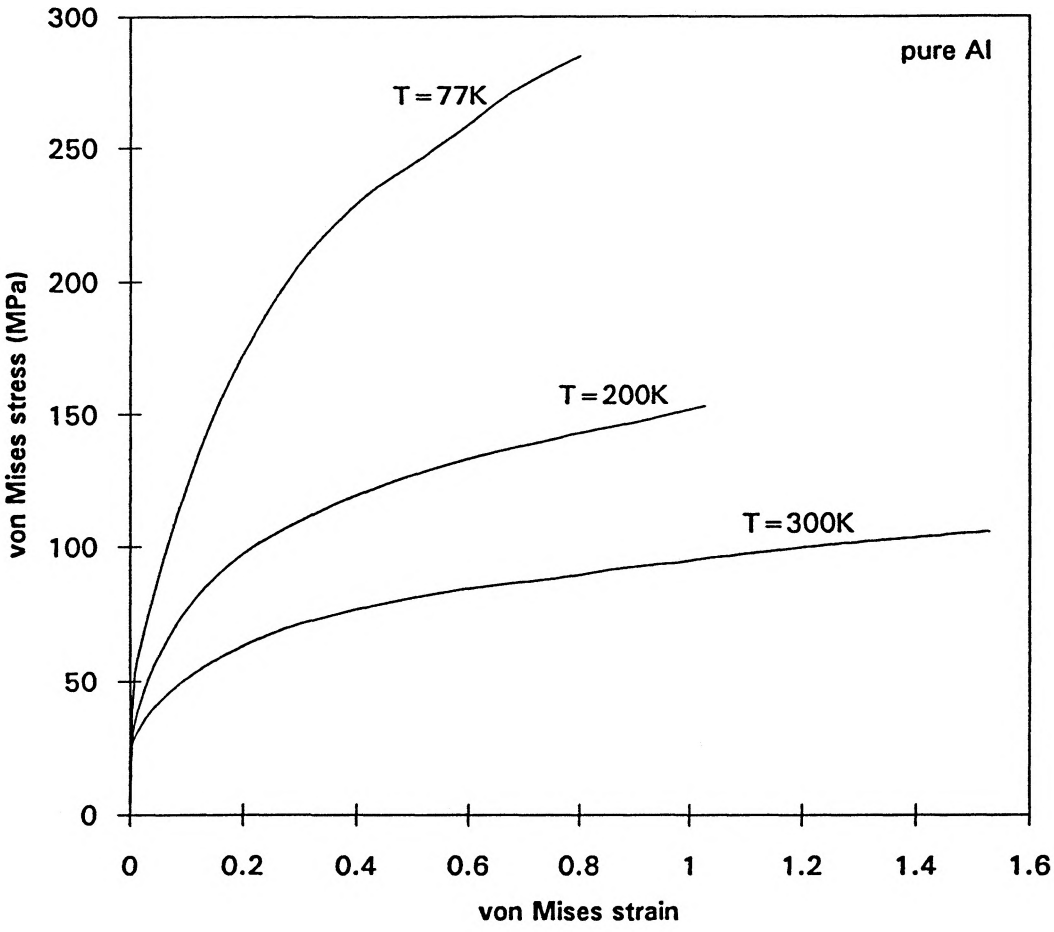

Figure 3.21/ Channel-die compression stress-strain curves for pure Al at 300K, 200K and 77K

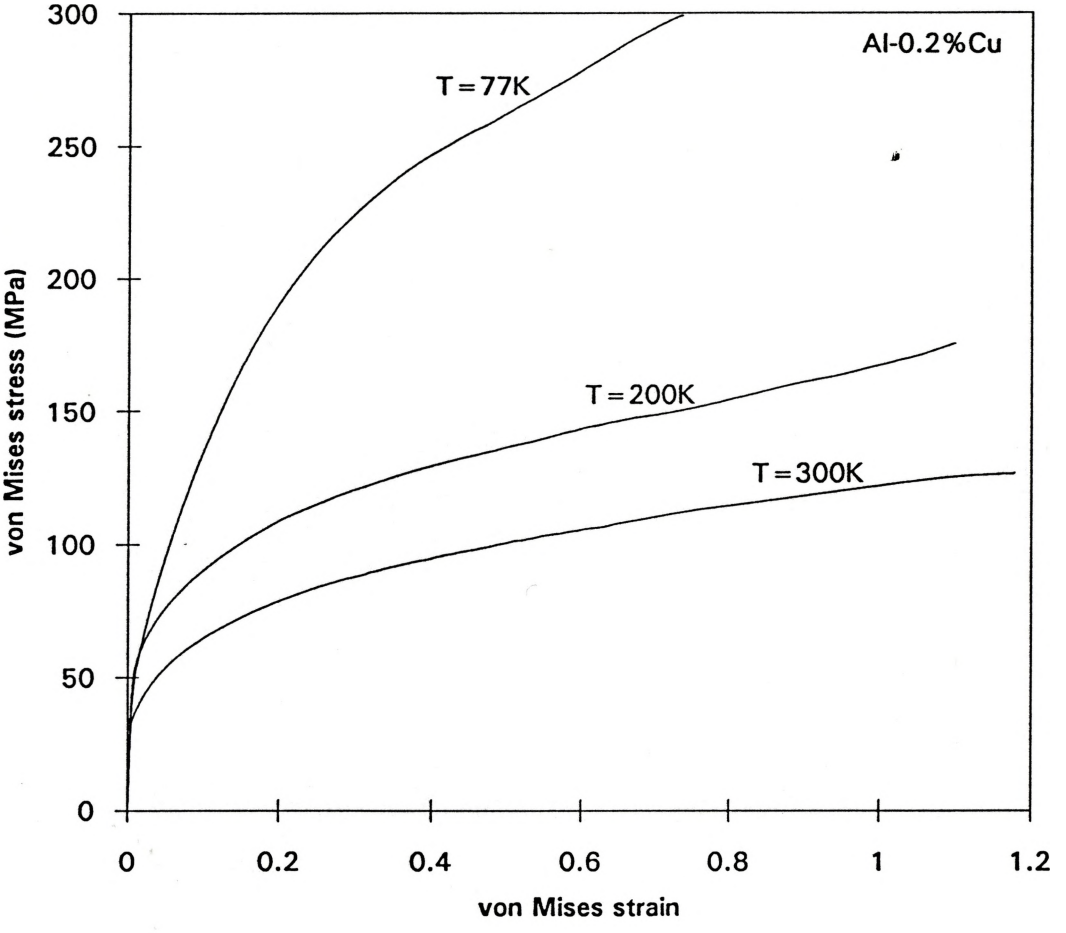

Figure 3.22/ Channel-die compression stress-strain curves for Al-0.2%Cu at 300K, 200K and 77K

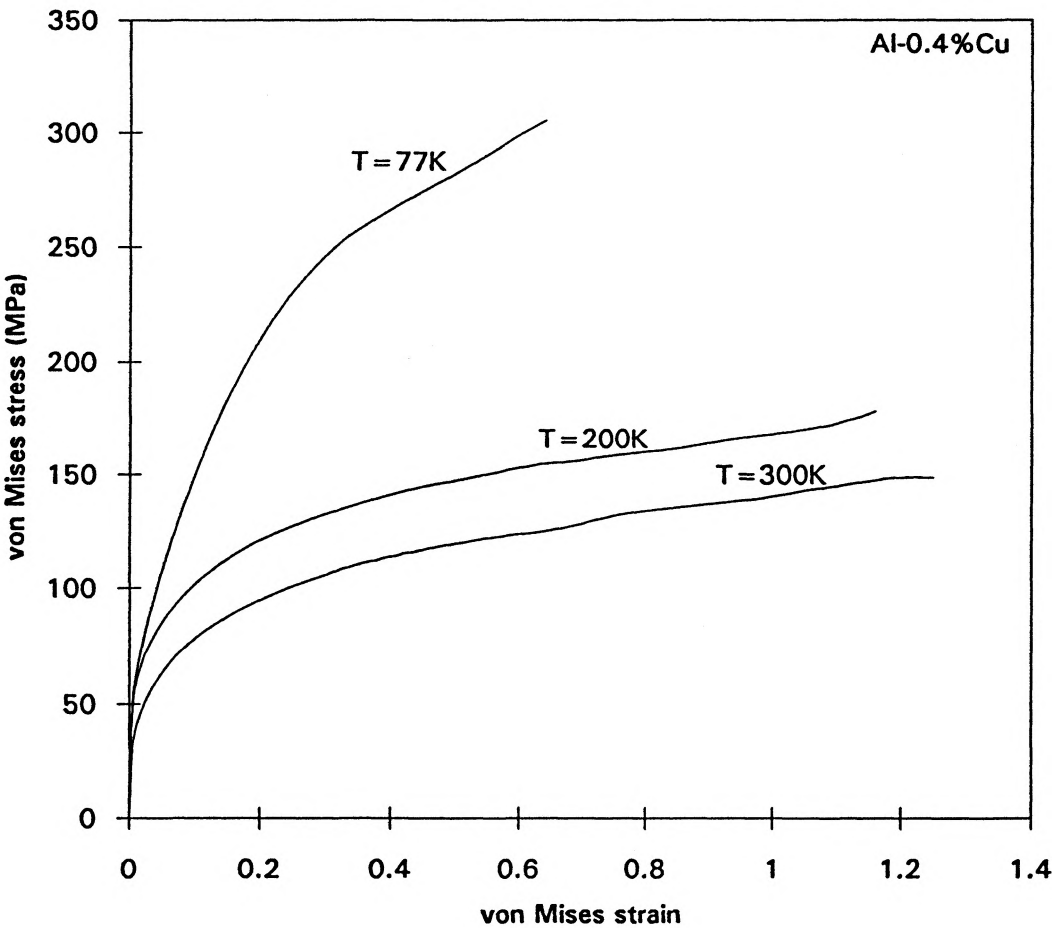

Figure 3.23/ Channel-die compression stress-strain curves for Al-0.4%Cu at 300K, 200K and 77K

the slope was calculated on the average of 20 points. The θ_{vm}/σ_{vm} curves were then smoothed. Finally both the stress and work hardening rate were normalized by the temperature-dependant shear modulus G. Values for G were obtained from Sutton (1953).

3.2.9.1/ Influence of alloying at constant temperature

Fig. 3.24, 3.25 and 3.26 show for each alloy the shear work hardening rate θ versus shear stress τ diagrams at the different temperatures.

At constant temperature, it can be seen that the addition of alloy increases the level of stress at which a given level of work hardening occurs. However, at large strains this influence vanishes, and stage IV work hardening rate is independent from the solute content.

3.2.9.2/ Influence of temperature at constant alloying

Fig. 3.27, 3.28 and 3.29 show for each testing temperature the shear work hardening rate θ versus shear stress τ diagrams at the different temperatures.

The shapes of these diagrams are drastically different from one temperature to another. At liquid nitrogen temperature the plot is first essentially linear. A very sharp transition leads to an almost constant stage IV where the work hardening rate is of the order of 10^{-3} G. At higher temperatures, however, the work hardening rate decreases very quickly with increasing stress, and the θ/τ curve is markedly concave. Stage IV is still observed at 200K and 300K, although not separated from the early part of the curve by a sharp transition. Stage IV work hardening rate is of the order of 2.10^{-4} G at 300K and 3.10^{-4} G at 200K.

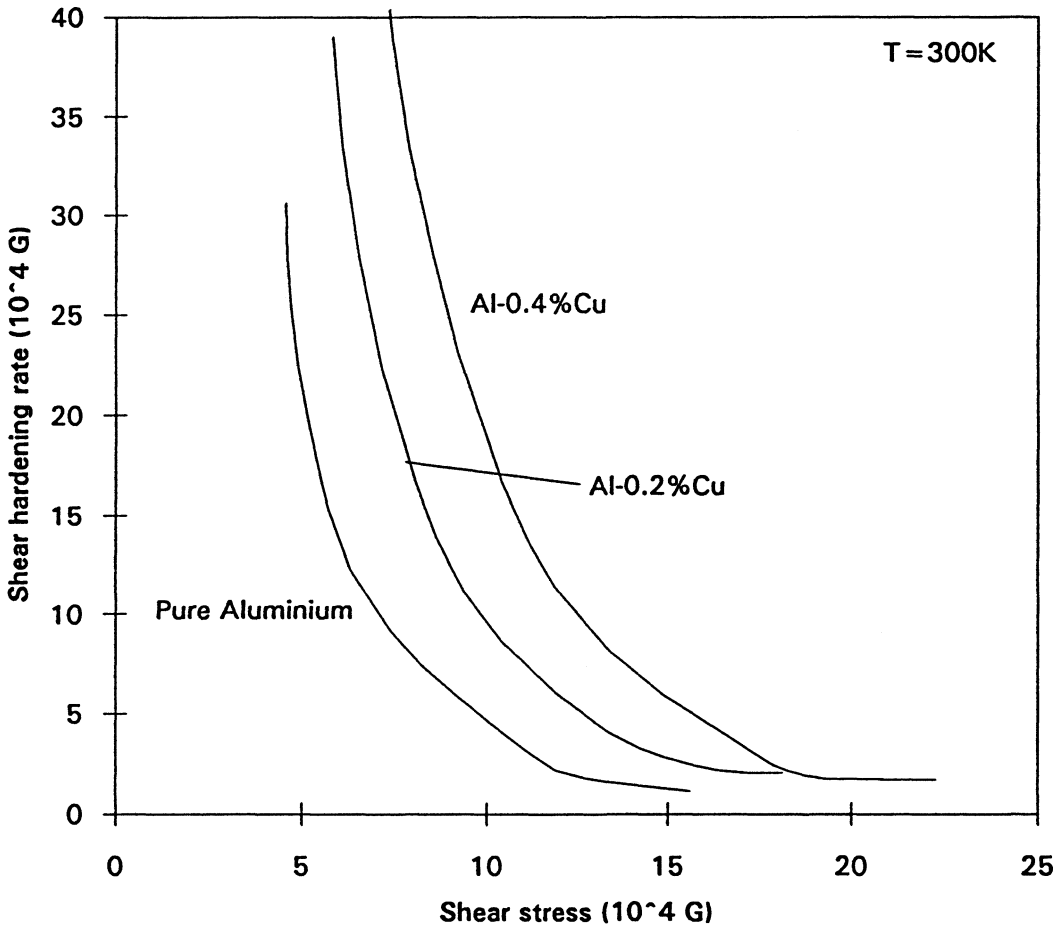

Figure 3.24/ Work hardening rate vs. stress curves for pure Al, Al-0.2%Cu and Al-0.4%Cu at room temperature

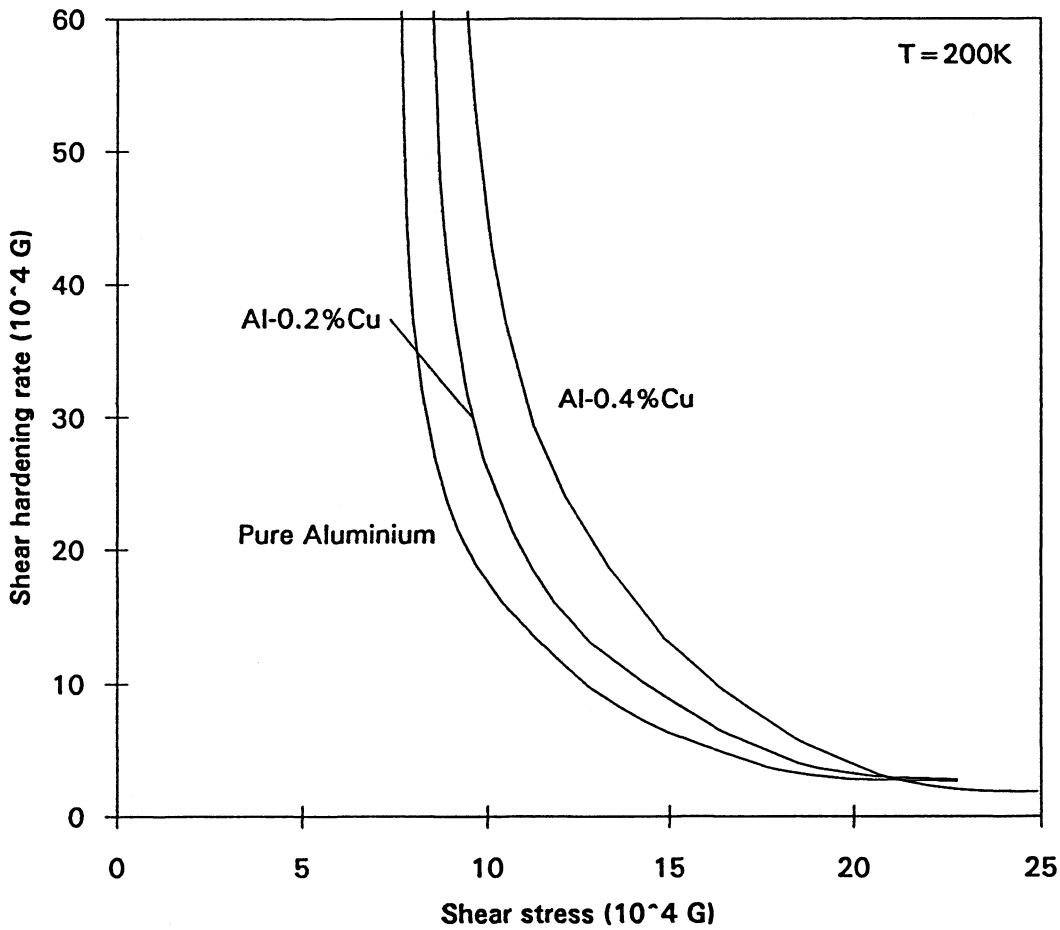

Figure 3.25/ Work hardening rate vs. stress curves for pure Al, Al-0.2%Cu and Al-0.4%Cu at 200K

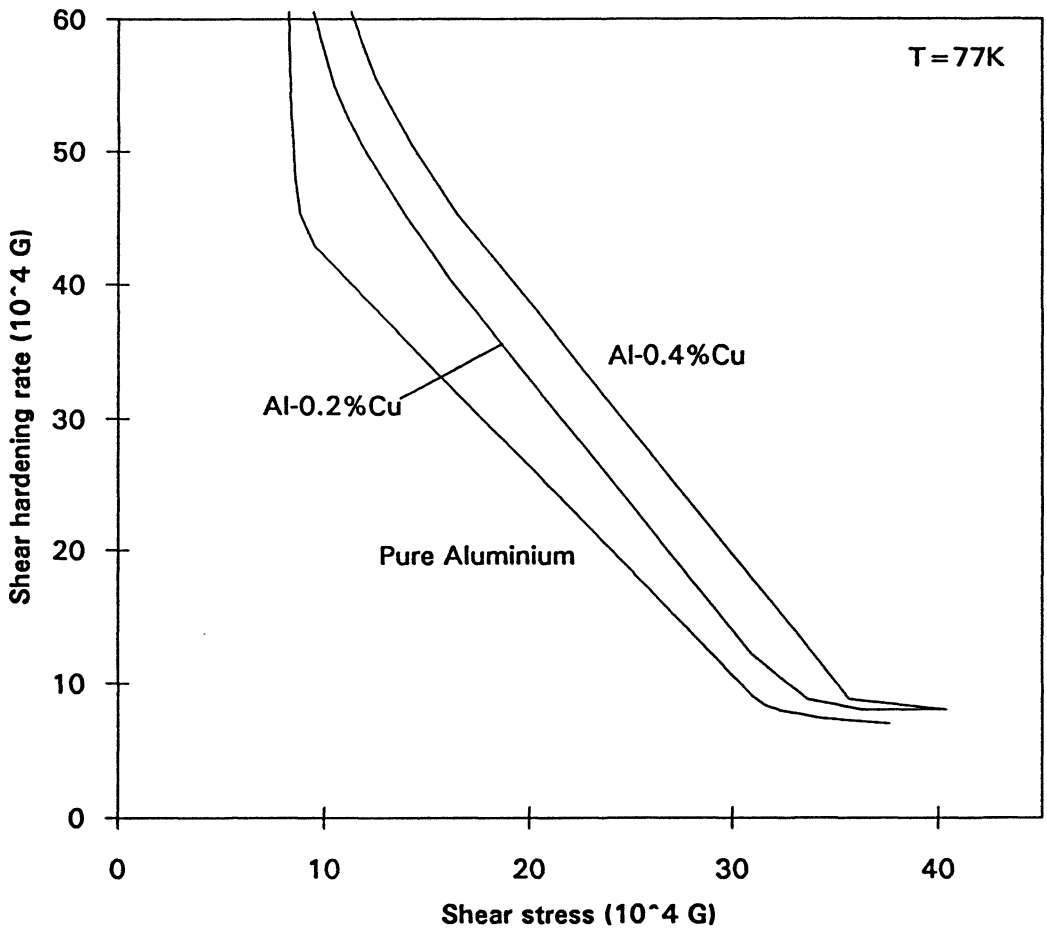

Figure 3.26/ Work hardening rate vs. stress curves for pure Al, Al-0.2%Cu and Al-0.4%Cu at 77K

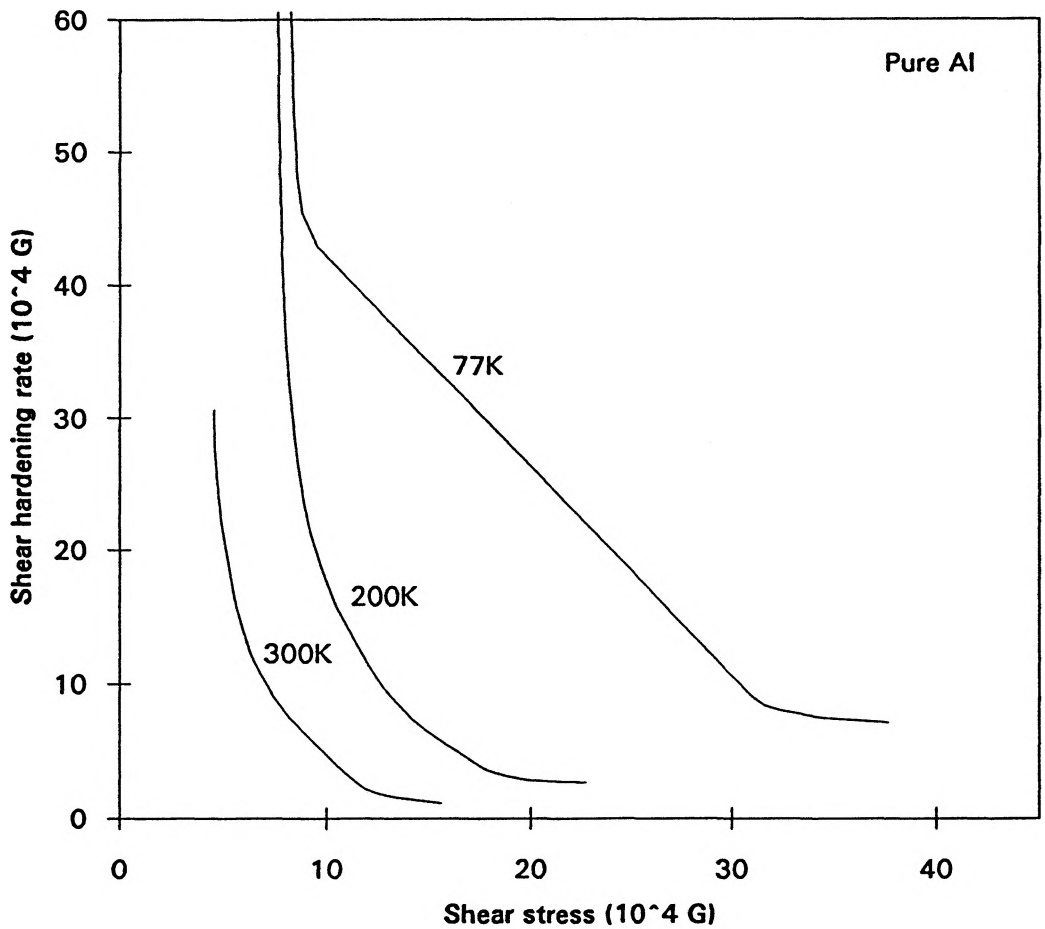

Figure 3.27/ Work hardening rate vs. stress curves for pure Al at 300K, 200K and 77K

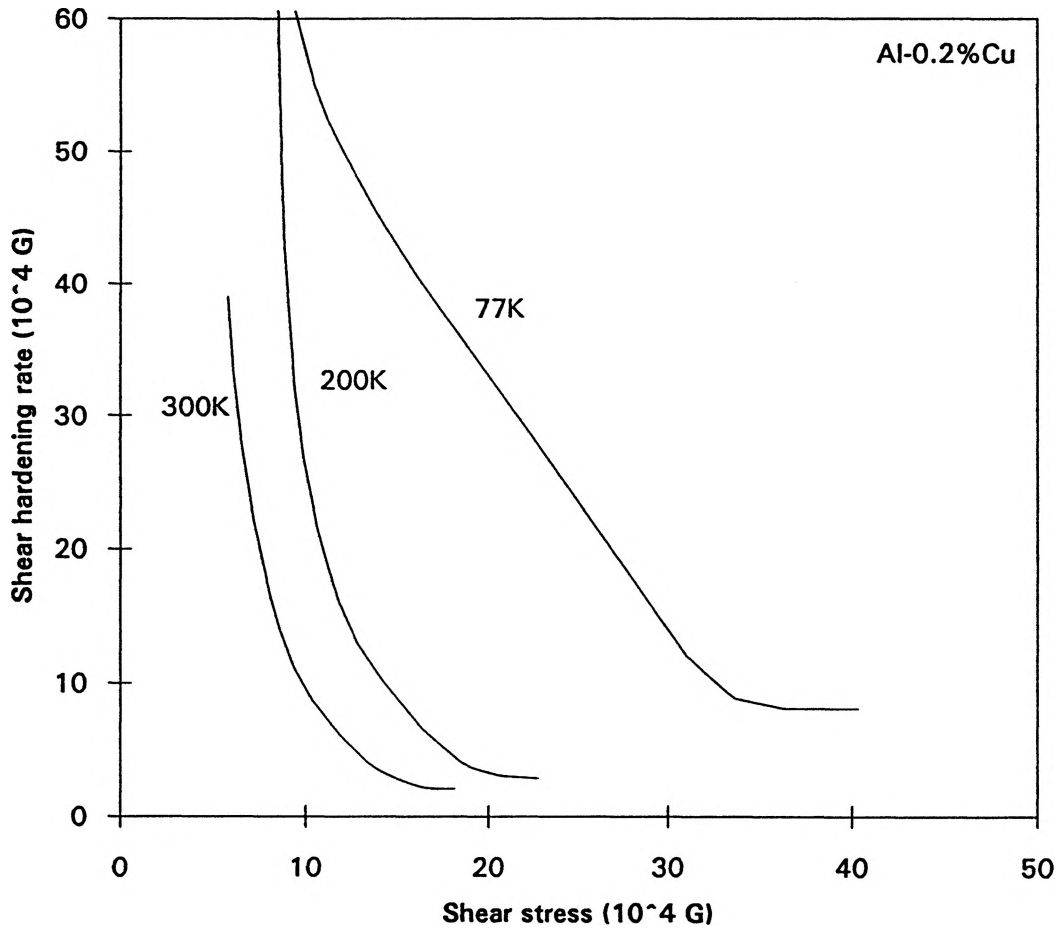

Figure 3.28/ Work hardening rate vs. stress curves for Al-0.2%Cu at 300K, 200K and 77K

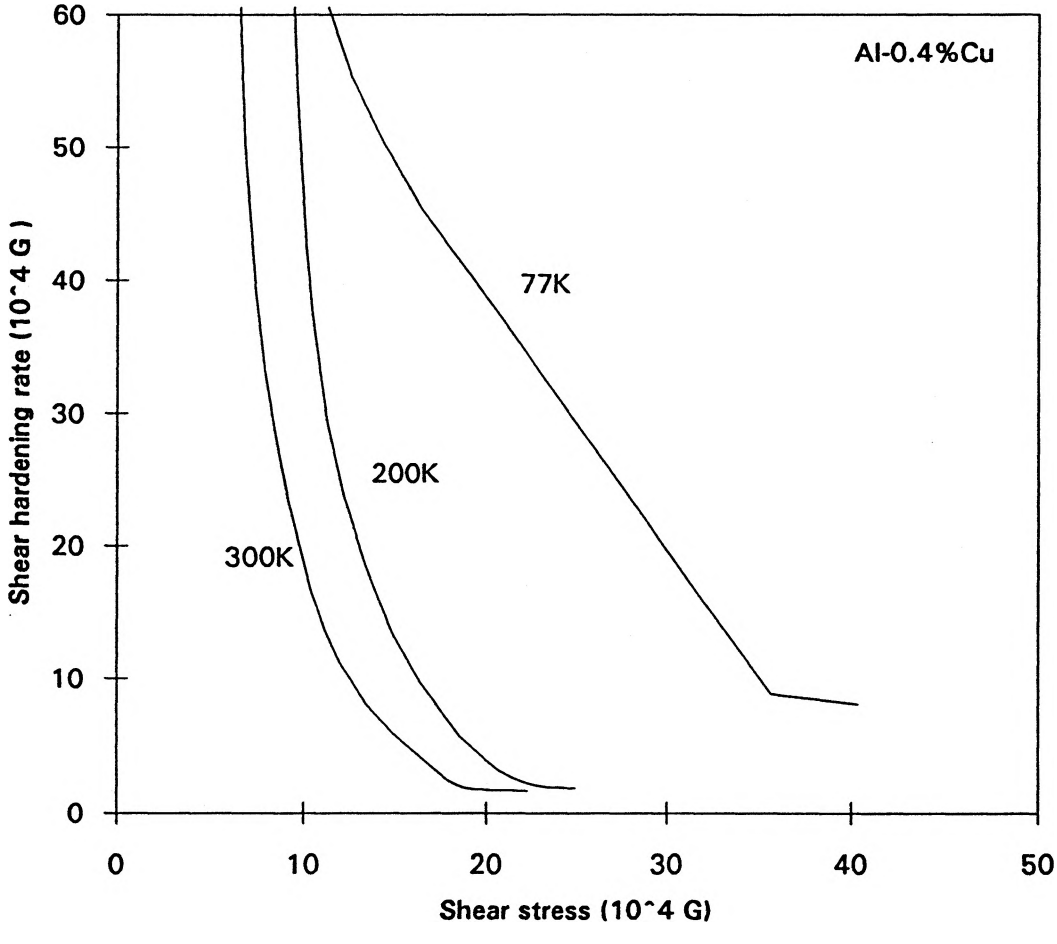

Figure 3.29/ Work hardening rate vs. stress curves for Al-0.4%Cu at 300K, 200K and 77K

3.3/ STRUCTURAL STUDIES

The purpose of the structural studies was to provide a general view of the evolution of the structure from the microscopic scale to the macroscopic scale that could be used as an input in the constitutive equations of the materials. This was achieved by investigating the material by various techniques: a slip line study by Nomarski contrast in the optical microscope, X-rays global texture analysis, local texture analysis by Backscattered Electron Kikuchi Patterns in the SEM, and TEM observations.

3.3.1/ The occurrence of shear bands

First of all, it is necessary to determine the extent at which inhomogeneous deformation occurs. This can qualitatively be achieved by looking at the sample surfaces after mechanical testing. Fig. 3.30 shows the specimen geometry and surface after 0.3 and 1.4 of true strain on the Al-0.4%Cu at room temperature. It appears that until strains of around 30% the deformation is quite homogeneous. However, when further deformation is imposed, inhomogeneous deformation occurs more extensively, and the geometry of the sample becomes less ideal. Fig. 3.31 shows an optical micrograph montage of the anodized lateral face of an Al-0.4%Cu sample deformed 100% at room temperature. Significant grains aspect ratios differences show that some regions have undergone extensive localization of shear.

In order to assess quantitatively the extent of inhomogeneous deformation, the

a)

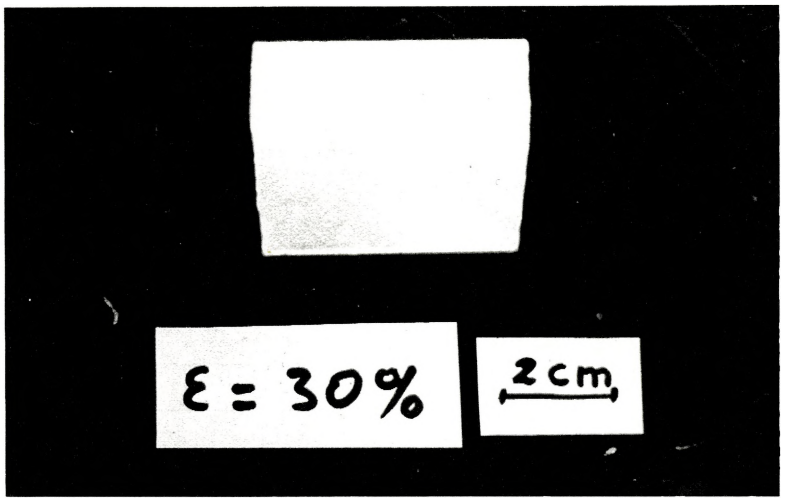

b)

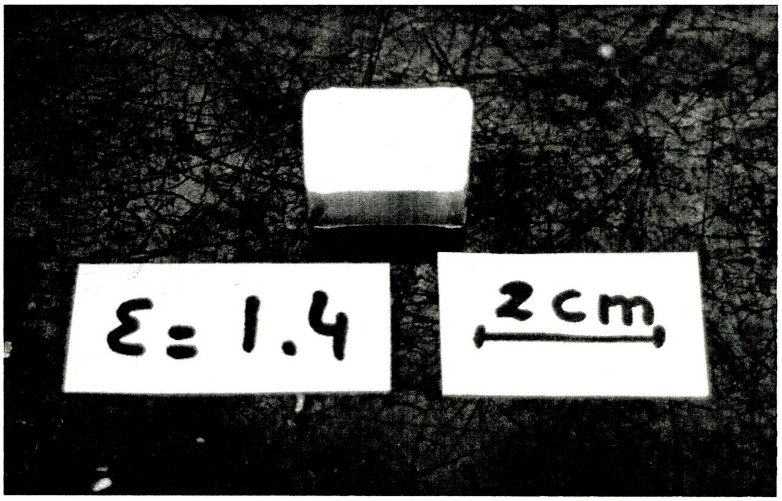

Figure 3.30/ Specimen geometry a) after 30% deformation b) after 140% deformation

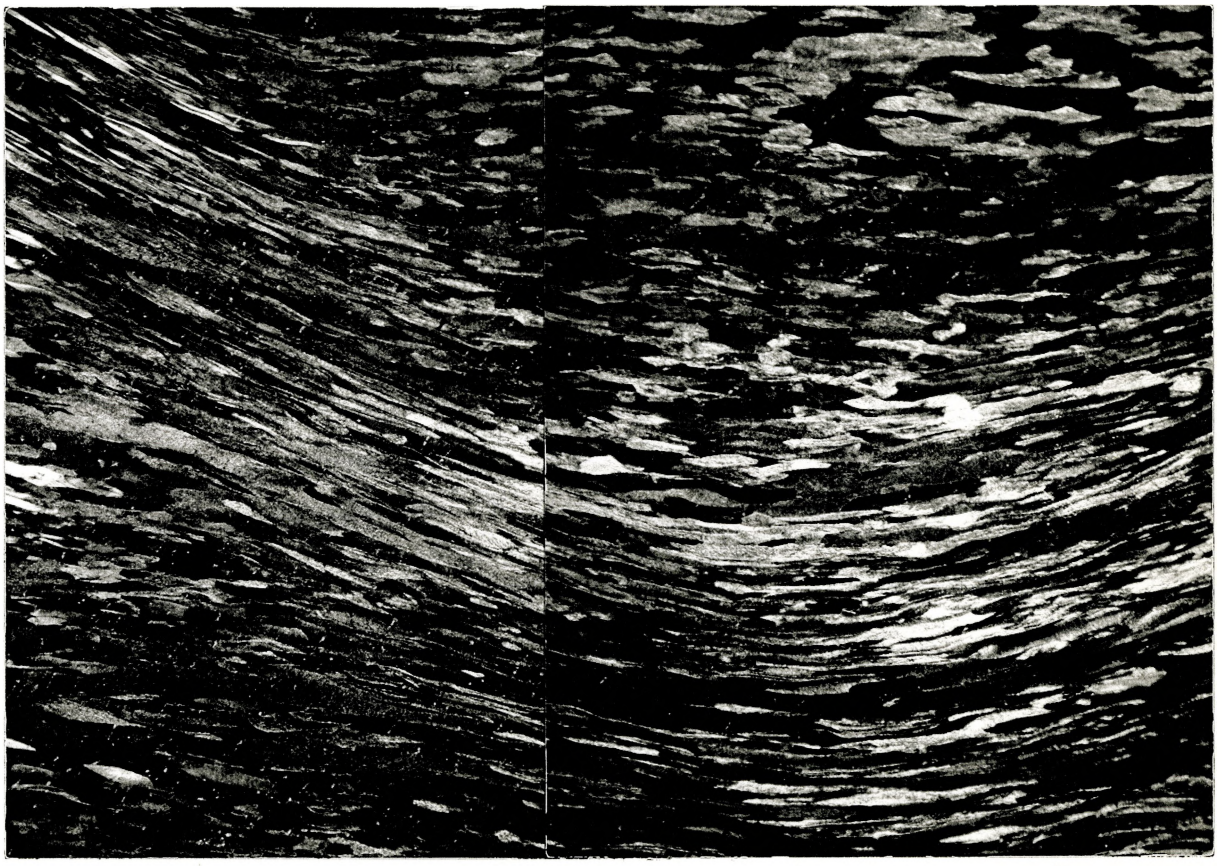

Figure 3.31/ Optical micrograph after anodization of the lateral face of an Al-0.4%Cu sample deformed 100% at room temperature

sample deformed to a true strain of 1 was cut parallel to the constrained surface and its Vickers hardness was measured at regularly spaced intervals, making a grid of 5 x 8. The results are summarized in Fig. 3.32. We can observe two peaks, one around H=45, and one around H=52, corresponding to the regions including no shear bands and shear bands, respectively.

3.3.2/ Slip lines study

The study of the orientation and the degree of localization of the slip lines is a useful tool to determine the angular relationships between the shear bands and the flow direction, and the mechanisms by which the microscopic shear bands propagate into the entire sample, becoming macroscopic shear bands.

The procedure to reveal the slip lines was the following : samples were deformed in channel-die compression at room temperature to certain strains (ranging from 0.3 to more than 1). One of the faces in contact with the die was polished (with electropolishing finish, see Appendix A) and the sample was placed again in the channel die, the polished surface being partly free. An extra deformation of approximately 2% was finally carried out to reveal the slip lines, and the sample surface was studied by Nomarski contrast under the optical microscope.

Samples of pure Aluminium were deformed to true strains of 0.3 and 1. Fig. 3.33 and 3.34 show optical micrographs of the slip lines present at these strains, as well as the general flow direction. In the intermediate strain case, the slip lines do not have a

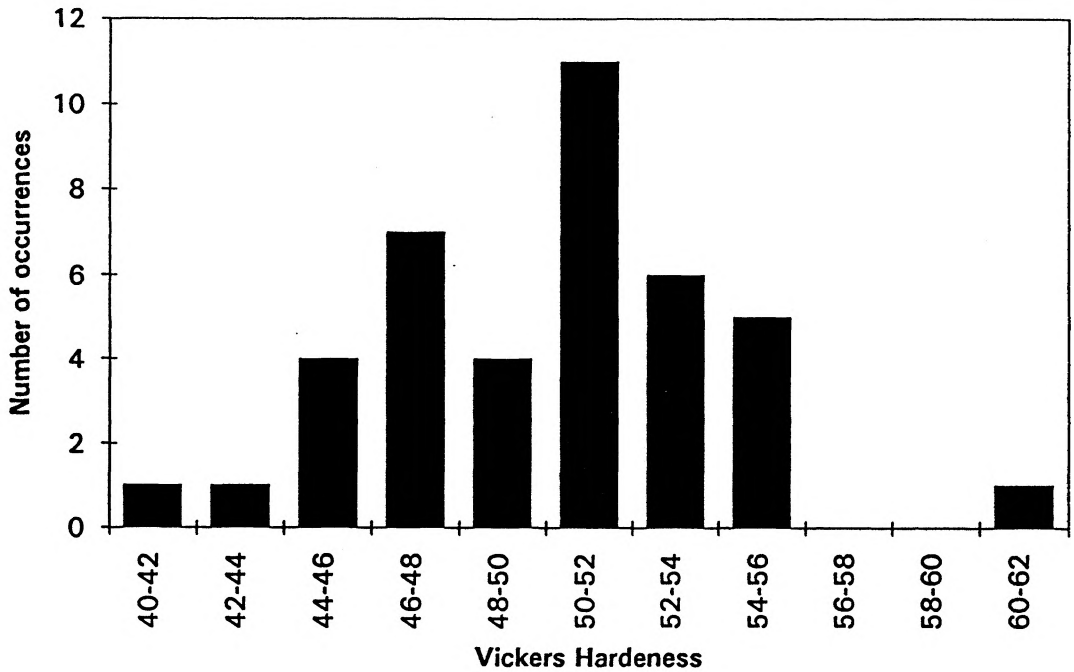

Figure 3.32/ Vickers hardness measurements performed on the lateral face of an Al-0.4%Cu deformed 100% at room temperature

Figure 3.33/ Slip lines for pure Al deformed 30% at room temperature. Line shows flow direction

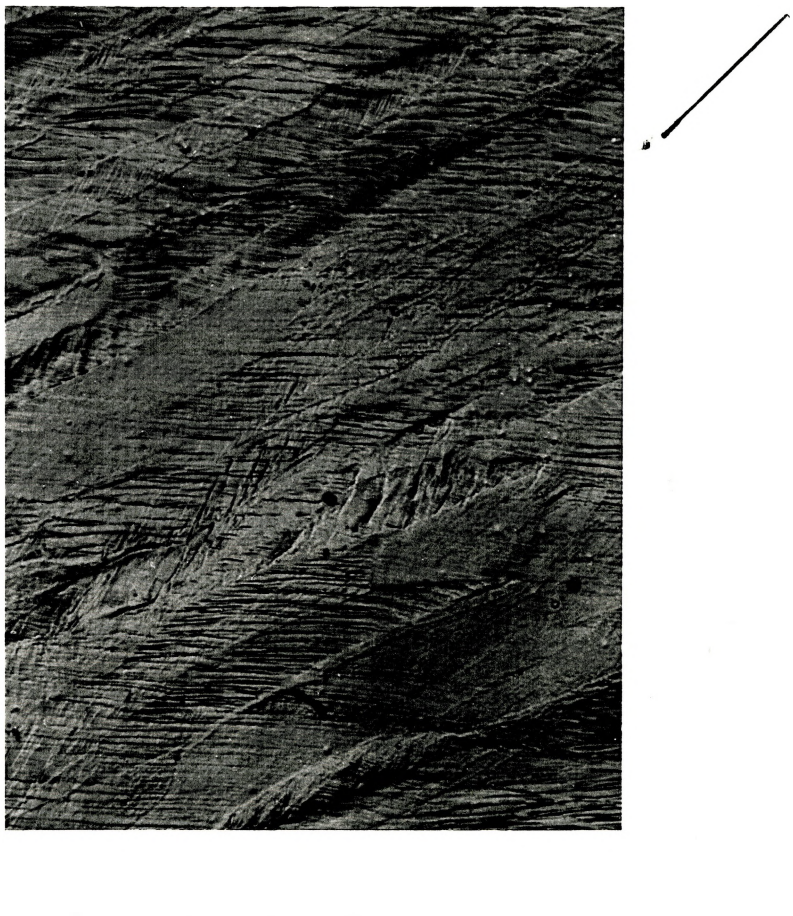

Figure 3.34/ Slip lines for pure Al deformed 100% at room temperature. Line shows flow direction

well defined orientation with respect to the flow direction : the active slip planes are determined by the orientation of each grain, and there can be large misorientations between the slip lines in different grains. Several slip systems are activated in order to accommodate the general shape change of the individual grains, and several sets of parallel slip lines are present within the same grains.

In the large strain case, the pictures were taken from the heavily sheared region. The sets of slip lines in the different grains were much more aligned in a common direction: the rotation of the different grains during the deformation brought the grains in a favourable orientation with respect to the plastic flow direction, and the slip lines misorientations from grain to grain were very small. Again, two sets of slip lines were present, and were symmetric with respect to the flow direction. These continuous sets of similarly oriented slip bands reveal the presence of shear bands. The same characteristic sets of slip lines can be observed in Al-0.2%Cu and Al-0.4%Cu deformed at room temperature to true strains of 1 (Fig. 3.35 and 3.36). The angles of these shear bands with the flow direction were measured from optical micrographs of all three alloys deformed to 100% to be of an average of 35.5°, with a standard deviation of 8°.

3.3.3/ Global texture study

3.3.3.1/ Measurement procedure

The texture measurements were performed at the Los Alamos National Laboratory (New Mexico, USA). In considering the experimental determination of textures in metals

Figure 3.35/ Slip lines for Al-0.2%Cu deformed 100% at room temperature. Line shows flow direction

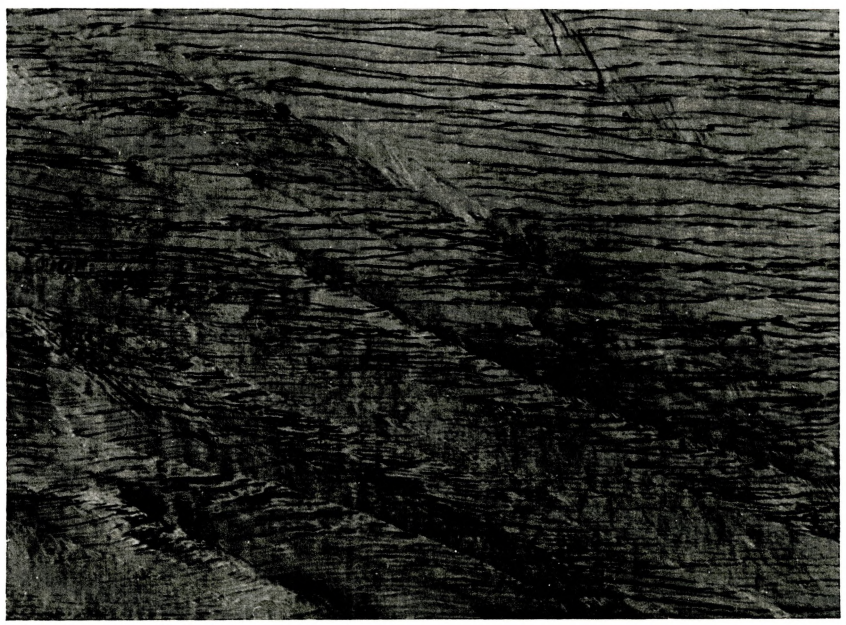

Figure 3.36/ Slip lines for Al-0.4%Cu deformed 100% at room temperature. Line shows flow direction

it is important to consider the nature of the measurement. A major consideration in determining the reliability of the measurements is the volume of material being sampled and how this changes as the orientation of the sample is changed. A combination of the X-ray spot size, its penetration depth, the grain size and the orientation of the sample in the goniometer cradle determines how many grains are being sampled. In the present case the penetration depth (50 μm) is smaller than the initial grain size (150 μm) so that only surface grains were being sampled. The sample area was of the order of 1 cm^2.

Experimental poles figures were measured using a Scintag texture goniometer using CuK_α X-ray radiation. Fig. 3.37 shows the definition of the angles for the goniometer cradle. θ is the Bragg angle corresponding to the measured figure pole, and is determined when the sample is placed in the eucentric goniometer. Measurements were made on the (111), (200) and (220) poles. The values of azimuth and angle of incidence were incremented by 5° stepwise from 0-355° and 0-80° respectively. At each position X-rays were counted for 1s. The input X-ray detector slit was set at 1 mm. All pole figures shown in this work will be equal-area projections. The equal-area projection has the advantage that the intensity of poles for a random sample is uniform over the entire projection (Poole, 1993). The experimental textures were corrected for defocusing and background effects based on experimental correction files from a random Aluminium sample. The incomplete pole figures (corrected for defocusing and background) were processed on a PC-based ODF analysis software package (Kallend *et al.*, 1991).

a)

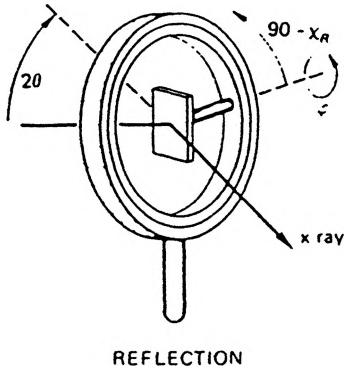

b)

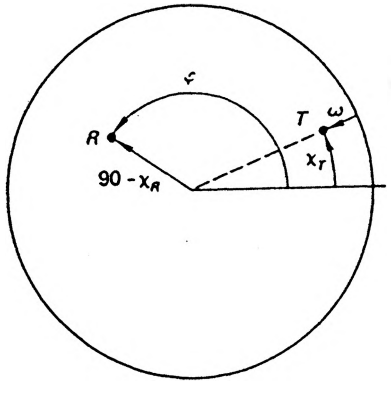

Figure 3.37/ Definition of the angles for X-ray texture measurements a) for goniometer and b) on corresponding projection

3.3.3.2/ Texture results

Texture measurements were first carried out on each of the three alloys in the annealed state, and deformed at room temperature to true strains of 0.3 and 1. The texture measurements were carried out on the constrained plane (i.e. the plane including the compression direction and the normal direction). However, for the sake of comparison with textures obtained by rolling, the data was converted in the "rolling" plane (i.e. the plane perpendicular to the compression direction). The initial figure poles of the three alloys are shown in Fig. 3.38. Figure poles after 30% of true deformation are shown in Fig. 3.39, and figure poles after true deformations of 1 are represented in Fig. 3.40. The initial textures show a lack of uniformity, probably due to the large grain sizes. After 30% of deformation, (111) pole figure show a slight evolution towards the rolling texture. After a deformation of 1, this texture is more characteristic, although still relatively weak. The texture development appears to be stronger in the pure aluminium than in the solid solutions.

3.3.4/ Local texture (BEKP) study

3.3.4.1/ Measurement procedure

The local texture measurements were performed on a Scanning Electron Microscope at Queen's University (Kingston, Ontario, Canada). Backscattered Electron

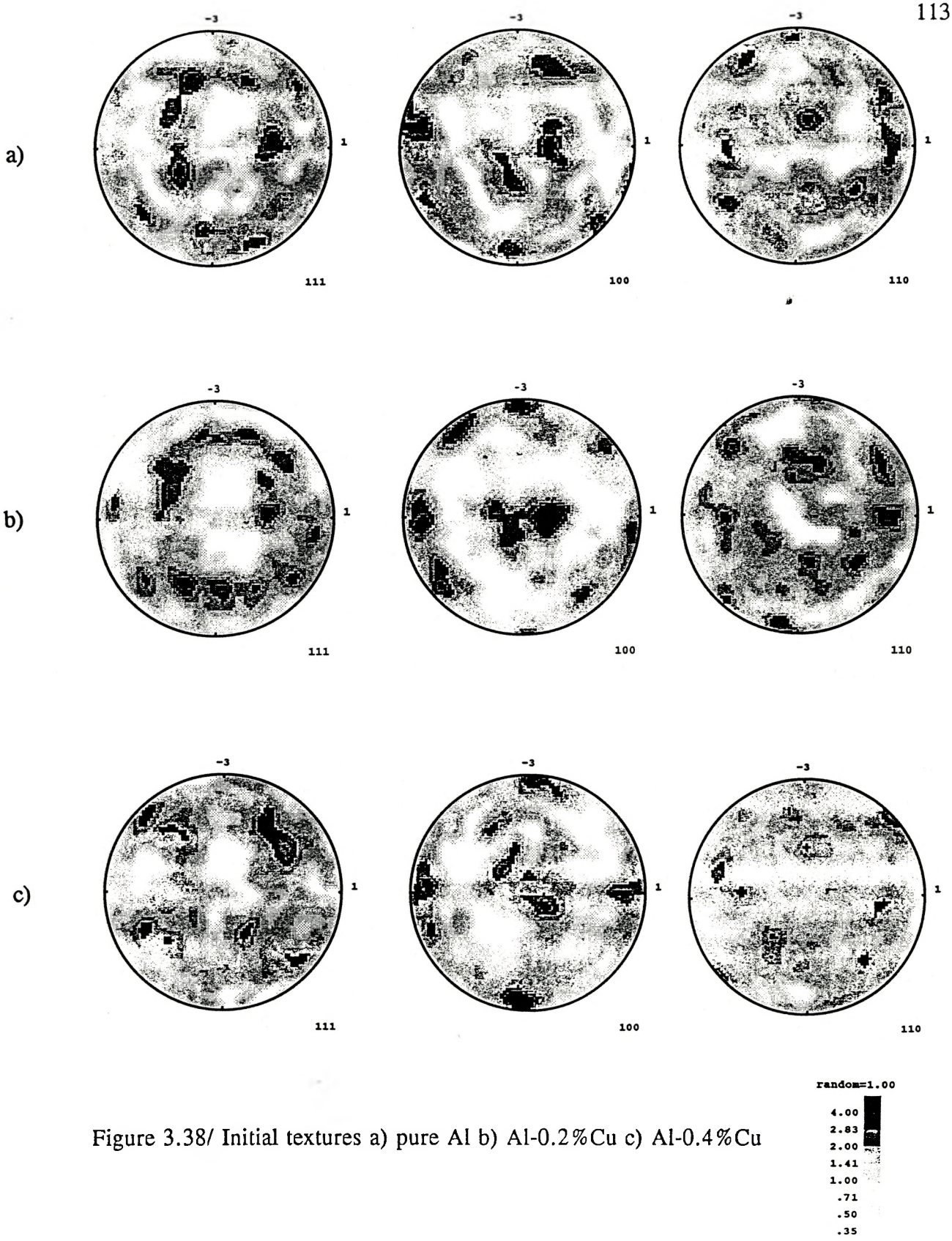

Figure 3.38/ Initial textures a) pure Al b) Al-0.2%Cu c) Al-0.4%Cu

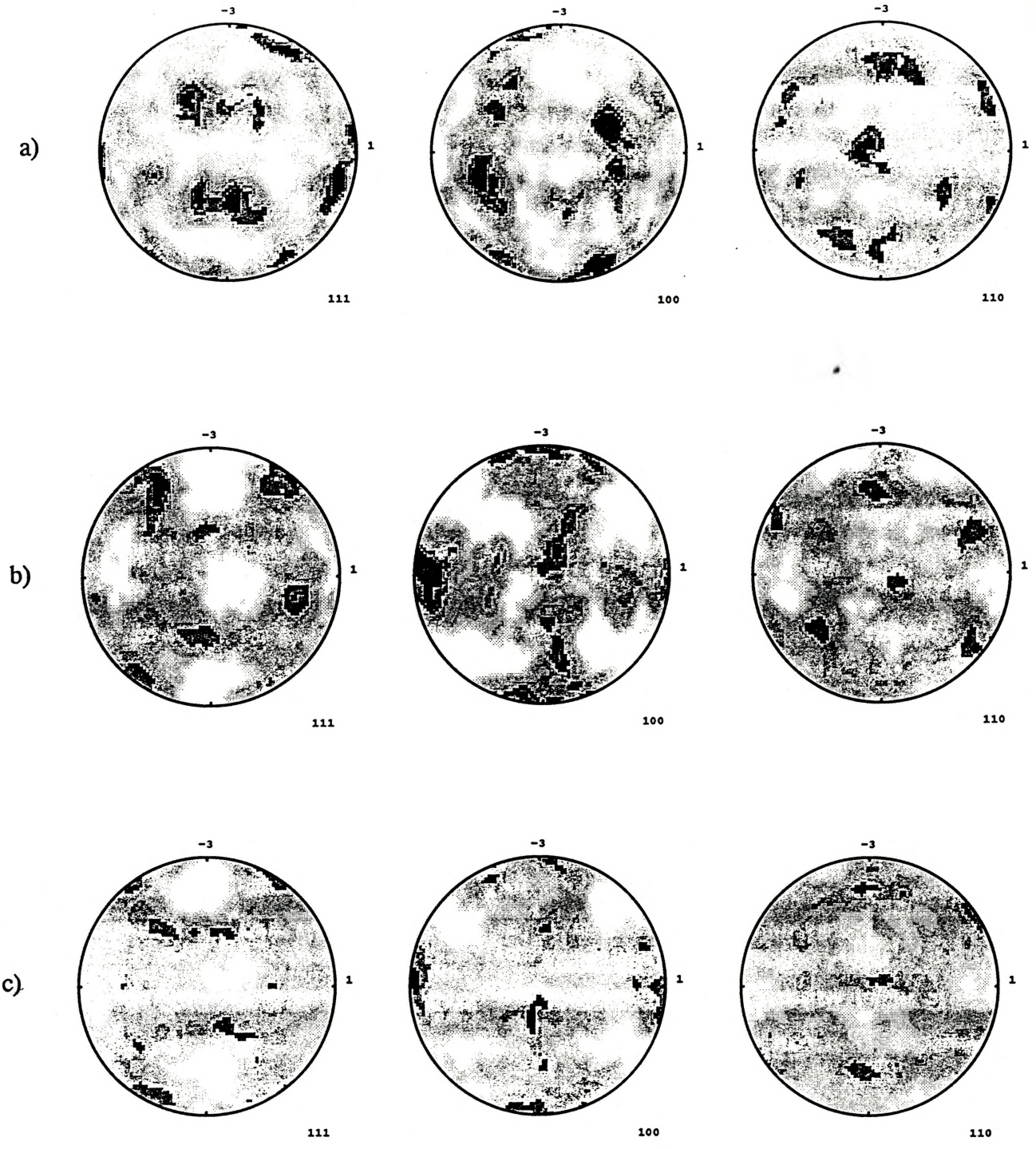

Figure 3.39/ Textures for a) pure Al b) Al-0.2%Cu c) Al-0.4%Cu deformed 30% by channel-die compression at room temperature

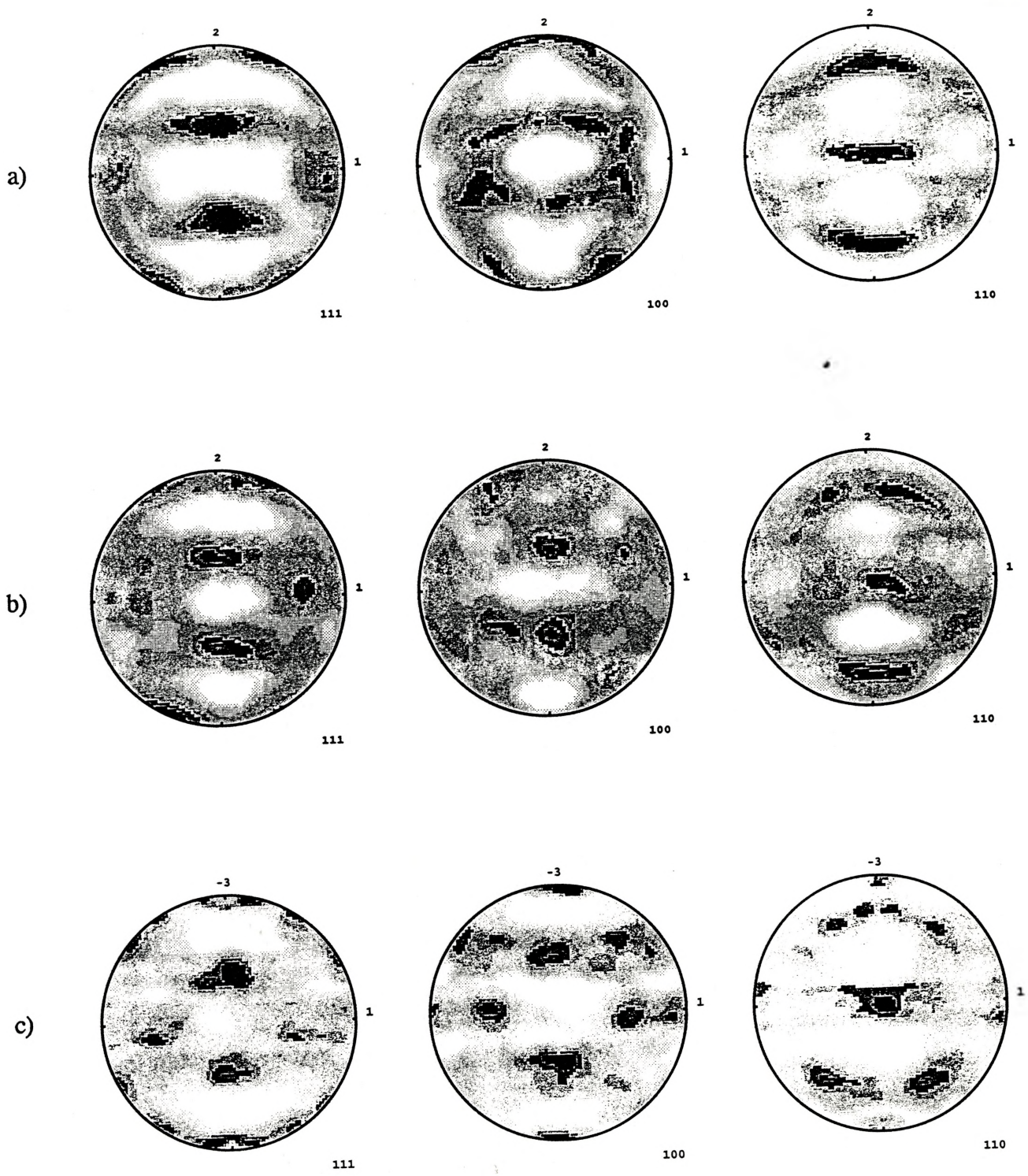

Figure 3.40/ Textures for a) pure Al b) Al-0.2%Cu c) Al-0.4%Cu deformed 100% by channel-die compression at room temperature

Kikuchi Patterns (BEKPs) are useful for determining the crystallographic texture of polycrystalline materials and crystal structures of unknown elements (Dingley and Randle, 1992; Randle, 1992). In order to obtain a BEKP the incident beam is focused and held stationary on the feature of interest on a specimen tilted 70° toward the BEKP detector. The spot is approximately 0.2 μm in diameter and 0.05 μm deep. Inside the specimen, the electrons are elastically and inelastically scattered. Some are scattered at high angles and exit the specimen. These backscattered electrons form the basis of the BEKP. Some of the backscattered electrons which satisfy the Bragg condition are diffracted into cones, constructing upon intersection with the plane of the detector an array of excess and default lines (Kikuchi lines). The arrangement of the Kikuchi lines is related to the crystallographic structure and the orientation of the specimen, with a very high angle sensitivity. These Kikuchi Patterns were recorded with a CCD camera, and corrected for background noise. They were then analysed with a semi-automated PC-based software package (by N. H. Schmidt): for each pattern three or four visible lines are drawn on the pattern by the operator. Knowing the crystallographic structure of the material investigated, the software searches for an orientation fitting the drawn lines. The complete calculated set of lines from this orientation is then displayed on the pattern. If the calculated orientation is correct, the match is perfect, and the operator saves the orientation. The complete operation lasts about 15 to 20s. Pole figures and inverse pole figures can finally be plotted from the saved orientations.

3.3.4.2/ BEKP results

The BEKP measurements were performed on Al-0.4%Cu deformed at room temperature to a strain of 1. The general purpose was to assess the difference of local texture between the region of the sample that had experienced intense localized shear (region SB) and the region that had deformed under pure plane strain conditions (region PS). Two sets of measurements were performed.

First the local crystallographic orientations were measured in both regions on a regular grid of 6x5 points (The size of each measurement spot was approximately 0.2 μm). The points were regularly spaced at 20 μm intervals. The inverse pole figures were then compared in the PS region and in the SB region. Inverse pole figures were plotted both referring to the "rolling plane" (which means in channel-die compression the plane perpendicular to the compression direction), and referring to the constrained plane, i.e. the plane including the flow direction and the compression direction.

Fig. 3.41 shows the inverse pole figures taken in regions PS and SB, referring to the rolling plane. We can see that in this representation, region PS experiences clustering around the {111} pole. In region SB, however, the orientations have migrated towards the {101} orientation. It has been shown by Aernoudt (1978) that the superimposition of shear on a pure rolling texture had a similar effect on the inverse pole figures (see Fig. 2.8). Although only a limited number of specimens points were processed here, the results provide at least a qualitative indication of the superposition procedure.

a)

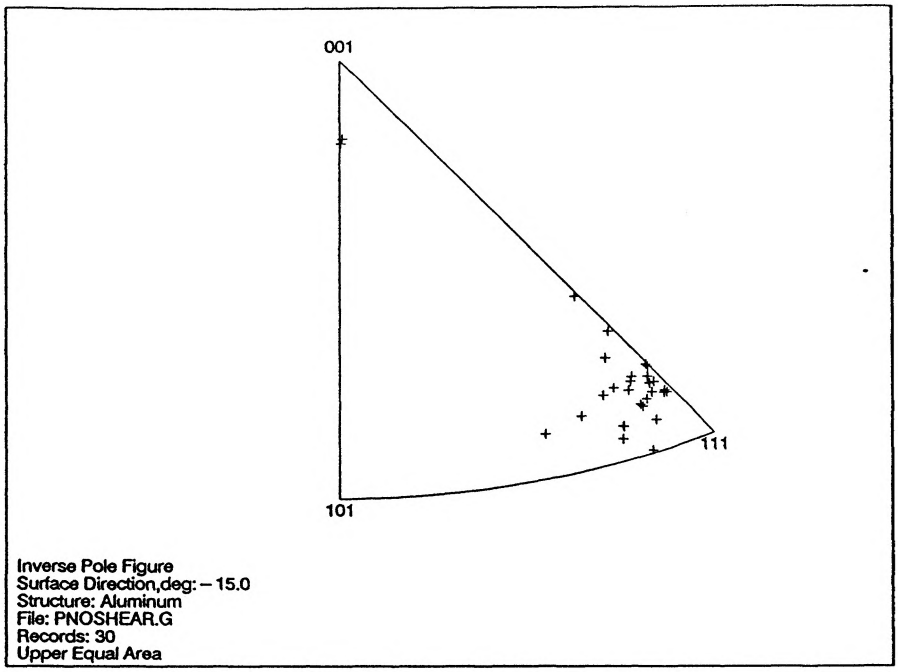

b)

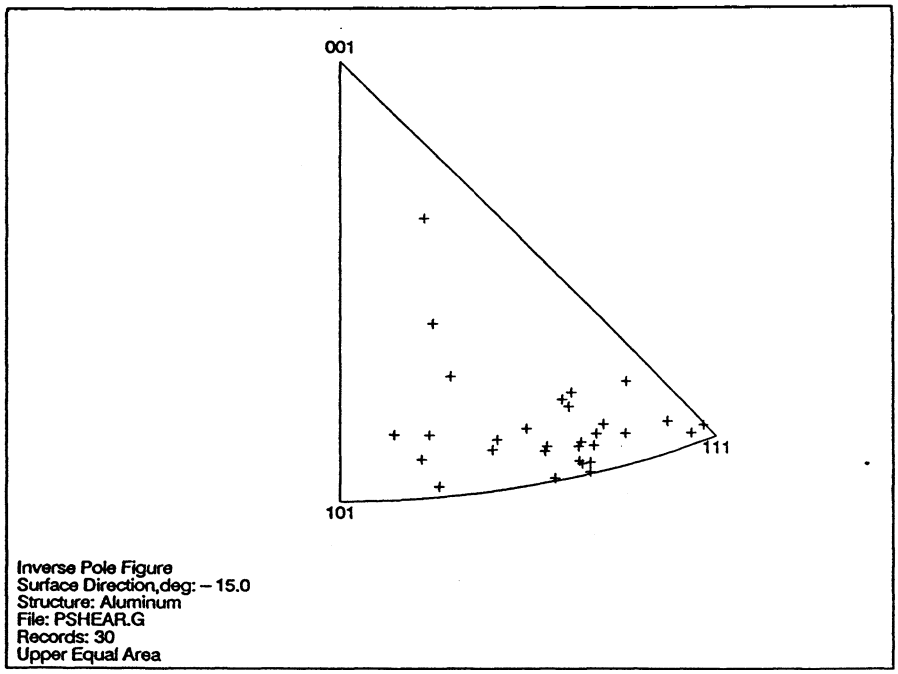

Figure 3.41/ Inverse pole figures (referring to the rolling plane) obtained by EBKP for Al-0.4%Cu deformed to a true strain of 1 at room temperature a) region free of shear bands b) shear banded region

The second experiment was to follow a line running from the PS region to the SB region. 120 measurements were made, regularly spaced at 20 μm intervals. These points were then separated in three groups, the first group corresponding to the PS region, the second group to a transition region and the third group to the SB region. The inverse pole figures were then compared in the two extreme groups, corresponding to the PS and the SB region. Again, these pole figures are referring to the "rolling" plane. As shown in Fig. 3.42, the tendency is similar to the first experiment: the shear banded region orientations are displaced towards the {101} pole.

3.3.5/ Electron Microscopy

Transmission Electron Microscopy (TEM) was performed on an Al-0.4%Cu sample deformed at room temperature to a true strain of 1. The purpose of this study was to determine the microstructural differences between the shear banded regions and the non shear banded regions of the sample. The experimental procedure for the sample preparation was the following :

The samples for TEM observations were obtained from two different regions of the deformed specimen : some in the shear banded region, some in the region not affected by them (see Fig. 3.30b for their respective positions with respect to the sample). The TEM samples were parallel to the constrained surface of the channel-die. Slices were first cut with the low-speed cutting saw, parallel to the constrained surface.

a)

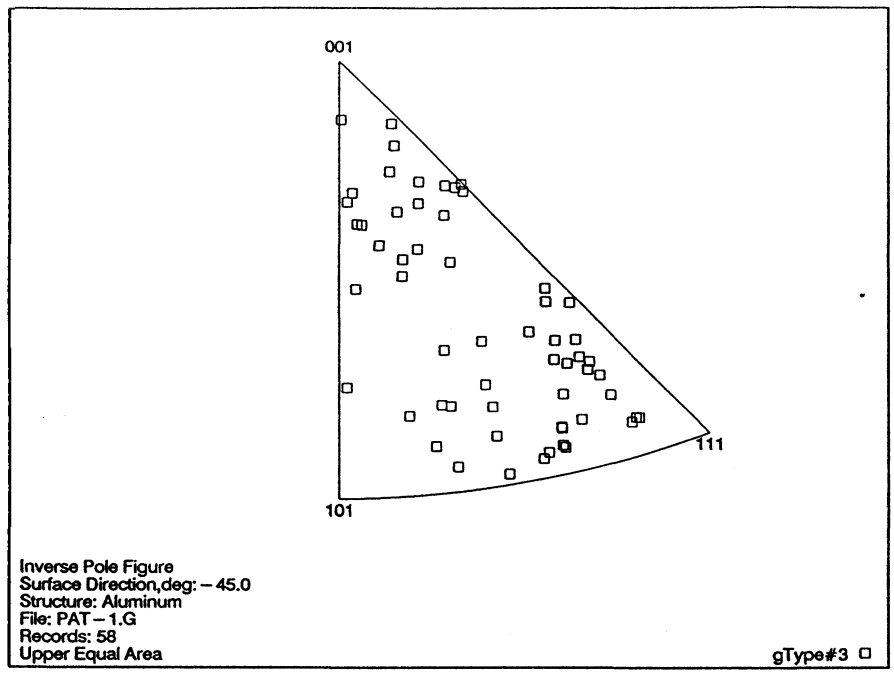

b)

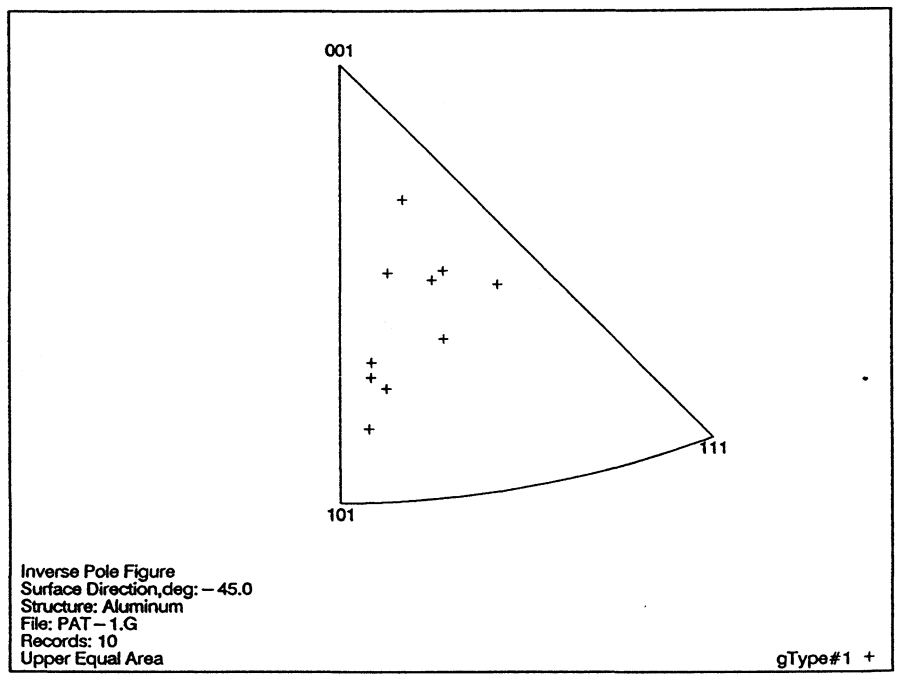

Figure 3.42/ Inverse pole figures (referring to the rolling plane) obtained by EBKP for Al-0.4%Cu deformed to a true strain of 1 at room temperature a) region free of shear bands b) shear banded region

Discs 3 mm in diameter were cut in these slices by spark cutting. These disks were then reduced to a thickness of approximately 70 μm by grinding with 1200 and 2400 SiC paper. The perforation was carried out by a dual electrojet, the electrolytic solution being composed of 25% nitric acid in methanol (working temperature : -40°C). The voltage used was 12V. The samples were finally observed in a Jeol TEM in bright field at different magnifications. The accelerating voltage used was 120 kV.

The cell structure is very well defined in both regions (Fig. 3.43 and 3.44): the cell walls are very sharp, and the cell interiors are almost dislocation-free. The shape of the cells is markedly different in both cases : in the unsheared region the grains are relatively equiaxed, which is to be expected from a relatively pure aluminium (see Rollett, 1988). In the shear band region, however, the dislocation cells are elongated, consistently throughout the sample. The average aspect ratio was measured to be approximately 4. As shown in the literature review, this is consistent with the presence of shear bands.

Macroscopic shear bands can be clearly seen in the sheared zone (Fig. 3.45). They are characterized by a very local disruption of the cell structure, with the presence of cells of a significantly smaller size. These shear bands make an angle of 35° with respect to the elongation direction of the cells. A reasonable assumption is that the dislocation cells are elongated in the direction of general flow (Hatherly and Malin, 1984). In this case the shear bands would be at an angle of 35° from the flow direction, which is consistent with the slip lines observations and the work present in the literature.

Figure 3.43/ TEM micrograph of Al-0.4%Cu deformed to a true strain of 1 at room temperature, shear banded region

Figure 3.44/ TEM micrograph of Al-0.4%Cu deformed to a true strain of 1 at room temperature, region free of shear bands

Figure 3.45/ TEM micrograph of Al-0.4%Cu deformed to a true strain of 1 at room temperature, shear banded region. Arrows show shear bands

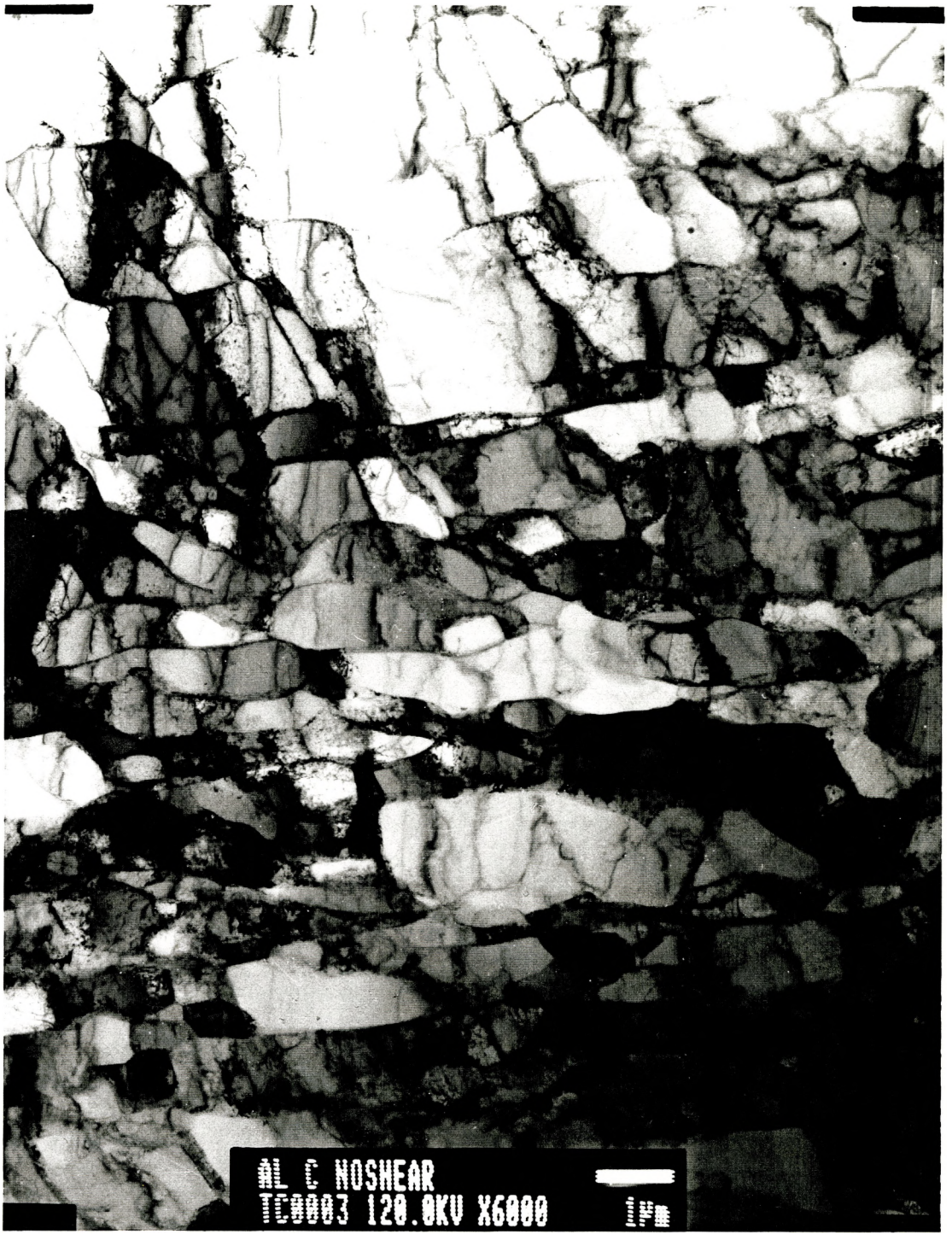

Figure 3.46/ TEM micrograph of Al-0.4%Cu deformed to a true strain of 1 at room temperature, region free of shear bands

In the unsheared zone, however, no shear bands could be observed (Fig. 3.46).

As a further observation of the localization of deformation, the cell size was measured in both regions. In the sheared region, the cell size was measured in three different areas to be respectively 0.75, 0.8 and 0.84 μm, giving an average value of 0.8μm. In the unsheared region, the grain sizes measured were 1.27, 1.44 and 1.55 μm, giving an average value of 1.4 μm. Since the cell size is a decreasing function of strain, this is a further indication that the level of strain experienced by the sheared zone was much higher than the level experienced by the unsheared zone.

CHAPTER 4

DISCUSSION

In this chapter the discussion will be organized as follows: first a discussion of the validity of the experimental method, second the structural evolution from the macroscopic scale to the microscopic scale. Finally we will attempt to model the work hardening behaviour that we observe for the materials studied in this work.

4.1/ VALIDITY OF THE MECHANICAL TESTING METHOD

In order to investigate phenomena such as dynamic recovery and stage IV of work hardening, one has to derive reliable data from the experimental output. The mechanical testing of a material is rarely direct: one is always measuring a combination of the ideal plastic flow behaviour, the possible effects of friction, and redundant work together with the characteristics of the testing equipment (e.g. machine stiffness). Moreover, testing to large strains can rarely been achieved without interruptions, during which static recovery occurs. It is appropriate to discuss the influence of the static recovery in channel die compression tests and to compare the results obtained by channel-die compression and other strain paths, namely tensile tests and free compression tests.

4.1.1/ Static recovery after straining

In the present work, the static recovery processes occurred when straining the materials at sub-zero temperatures (77K and 200K), followed by letting the alloys recover at room temperature prior to re-straining them at the same low temperature.

This type of recovery process has been investigated in the past, as in the works of Cherian *et al.* (1949), Lytton *et al.* (1962), Tietz *et al.* (1962), Hasegawa and Kocks (1979), Hasegawa and Yakou (1980), Hasegawa and Yakou (1982) and Kwiecinski and Wyrzykowski (1993) (although in these cases the material was deformed at room temperature, recovered at higher temperatures, and restrained at room temperature). These works concentrated on the decrease in the stress level that occurs when straining is resumed after static recovery. From these works one can state some characteristics about the stress-strain curves obtained after recovery:

- for mild recovery treatments the yield stress after restraining is lower than the flow stress obtained at the end of the first deformation process, but this difference vanishes after a short strain interval. The recovered material then experiences the same stress levels as the non recovered material;
- for stronger recovery treatments a larger yield stress drop upon restraining is observed, and the stress-strain curve always stays below the non-recovered stress-strain curve;
- the work hardening rate vs. stress curves of the deformation before and after recovery are continuous, except for a short transient;

We confirmed in this study that it is useful for this type of investigation to

represent the data in work hardening rate versus stress diagrams. The θ/τ curves, when represented for the channel-die compression tests at low temperatures, including the recovery taking place at room temperature, were consistently defining a continuous curve, with the exception of a short transition period. As it has been shown in the experimental investigation section, the stress-strain curve can then be made perfectly continuous by a simple shift in strain.

This approach implies that the recovery process between the two stages of deformation is equivalent to a loss of strain, or more specifically a loss of the structure stored by straining. When the material is restrained, it experiences first a transition period, during which the material stores dislocations at a high rate. When the stress level reaches the same level as that in prestrain the material experiences the same work hardening rate level and the same subsequent deformation process. The existence of the transient proves that the work hardening rate is not uniquely determined by the set of variables flow stress, temperature and strain rate. In other words, there is no equation of state for the material based on these variables. On the other hand, we observe that once the material upon restraining has reached the pre-strain stress level, its work hardening rate is identical to the pre-strained work hardening rate at the same stress. This tends to indicate that the structure obtained after recovery and restraining up to the former stress level is the same as that produced before recovery.

This would support the view that the recovery mechanisms observed here are of the "metarecovery" type, to follow the terminology of Cherian *et al.* (1949). In this case

the sequence of mechanisms would be as follows: recovery leaves unchanged the structure of the material (e.g. the cell size) and affects only a fraction of the dislocation density. Upon restraining the structure stays unchanged and the high work hardening rate is caused by the storage of dislocations of the same type of the dislocations previously recovered. When this process is complete, the state of the material is identical to the state before recovery happened and the material has the same subsequent behaviour as the unrecovered material.

An other possibility is that there would be two separate populations of dislocations, as has been proposed by Cottrell *et al.* (1953): the first would be very sensitive to static recovery, and the second would be insensitive to mild recovery treatments. Typically the first population would include dislocations which can be moved by thermal activation, and the second dislocations that can be moved only by long-range stresses. During static recovery the first population would first recover. When the material is restrained, the high work hardening rate which is first observed would be caused by the storage of these "soft" dislocations. This approach would explain the lack of an equation of state: here the overall stress and the work hardening rate do not only depend on the dislocations density, but on the repartition between two separate populations of dislocations.

This mechanism may well explain the phenomena taking place for very small recovery treatments. However, we observed in this study that the transient state strain extent (or the equivalent loss of strain) could as high as 20% in the case of severe

recovery treatments after high strains. It seems unlikely that the material would keep a constant structure during the first 20% of restraining before it reaches its former stress level.

No systematic study of the influence of the dependence of the strain shift with recovery time, temperature and amount of previous straining was undertaken. The time during which the samples were held at room temperature was not controlled, and the amount of initial straining before recovery was also different from sample to sample. Moreover, such study would be very difficult in a channel-die because of the uncertainty on the yield point behaviour. However, we can state that after 30% of initial straining, recovery of 1/2 hour to 1 hour at room temperature was (in strain equivalents) about 5% for room temperature testing, 11% for testing at 200K, and 17% for testing at 77K.

The same approach can be used with the data mentioned above. We can see in Fig. 4.1 the initial curves and the superimposed displaced stress-strain curves for the material subject to recovery treatments at 373K, 473K and 623K (form Kwiecinski and Wyrzykowski, 1993). The continuity by displacing the position on the strain axis is observed for the two first treatments, but not for the last treatment of 1h at 623K. During this last treatment the sample will probably have recrystallized, causing major changes in the structure. The same type of observations can be made in regard to the other works cited above.

In order to reach a more complete understanding of the recovery processes after

a)

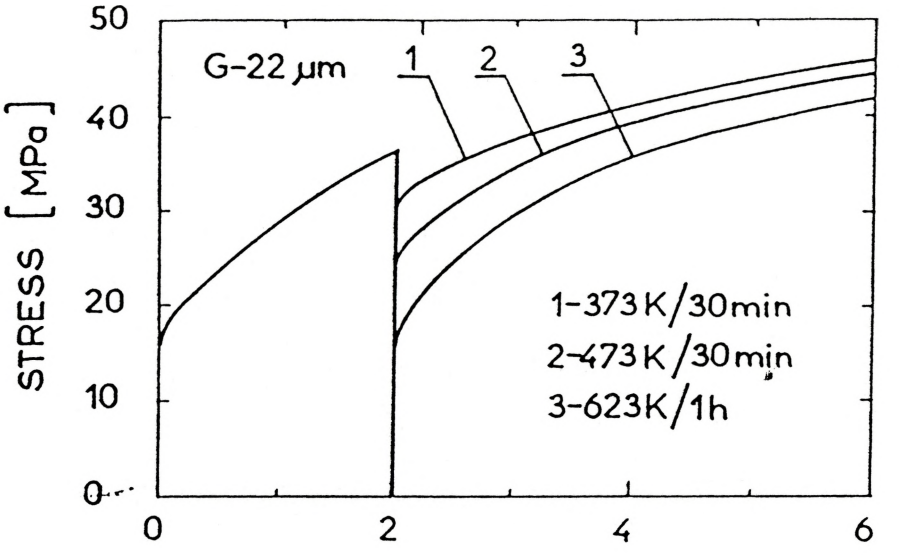

b)

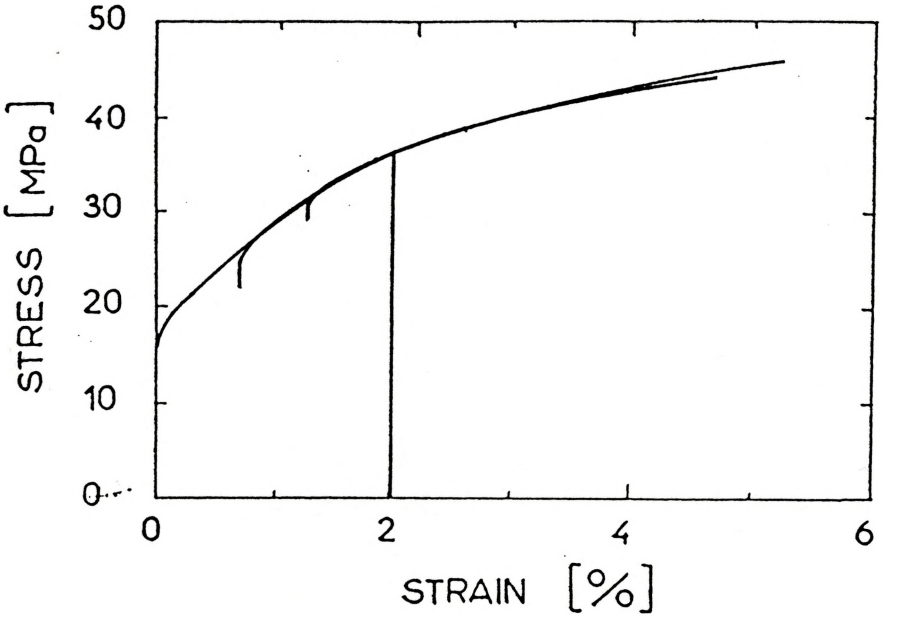

Figure 4.1/ a) The effect of 2% of prestrain and annealing temperature for constant time of 30 min on the room temperature stress-strain behaviour of Aluminium (from Kwiecinski and Wirzykowski, 1993) b) Curves 1 and 2 in Fig. 4.1a) have been translated on the strain axis to match the stress level before annealing

plastic straining and the subsequent restraining, it is clearly necessary to obtain more reliable and systematic data. There is a need for the ability to measure precisely the stress drop upon recovery and the equivalent strain loss upon restraining. Recovery treatments need to be done at various times, various levels of prestrain and during various times. However, on a very practical point of view, the phenomena observed in this work, if not interpreted quantitatively, provide a good tool for constructing reliable envelopes for stress-strain curves of interrupted tests.

4.1.2/ Comparison between various deformation paths

The mechanical properties of the three alloys considered in this thesis were studied using three different deformation procedures: channel-die compression, free compression and uniaxial tensile testing. These three deformation procedures enabled an investigation of the mechanical properties of the material to be performed using various strain paths and frictional effects: both tensile tests and free compression tests involve uniaxial deformation, and channel die compression involves plane strain deformation. In tensile testing the material does not experience any friction; in free compression the friction is limited to the top and bottom faces of the sample; in channel-die compression the friction occurs on four of the six faces of the sample. Therefore, the comparison between these three procedures (in equivalent von Mises strains and stresses) should provide a good assessment of the validity of channel-die compression as a mechanical testing method at large strains.

Fig. 3.14 shows the stress-strain curves obtained by the three deformation procedures for pure Aluminium at room temperature. It can be seen that the behaviour is very similar both in terms of stress levels and work hardening rates for the tensile test, free compression test and channel die compression test. Fig. 3.17 shows the stress-strain curves obtained by the three deformation procedures for pure Aluminium at 77K. Again, the agreement between the free compression test and the channel die compression test is very good. Such agreement has previously been demonstrated by Kocks *et al.* (1988) for Aluminium alloys.

We can see, however, that pure Aluminium tested in tension with very small cross-sections shows much lower levels of stress, both at room temperature and at liquid Nitrogen temperature. To explain this fact, it is useful to consider the grain size of the material under study. Although the average grain size was 150 μm, it was quite inhomogeneous, and could become locally larger than 500 μm. As pointed out by McGregor Tegart (1967), the deformation mode is then different from the deformation mode of a true polycrystal: the number of slip systems is lower than that required for the homogeneous deformation of a polycrystalline aggregate. The resulting orientation factor is hence smaller, and so is the macroscopic flow stress. The easier slip in the surface grains leads to a very heterogeneous surface. This effect of the number of grains per cross-section has been studied previously by Fleischer and Hosford (1961), see Fig. 4.2.

In conclusion, the correction of the effects of static recovery between straining

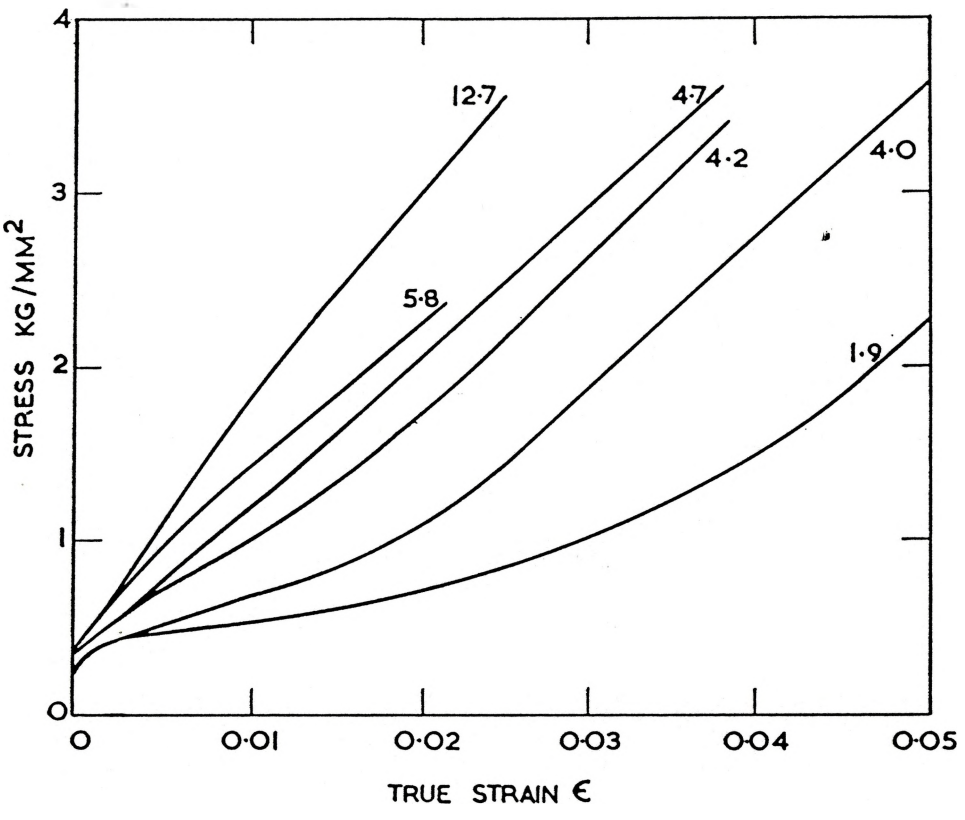

Figure 4.2/ Influence of number of crystals per cross-section on stress-strain curves for aluminium polycrystals at 4.2K (after Fleischer and Hosford, 1961)

passes in channel-die compression and the validation of the channel-die results by investigation of other strain paths proved that channel-die compression was a reliable procedure to test the materials under study to large strains.

4.2/ EVOLUTION OF THE STRUCTURE

In investigating the structural evolution of the materials during deformation, the purpose was to provide a link between the macroscopic and microscopic scales, and between the moderate and large strains. Given the limited amount of time available for the present study, preference was given to a survey of the structures by various experimental techniques covering a variety of scale levels rather than the thorough study of only one of these. The macroscopic scale was studied by optical microscopy (slip lines and grain shapes) and global texture measurements, and the microscopic scale was studied by local texture measurements in the Scanning Electron Microscope using Back-Scattering Kikuchi Patterns and limited observations in the Transmission Electron Microscope. The purpose was notably to determine the occurrence and characteristics of macroscopic shear bands during the deformation process in order to understand their role in the texture evolution and their influence on the mechanical properties.

4.2.1/ Moderate strains: ideal plane strain compression

A material tested by channel-die compression would ideally flow homogeneously

by plane strain, developing an idealised copper texture. In the present experiments, the deformation at moderate strains (up to 30%) was shown to be homogeneous: the specimen surfaces did not show any inhomogeneous deformation and the slip lines were highly misoriented from grain to grain, not showing any sign of shear banding. The texture developed towards a Copper texture for all three alloys. It is important to note that due to the large initial grain size (approximately 150 μm), the texture of the undeformed material was rather inhomogeneous, with the consequence that texture evolution during deformation is more difficult to determine and more likely to be different from the texture developed from a perfectly random oriented sample.

4.2.2/ Large strains: the influence of shear bands formation

The slip lines study showed that macroscopic shear bands (MSBs) started to occur at strains of about 50%, which is in general agreement with the literature (Dève and Asaro, 1989). On Al-Mg-Mn alloys deformed by the same channel-die compression apparatus, Duly (1993) observed MSBs initiation at much lower strains (10 to 20%). However, these alloys exhibit dynamic strain ageing and a low work hardening rate versus stress ratio, both of which favour deformation by the shear band mode.

Shear bands appeared to be responsible for an important fraction of the deformation in subsequent deformation. This was evidenced both by the observation of the grains aspect ratios in the regions experiencing shear banding and by the hardness measurements inside and outside the shear bands. Grains aspect ratios for Al-0.4%Cu

deformed 100% at room temperature could reach 20 in the shear banded regions, as compared to 5 on average in the unsheared regions. This difference means a very substantial difference in the strains experienced by the two regions. One can argue that the Vickers hardness spread is relatively small between the two regions. However, at room temperature and large strains the work hardening rate of Al-0.4%Cu is very small and a large difference in the amount of strain will only make a small difference in the local hardness of the material. Moreover, the texture evolution difference tends to reduce the true stress gradient in the material. The consequences of the strain difference was further assessed by the TEM study: thin foils cut from the shear banded region and the non sheared banded region showed subgrain sizes of 0.8 μm and 1.4 μm. Moreover, the subgrains in the shear banded region were elongated, which is a further indication of higher strain levels.

The mechanism of shear bands formation appeared to be in agreement with the mechanism proposed by Harren *et al.* (1988). Slip bands observations showed that at moderate strains (30%) slip lines were highly misoriented from grain to grain. Although grain-size shear bands (GSBs) may be present at this stage, no MSBs could be distinguished. At large strains (100%), the slip lines were aligned in well-defined directions, defining MSBs. Two families of MSBs were often observed in the same grains; these are often referred to as positive shear bands and negative shear bands. The shear band planes appeared to be locally bent close to a grain boundary in order to accommodate the small misorientations still existing between the MSBs. These

observations were confirmed by the TEM observations: it was observed that among a distribution of elongated and large dislocation cells there exists planes consisting of very small dislocation cells, suggesting a very highly localized deformation. These planes were identified as shear bands, and their volume fraction was found to be very small, which is to be expected in high SFE materials.

Shear band angles were measured both on a macroscopic scale by the slip line angles and on the microscopic scale by the TEM observations. In both cases the measured angles were 35°, which is excellent agreement with the literature. It also assessed the relationship between the microscopic observations of shear bands (typical magnifications X6,000 to X20,000) and their macroscopic observations (typical magnifications X300). The only troubling fact was the large spread of the shear band angles as measured by slip lines (standard deviation 8°). This can result from two different causes: either the formation of MSBs was still in a transient state, or a wide range of orientations are almost equally favourable to the development of shear bands. The first possibility seems the most likely: the average shear band angles are very consistent in the literature, and microscopic observations showed less dispersed orientations than macroscopic measurements.

Once the various mechanisms of formation and the characteristics of shear bands are determined, it is of interest to include them in the prediction of the general mechanical properties of the alloy, notably by relating the appearance of shear bands to the texture evolution. This was done both by global X-ray texture measurements and by

SEM local texture measurements.

As far as texture evolution is concerned, the effect of shear banding on plain strain compression can be simply approximated by superimposing shear to plane strain compression in the prediction of the deformation textures. The effect of this procedure is to reduce the sharpness of the rolling texture by moving a fraction of the expected rolling texture component towards the shear texture (see Aernoudt, 1978). After large strains at room temperature it was observed that the texture was stronger for pure Aluminium and weaker for Al-0.4%Cu. This seems to indicate that shear bands developed to a greater extent in the solid solution than in the pure Aluminium. The fact that solutes enhance the tendency to form shear bands and that it is difficult to observe them in pure Aluminium is due to two possible mechanisms, as has been discussed in the literature review: first, the addition of solutes increases the level of stress for a given level of work hardening rate. The ability to resist plastic instabilities, measured by the ratio θ/τ, is therefore reduced by the addition of solutes. Second, solutes may provoke stress serrations which are a factor in initiating instability.

The results of local texture measurements by BEKPs were in qualitative agreement with the global texture measurements: at large strains in Al-0.4%Cu the local texture in the region experiencing shear banding was found to have migrated towards a combined texture plane strain + shear as compared to the local texture in the non shear banded region.

4.3/ MODELLING THE WORK HARDENING OF SOLID SOLUTIONS

In the present study, we obtained a general view of the evolution of the microstructure and the possible influence this could have on the mechanical properties. However, this experimental evidence is insufficient to support a detailed model since it cannot assess the detailed microstructural features involved in stage IV. Therefore, we will attempt in this section to present a phenomenological view of moderate and large strain deformation and present tentative models which describe in a qualitative sense the major experimental observations.

4.3.1/ Phenomenology of work hardening

The experimental data presented in Chapter 3 showed that θ/τ plots are able to separate the sequence of stages involved in large strain deformation. The results presented in this work suggested several important observations that will have to be taken into account in any modelling attempt.

The first important parameter acting on work hardening is the influence of temperature on the moderate strain behaviour. It has been shown in this study that increasing the temperature increased the curvature of the θ/τ plot: at 77K this plot is linear, and it becomes extremely concave when the temperature is raised to room temperature. This has also been observed for pure Aluminium by Rollett (1988).

The influence of solutes is not only to raise the yield stress of the material, but

also to raise its work hardening capacity. In the present study it appears that the addition of solutes to pure Aluminium is equivalent to translating the θ/τ plot along the stress axis. This is shown in Fig. 4.3. At each temperature, the plots for pure Aluminium and its solid solutions could be almost perfectly superposed by a translation along the stress axis. It should be noted that the superposition is less good at the beginning of the curves, which corresponds to the range of strain of the channel-die compression test where the data is less precise.

The work hardening behaviour at large strains needs to be addressed. The main characteristics of stage IV work hardening that have been suggested by this study are in general agreement with the existing literature:

- the stage IV of deformation was observed consistently both in pure Aluminium and in the solid solutions over a range of temperatures. Stage IV is observed over a wide range of strains;
- increase of testing temperature leaded to a decrease in the sharpness of the stage III - stage IV transition;
- the stage IV work hardening rate was approximately independent of alloying content. It is interesting to point out that some previous studies showed no influence of solutes on stage IV over very large solutes ranges (Hughes and Nix, 1989, for Ni-Co alloys up to 30% Co), whereas other studies showed that increasing solute content lead to increasing stage IV level, the two being related by $\theta_{IV}=c.\tau_{IIIs}$ where τ_{IIIs} is stage III saturation stress and c a constant (Rollett, 1988). The solute content range studied in this work was too

Curve	1	2	3	4	5	6
Material	Al	Al-0.2Cu	Al-0.4Cu	Al	Al-0.2Cu	Al-0.4Cu
Shift (10^4 G)	0	-2.9	-5.7	0	-1.5	-3.5

Curve	7	8	9
Material	pure Al	Al-0.2Cu	Al-0.4Cu
Shift (10^4 G)	0	-2.5	-5.5

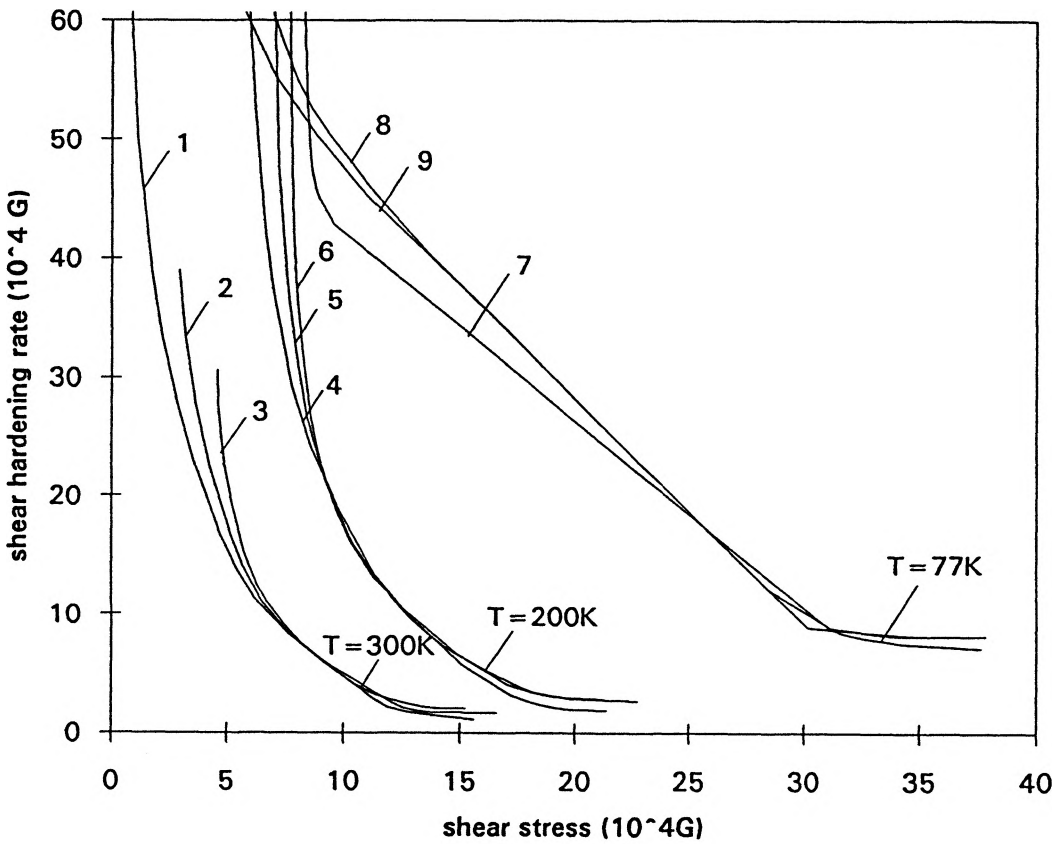

Figure 4.3/ θ/τ plots for Al-0.2%Cu and Al-0.4%Cu (from Fig. 3.24, 3.25 and 3.26) translated on the stress axis to superpose the plots for Pure Aluminium. The magnitude of the translation is shown in the table above

limited to decide between the two possibilities;

- stage IV work hardening rate decreased with increasing temperature. It is interesting to note here that the level of work hardening rate was very consistent with the literature at room temperature (of the order of 2.10^{-4} G), but was significantly higher than expected at liquid nitrogen (close to 10^{-3} G). It should be stressed here that the amount of previous data available for large strain deformation at liquid nitrogen temperature is very small, currently limited to the work of Rollett (1988). In his case, stage IV of work hardening at liquid nitrogen temperature for Aluminium was found not to exceed 3.10^{-4} G. This difference in behaviour may be due to the difference in deformation procedure, between plane strain compression and torsion of thin-wall tubes.

The aim of the next section is to develop constitutive equations for the work hardening behaviour at large strains of the alloys under investigation that will represent the various observations outlined above. We will first attempt to model the work hardening at moderate strains, then discuss the influence of solutes on the work hardening, and finally discuss the behaviour at large strains. Because of the lack of quantitative structural evidence (e.g. TEM evidence), we will make no attempt to base the modelling on structural parameters, such as cell size or misorientation. The modelling will be based simply on the evolution of the dislocation density on the basis of phenomenological accumulation and recovery rates.

4.3.2/ Modelling of moderate strains

In investigating the moderate strains work hardening rate behaviour one has to take into account all the appropriate physical mechanisms. There is wide recognition that moderate strains are controlled by the extent of dynamic recovery. The following modelling process will try to develop constitutive equations representing the experimental evidence by considering the evolution of dynamic recovery processes with temperature.

4.3.2.1/ Standard model for a Voce law

It was shown in section 2.3.2.4/ that the Voce law could be written in terms of dislocation density evolution rate:

$$\frac{d\rho}{d\gamma} = A\sqrt{\rho} - B\rho \qquad (4.1)$$

The first term is the storage rate. It is purely geometrical and does not depend on the temperature or the solute content. This term represents stage II of work hardening rate and has been modelled by Kocks (1966) in his Aerial Glide model, assuming the dislocation storage to be the result of the formation of Orowan loops around the hard spots of the microstructure and their subsequent relaxation on other slip systems.

The second term is the dynamic recovery rate. It can be interpreted as follows: let us consider that two dislocations annihilate if their slip planes are less than a critical distance y_0 apart. This critical distance can be a critical cross-slip distance or a dipole annihilation distance, for instance. Now consider a dislocation of unit length. During the

time dt, the length of dislocation that is captured at a distance less than y_0 from this dislocation is (ρ.v.dt.$2y_0$), where v is the average dislocation speed. The length of dislocation recovered during dt by this process will be twice this value. When considering the complete dislocation density we can hence write:

$$\frac{d\rho^-}{dt} = 4\rho^2 v y_0 \qquad (4.2)$$

We can write the strain rate

$$\dot{\gamma} = \frac{d\gamma}{dt} = \rho v b \qquad (4.3)$$

hence the recovery rate becomes:

$$\frac{d\rho^-}{d\gamma} = -4\frac{\rho}{b} y_0 \qquad (4.4)$$

which represents the recovery term of Eq. 4.1 with $B=y_0/b$. This model produces a linear θ/τ plot, with an initial work hardening rate of $\theta=\alpha GbA/2$, typically G/200.

4.3.2.2/ Effect of temperature

In the above interpretation of the standard Voce model, y_0 represents the occurrence of a thermally activated recovery mechanism (e.g. cross-slip or climb), and therefore it is expected that it will vary exponentially with temperature:

$$y_0 = y_0^0 \exp\left[-\frac{E_1}{kT}\right] \qquad (4.5)$$

Thus the slope of the θ/τ diagram will increase with increasing temperature, but the initial work hardening will stay constant, as is observed experimentally.

However, when the temperature increases, it is observed that the θ/τ plot looses its linearity and becomes more and more concave. We hence have to refine the above analysis with respect to the temperature dependence.

One effect that has to be taken into effect is the pinning of dislocations on the trees of the forest. This subtracts a line tension factor to the interaction force between two dislocations trying to annihilate. This line tension has the form of $Gb\sqrt{\rho}$. However, this factor has a relatively weak contribution to the critical recovery length and is not sufficient by itself to explain the observed curvature.

The study of static recovery showed that there exists two different populations of dislocations: some constituting weak obstacles that can be overcome easily, some constituting stronger structures, that recover with more difficulty. This one population can be subgrain walls or strong dislocation junctions. It is apparent that the proportion of these strong obstacles is dependant both on the temperature and the stress level. This can be seen from the dependence of the Cottrell-Stokes ratio on deformation: it is observed that during stage II the strain rate sensitivity is proportional to the stress, but that stage III leads to an increasing divergence from this law. This divergence from the Cottrell-Stokes law is caused by a change in the ratio between weak obstacles and strong obstacles: when one increases the stress or the temperature, the dislocation structure

evolves towards a low energy structure consisting of cells and then subgrains. The more developed the structure, the stronger the dislocation pinning. We can describe this by adding another term, thermally activated and depending on the mean dislocation spacing, to the interaction force between two dislocations trying to annihilate.

We called the critical spacing for annihilation in the absence of these two mechanisms y_0. Therefore the critical interaction force for annihilation is Gb/y_0. When we take into account the presence of the line tension and of the strong obstacles, we can write that annihilation will occur for a critical spacing y_c which will yield:

$$\frac{Gb}{y_c} - Gb\sqrt{\rho} - qGb\sqrt{\rho} = \frac{Gb}{y_0} \qquad (4.6)$$

On the left-hand side, the first term represents the interaction force between two dislocations at the new critical spacing y_c, the second term represents the force due to the line tension, and the third term represents the back stress due to the strong obstacles. $q=q_0 \exp(-E_2/kT)$ is a thermally activated factor representing the influence of temperature on the development of the microstructure. We can solve Eq. 4.6 for y_c:

$$y_c = \frac{y_0}{1 + y_0\sqrt{\rho}\,(1+q)} \qquad (4.7)$$

In order to obtain the new form of the θ/τ plot we just need to replace y_0 by y_c in Eq. 4.4. The work hardening rate law becomes:

$$\theta = \frac{\alpha Gb}{2}\left[A - \frac{4}{b}\frac{\tau y_0/\alpha Gb}{1 + (q+1)\,(\tau y_0/\alpha Gb)}\right] \qquad (4.8)$$

The θ/τ plot hence becomes an hyperbola. At low temperatures, q will be very small; furthermore, it appears that $\tau y_0/\alpha Gb$ stays small compared to 1 up to large strains. Hence the θ/τ plot will be almost linear and very close to the standard Voce law. However, when the temperature increases, two phenomena take place: the magnitude of the initial slope of the θ/τ plot increases, and the divergence from the Voce law becomes stronger. The combined effect will be to increase the concave curvature of the θ/τ plot. We see also that the slope of the θ/τ plot at the intersection of this hyperbola with the stress axis decreases with temperature. This represents well the fact that the transition between stage III and stage IV becomes less sharp as temperature increases.

It is interesting to point out that we can arrive to an equivalent result if we simply state that because of the increasing proportion of dislocations that become strong obstacles, only a certain proportion of them is capable of dynamic recovery. This proportion f varies with temperature and dislocation density and one can obtain Eq. 4.8 by stating that

$$f = \frac{1}{1 + (1+q)\, y_0\sqrt{\rho}} \qquad (4.9)$$

We see that this model can really be interpreted in two different ways: the evolution of the character of the dislocations can either be seen as making dynamic recovery more difficult by inhibiting their movement, or as decreasing the number of dislocations available for the dynamic recovery events.

4.3.3/ Modelling large strains

In discussing stage IV of work hardening, one has to address a fundamental question: What structure may be stored in stage IV that is superimposed on all previous structures and which can produce the low rate of hardening in the material? We have seen in the literature review the difficulties encountered by the modelling of the work hardening at large strains, or stage IV. As reviewed by Mecking and Grinberg (1979), many mechanisms may be responsible for stage IV, and there is no definitive experimental evidence to assess any of them. Therefore one has to be very careful in the process of modelling large strain deformation, as any model will include some *ab initio* assumptions.

One possible cause for stage IV could be the evolution of the texture and a change in Taylor factor. This is unlikely for various reasons. First, it has been observed that the texture evolution is different in the pure metal and in the alloy, whereas their stage IV behaviour is identical. Second, the texture evolution in various deformation paths is very different, although their work hardening behaviour is very similar.

A more likely possible cause for stage IV could be the occurrence of shear bands. Indeed, shear bands appear at about the same strain levels as stage IV does. Shear band formation can affect the stress levels in two ways. First they influence the texture evolution. However, the discussion above dismissed texture evolution as a possible cause for stage IV. Second, they can affect the overall stress level by localizing an important part of the deformation in a small volume fraction of the material. The increase in flow

stress during stage IV would then be the building up of internal stresses to accommodate the resultant strain gradients. However, there is no evidence that these stresses may cause such a work hardening. Finally, there is no evidence for shear band formation in torsional experiments, although torsion experiments also exhibit stage IV.

In reviewing the experimental data it appears that the level of work hardening during stage I and stage IV is of the same order of magnitude. It is known that the dislocation storage mechanism leading to the weak work hardening in stage I is the storage of dislocation multipoles. Rollett (1988) suggested that this process is present throughout the deformation, and developed a model for stage IV of work hardening based on the accumulation of dislocation debris (see the literature review). The stage I storage process is screened by high levels of work hardening during stage II and III, but reappears when these processes come to exhaustion at the end of stage III, causing stage IV. We can think about this in terms of two different deformation regimes, one laminar and one turbulent, as pointed out by Cottrell (1953):

" [...] in the ideal form of this translational slip, or 'laminar flow', there is no work hardening. Crystals which show strong work hardening, such as those of cubic metals, do not slip like this but in a more complex manner [...] which involves inhomogeneous lattice rotations and bending, and slip on intersecting families of planes. We shall call this second kind of slip 'turbulent plastic flow', borrowing a term suggested by an obvious hydrodynamical analogy."

Following this view, stage I can be considered a stage of laminar flow, and

therefore low work hardening rate. After a turbulent flow transient, composed of stage II and III, the turbulent dislocation storage capabilities of the material are exhausted. At large strains the laminar flow of dislocations through the sample is renewed. In stage I the low but finite work hardening rate was caused by the accumulation of dipoles, in stage IV this work hardening rate is caused by the accumulation of dislocation debris resulting from the annihilation events. These debris are quite similar in nature to the multipoles of stage I: they are thought to be prismatic loops resulting from the collapse of dislocation dipoles. Therefore it is natural that the work hardening rate levels in stage I and stage IV are of the same order of magnitude.

This interpretation of stage IV can also explain the temperature dependence of stage IV: as temperature increases a greater proportion of these debris becomes unstable (collapse of loops resulting in rows of vacancies, for instance), therefore decreasing the efficiency of the hardening process.

In conclusion, a model based on the accumulation debris seems to be consistent with our view of moderate deformation and to explain the principal experimental characteristics of stage IV. However, reliable stage IV modelling requires some definitive experimental data which is extremely difficult to obtain. Such data needs to be obtained by direct observations, such as line broadening in X-ray diffraction for the measurements of internal stresses, or weak-beam transmission electron diffraction for the characterization of dislocation debris. These techniques are extremely difficult to put into practice in the case of heavily deformed metal and one is reduced to indirect

measurements, such as Bauschinger effect for internal stresses, strain-rate sensitivity measurements to assess the arrangement of dislocations in various populations. Although these experimental techniques are very useful to determine the phenomenology of deformation, they will not give us any definitive answer on the actual mechanisms involved in large strain deformation.

4.3.4/ Influence of the solutes on work hardening

In discussing the influence of solutes on work hardening it is first necessary to correct the data for yield stress solution hardening. This correction obviously translates the θ/σ plot on the stress axis by a constant stress value. However, as we have discussed above, this is not sufficient to explain the large difference in work hardening behaviour between the pure metal and its alloys.

It is unlikely that the dislocation storage rate is influenced by the solute content: this is a strictly geometrical process. However, dynamic recovery is very likely to be influenced by solute content, through the critical distance for annihilation y_c (as defined in section 4.4.2). Let us take the first model of work hardening presented in section 4.4.2, which results in a Voce law. One can say that in the absence of solute dislocation annihilation will occur if the interaction between the two dislocations reaches a certain stress level σ_0:

$$\frac{Gb}{y_0} = \sigma_0 \qquad (4.10)$$

If there is now a local solute concentration c in the dislocation region one would expect the critical stress for annihilation to rise, *viz.*:

$$\frac{Gb}{Y_c} = \sigma_c = \sigma_0 + Kc \qquad (4.11)$$

The effect of the solute on the critical annihilation stress is likely to be more complicated than linear but given the limited range of solute contents studied we may just take the simplest law in order to obtain a qualitative model. From Eq. 4.11 we can deduce the influence of solute content on the critical annihilation distance:

$$Y \simeq Y_0 - \frac{K}{\sigma_0} c \qquad (4.12)$$

If there is no segregation at the dislocation core the solute concentration c is equal to the average solute concentration c_0. The effect of the solute is in this case to pivot the θ/τ plot around its intersection with the work hardening axis, exactly as the temperature would do. However, this is not what is observed experimentally: the addition of solutes does not pivot the θ/τ plots, but translates them on the stress axis. This can be explained if we take into account the segregation at the dislocation core. During the deformation, a dislocation collects solutes atoms when gliding, and notably as it is bowing to its equilibrium curvature. We can qualitatively state that the amount of solute collected during this bowing process is proportional to the area swept by the dislocation, which is of the order of $(1/\sqrt{\rho})^2$. This solute is distributed along the length of the dislocation, which is of the order of $1/\sqrt{\rho}$. Hence we will have:

$$c \propto c_0 b \frac{1}{\sqrt{\rho}} \qquad (4.13)$$

The influence of solute content on the critical annihilation distance can therefore be written as:

$$Y_c = Y_0 - \frac{K' b}{\sigma_c} \frac{c_0}{\sqrt{\rho}} \qquad (4.14)$$

where K' is a constant. This formulation is equivalent to a translation of the θ/τ plot on the stress axis, which corresponds well to the experimental observations. Moreover, this translation is proportional to K'c. We can see in Fig. 4.3 that the amount of translation is actually approximately proportional to the solute concentration. We observe also that the amount of translation in the experimental data is much larger at room temperature than at lower temperatures. This is well represented by the factor K', which represents a solution hardening efficiency: when the temperature increases, more segregation can occur on the dislocation due to the increased mobility of the solute atoms.

CHAPTER 5

CONCLUSIONS AND FUTURE WORK

5.1/ CONCLUSIONS

Channel-die compression was shown in this work to be a reliable procedure capable of testing materials to large strains and various temperatures, including liquid Nitrogen temperature. A reliable correction for the static recovery taking place between consecutive tests at low temperatures was applied, and the stress-strain curves after correction were in good agreement with stress-strain curves obtained by tensile tests and free compression tests.

The structural evolution during deformation was studied by optical microscopy for slip line studies, by X-ray diffraction for global texture measurements, by Electron Back-Scattering Kikuchi Patterns for local texture measurements, and by Transmission Electron Microscopy for microstructural information. These experimental techniques provided a global view of the evolution of the structure at large strains, from a macroscopic scale to a microscopic scale.

Intense shear banding was evidenced at large strains (after approximately 50% deformation). At large strains it was shown that the amount of deformation taking place in the shear banded regions was significantly higher than outside the shear banded

regions. The angle of the shear bands with respect to the direction of deformation was found to be of 35°.

The evolution of the texture was shown to correspond to pure plane strain compression at moderate strains. At higher strains, the texture evolution included some components of shear texture in addition to plane strain compression texture. The shear component increased with solute content.

The mechanical tests were interpreted by work hardening rate vs. stress plots. At moderate strains the work hardening rate decreased dramatically with increasing temperature. Moreover, temperature modified the shape of these θ/τ plots: At 77K stage III was represented by a straight line, whereas it showed increasing concave curvature at 200K and 300K. The addition of solute was shown to simply result in a translation of the θ/τ plot on the stress axis. At large strains all three materials experienced a stage of continuing constant work hardening rate at a low level, which is usually called stage IV of work hardening. Stage IV work hardening rate was in the range of 2.10^{-4}G (at room temperature) to 10^{-3}G (at 77K). It was shown to be independent of solute content and to be a decreasing function of temperature. The transition between stage III and stage IV on the θ/τ plot was very sharp at 77K and very progressive at room temperature.

Phenomenological models were developed to account for the experimental results outlined above, based on the dislocation density evolution rate, and its separation in a storage rate and a dynamic recovery rate. Moderate strains were modelled taking into account the evolution of the dislocation density into two different populations during the

deformation and the evolution of the ratio between these two populations. The influence of solutes on work hardening was modelled by considering how segregation of solute atoms at the dislocation cores influences the dynamic recovery events. Finally, stage IV of work hardening was considered to be a stage of laminar flow following the turbulent flow occurring during stage III, and similar in nature to stage I of deformation. Work hardening was considered to arise from the storage of dislocation debris resulting from the dynamic recovery events.

5.2/ FUTURE WORK

Channel-die compression offers a good potential for future studies. It is capable of providing continuous stress-strain curves up to large strains in plane strain compression conditions, similar to many industrial processes. It is particularly suited for deformation at various temperatures since the temperature control is easy and precise.

Static recovery occurring between consecutive tests is inherent to channel-die compression at cryogenic temperatures. The study of the influence of these recovery processes on subsequent straining has shown interesting phenomena. However, channel-die compression is not a suitable procedure for studying these recovery processes. A detailed and systematic study of recovery of deformed structures and subsequent restraining would be of great interest, notably at large strains and in relation to the evolution of the Cottrell-Stokes ratio by strain rate sensitivity measurements.

In this work tentative models were developed in order to explain the phenomenology of work hardening. However, much more experimental evidence is needed to support any modelling of large strain deformation. There is clearly a need for reliable experimental methods to characterize the evolution of the structure during deformation, and notably some structural parameters such as internal stresses and the presence of dislocation debris. With these restrictions, it would be of interest to pursue the study of the work hardening rate evolution at large strains over a wider variety of temperatures and solute contents in order to refine its phenomenology which is still unclear to a significant extent.

APPENDIX A

ELECTROPOLISHING AND ANODIZING METHODS

A1/ ELECTROPOLISHING

Solution: 25% Nitric acid and 75% Methanol

Temperature: -40°C

Voltage: 20 V

Time: approximately 30 s

Wash thoroughly in methanol

Do not store solution

Wear gloves and safety glasses

A2/ ANODIZING

Solution:

- Orthophosphoric acid	8 ml
- Hydrofluoric acid	3.2 ml
- Boric acid	1.3 g
- Oxalic acid	0.7 g
- Carbitol	17 ml
- water	10 ml

Temperature: +40°C

Voltage: 20 V

Time: approximately 30 s

Wash thoroughly in cold water for 1 min

Dry in air

Wear gloves and safety glasses

Use under fumehood

REFERENCES

AERNOUDT,E. (1978): Calculation of deformation textures according to the Taylor model. In: Proceedings of the Fifth International Conference on Textures of Materials. Vol. 1. (Eds: GOTTSTEIN,G.; LUCKE,K.) Springer-Verlag, Berlin, 45-64.

ALBERDI,J.M.G. (1984): Large plastic deformation in polycrystalline Cu and Al at low temperatures., University Navarra, Spain.

ANAND,L.; SPITZIG,W.A. (1982): Shear band orientations in plane strain. Acta Metall. 30, 553-561.

ARGON,A.S.; HAASEN,P. (1993): A new mechanism of work hardening in the late stages of large strain plastic flow in f.c.c. metals and diamond cubic metals. Acta Metall. 41(11), 3289-3306.

BACKOFEN,W.A. (1972): Deformation processing. Addison-Wesley Publishing Company, Inc., Reading, Mass.

BASINSKI,S.J.; BASINSKI,Z.S. (1966): Recrystallization, grain growth and textures. American Society of Metals, Ohio. (N)

BASINSKI,Z.S. (1974): Forest hardening in f.c.c. cubic crystals. Scripta Metall. 8, 1301-1308.

BASINSKI,Z.S.; BASINSKI,S.J. (1992): Fundamental aspects of low amplitude cyclic deformation in face-centered cubic crystals. Progr. Mat. Sc. 36, 89-148.

BECKER,R. (1991): Analysis of texture evolution in channel die compression - I. effects of grain interaction. Acta Metall. 39(6), 1211-1230.

BECKER,R.; LALLI,L.A. (1991): Texture evolution in channel-die compression part II: effect of grains which shear. Text. Microstr. 14-18, 145-150.

BERVEILLER,M.; BOUAOUINE,H.; FAKRI,N.; LIPINSKI,P. (1988): Texture transition, micro shear bands and heterogeneous plastic strain in f.c.c. and b.c.c. metals in rolling. Text. Microstr. 8-9, 351-379.

BIRD,J.E.; NEWMAN,K.E.; NARASIMHAN,K.; CARLSON,J.M. (1987): Heterogeneous initiation and growth of sample-scale shear bands during necking of Al-Mg sheet. Acta Metall. 35(12), 2971-2982.

BLICHARSKI,M.; BECKER,R.; HU,H. (1993): Deformation texture of channel-die

deformed aluminium bicrystals with S orientations. Acta Metall. 41(7), 2007-2016.

BONNEVILLE,J.; ESCAIG,B.; MARTIN,J.L. (1988): A study of cross-slip activation parameters in pure Copper. Acta Metall. 36, 1989-2002.

BRONKHORST,C.A.; KALIDINDI,S.R.; ANAND,L. (1991): An experimental and analytical study of the evolution of crystallographic texture in FCC materials. Text. Microstr. 14-18, 1031-1036.

BROWN (1972): Role of deformation shear banding in the stability of the rolling textures of Aluminium and an Al-0.8% Mg alloy. J. Inst. Metals 100, 341-345.

BUTLER,J.F.Jr; HU,H. (1989): Channel-die compression of Aluminium single crystals. Mat. Sc. Eng. A114, L29-L33.

CANOVA,G.R.; KOCKS,U.F.; STOUT,M.G. (1984): On the origin of shear bands in textured polycrystals. Scripta Metall. 18, 437-442.

CHANDRA,H. (1979): Substructural studies at large strains in aluminium., McMaster University, Hamilton, Ontario, Canada.

CHANG,S.-C.; HOU,D.-H.; CHANG,Y.-K. (1989): The effect of textures and grain shape on the shear band formation in rolled f.c.c. metals. Acta Metall. 37(7), 2031-2033.

CHERIAN,T.V.; PIETROKOWSKI,P.; DORN,J.E. (1949): Some observations on the recovery of cold worked aluminium. Trans. Amer. Inst. Min. Met. Eng. 185(12), 948-956.

COTTERILL,R.M.J. (1977): Does dislocation density have a natural limit? Physics Lett., A 60, 61-62.

COTTRELL,A.H. (1953): Dislocations and plastic flow in crystals. Clarendon Press, Oxford.

COTTRELL,A.H.; STOKES,F.R.S.; STOKES,R.J. (1955): Effects of temperature on the plastic properties of aluminium crystals. Proc. Roy. Soc. London, A 233, 17-34.

DEVE,H.E.; ASARO,R.J. (1989): The development of plastic failure modes in crystalline materials : shear bands in f.c.c. polycrystals. Met. Trans., A 20, 579-593.

DIEHL,J. (1956): Tensile tests of Cu single crystals. Zeit. f. Metall. 47, 331.

DINGLEY,D.J.; RANDLE,V. (1992): Review - Microtexture determination by electron back-scatter diffraction. J. Mat. Science 27, 4545-4566.

DULY,D. (1993): Precipitation in a Al-0.7 wt% Mn-1 wt% Mg -0.09 wt% Si alloy and

influence of this precipitation on the mechanical properties at large strains of the alloy. Post-doctoral report, McMaster University, Hamilton, Ontario.

EMBURY,J.D.; FISHER,R.M. (1966): The structure and properties of drawn pearlite. Acta Metall. 14, 147-159.

ESCAIG,B. (1968): Sur le glissement dévié des dislocations dans la structure cubique à faces centrées. J. de Phys. 29, 255.

ESSMANN,U.; MUGHRABI,H. (1979): Annihilation of dislocations during tensile and cyclic deformation and limits of dislocation densities. Phil. Mag., A 40(6), 731-756.

ESSMANN,U.; RAPP,M. (1973): Slip in Copper crystals following weak neutron bombardment. Acta Metall. 21, 1305-1317.

FARGETTE,B.; WHITWHAM,D.; DINER,O. (1968): Bronzes conducteurs - Cuivres au cadmium et à l'étain - influence sur les propriétés mécaniques et électriques de la déformation à froid et du recuit. Rev. de Métall. 65, 679-690.

FLEISCHER,R.L.; HOSFORD JR,W.F. (1961): Easy glide and grain boundary effects in polycrystalline Aluminium. Trans. Metall. Soc. AIME 221, 244-247.

FRANCIOSI,P.; STOUT,M.G.; O'ROURKE,J.; ERSKINE,B.; KOCKS,U.F. (1987): Channel-die tests on Al and Cu polycrystals: study of the prestrain history effects on further large strain texture. Acta Metall. 35(8), 2115-2128.

FRIEDEL,J. (1956): Les dislocations. Gauthier-Villars, Paris.

FRIEDEL,J. (1957): in : Dislocations and mechanical properties of crystals. Wiley, New York.

FRIEDEL,J. (1959): in : Internal stresses and fatigue of metals. Elsevier, Amsterdam.

FRIEDEL,J. (1964): Les dislocations. Pergamon Press, Oxford.

GILMAN,J.J. (1964): Influence of dislocation dipoles on physical properties. Disc. Faraday Soc. 38, 123-137.

GIL SEVILLANO,G.; VAN HOUTTE,P.; AERNOUDT,E. (1981): Large strain work hardening and textures. Progr. Mat. Sc. 25, 69-412.

GLEITER,H. (1988): Microstructural aspects of strengthening and toughening of metals, crystalline metallic alloys and semicrystalline polymers. Mat. Forum 11, 140-165.

HAASEN,P. (1967): in : Lattice defects and their interactions. Hasiguti, New York.

HARREN,S.V.; DEVE,H.E.; ASARO,R.J. (1988): Shear band formation in plane strain compression. Acta Metall. 36(9), 2435-2480.

HASEGAWA,T.; KOCKS,U.F. (1979): Thermal recovery processes in deformed aluminium. Acta Metall. 27, 1705-1716.

HASEGAWA,T.; YAKOU,T. (1980): Effects of stress reversal and thermal recovery on stress vs strain behaviour in aluminium. Scripta Metall. 14, 1083-1087.

HASEGAWA,T.; YAKOU,T.; KOCKS,U.F. (1982): Length changes and stress effects during recovery of deformed aluminium. Acta Metall. 30, 235-243.

HATHERLY,M.; MALIN,A.S. (1984): Shear bands in deformed metals. Scripta Metall. 18, 449-454.

HIRSCH,J.R. (1990): Correlation of deformation texture and microstructure. Mat. Sc. Techn. 6(11), 1048-1057.

HODIERNE,F.A. (1963): A torsion test for use in metalworking studies. J. Inst. Metals 91, 267-273.

HOSFORD,W.F.; CADDELL,R.M. (1993): Metal forming. PTR Prentice Hall, Englewood Cliffs, NJ.

HUGHES,D.A. (1986): Strain hardening of F.C.C. metals and alloys at large strains. Ph.D., Stanford University, CA.

HUGHES,D.A.; NIX,W.D. (1988): The absence of steady-state flow during large strain plastic deformation of some f.c.c. metals at low and intermediate temperatures. Met. Trans., A 19, 3013-3024.

HUGHES,D.A.; NIX,W.D. (1989): Strain hardening and substructural evolution in Ni-Co solid solutions at large strains. Mat. Sc. Eng. A122, 153-172.

JACKSON,P.J. (1985): Dislocation modelling of shear in f.c.c. crystals. Progr. Mat. Sc. 29, 139-175.

KALLEND,J.S.; KOCKS,U.F.; ROLLETT,A.D.; WENK,H.-R. (1991): Operational texture analysis. Mat. Sc. Eng. A132, 1-11.

KAMIJO,T.; FUJIWARA,A.; INAGAKI,H. (1991): Shear bands in high purity aluminium. Scripta Metall. 25, 949-954.

KOCKS,U.F. (1964): Latent hardening and secondary slip in Al and Mg. Trans. Metall. Soc. AIME 230, 1160.

KOCKS,U.F. (1966): A statistical theory of flow stress and work hardening. Phil. Mag., 13, 541-566.

KOCKS,U.F. (1976): Laws for work hardening and low temperature creep. J. Eng. Mat. Techn. 98, 76-85.

KOCKS,U.F.; STOUT,M.G.; ROLLETT,A.D. (1988): The influence of texture on strain hardening. In: Proceedings of the 8th Conference on the Strength of Metals and Alloys, Tampere, Finland. Vol. 1. (Eds: KETTUNEN,P.O.; LEPISTO,T.K.; LEHTONEN,M.E.) Pergamon Press, Oxford, 25-35.

KORBEL,A.; DOBRZANSKI,F.; RICHERT,M. (1983): Strain hardening of aluminium at high strains. Acta Metall. 31(2), 293-298.

KORBEL,A.; MARTIN,P. (1986): Microscopic vs macroscopic aspect of shear band formation. Acta Metall. 34(10), 1905-1909.

KORBEL,A.; RICHERT,M. (1985): Formation of shear bands during cyclic deformation of aluminium. Acta Metall. 33(11), 1971-1978.

KRITZINGER,S.; SMALLMAN,R.E.; DOBSON,P.S. (1969): The formation and annealing behaviour of multifaceted loops in an Al-Mg alloy. Acta Metall. 17, 49-58.

KROKHA,V.A.; ERMANOK,M.Z. (1991): Validity of the exponential law for the hardening of aluminium and aluminium based alloys. Russ. Metall. Met. 1, 150-153.

KUHLMANN-WILSDORF,D. (1968): Work hardening. ed. Gordon & Breach, New York.

KUHLMANN-WILSDORF,D. (1985): Theory of work hardening 1934-1984. Met. Trans., A 16, 2091-2108.

KWIECINSKI,J.; WYRZYKOWSKI,J.W. (1993): The effect of recovery annealing after small plastic deformations on the yield strength of polycrystalline aluminium. Acta Metall. 41(11), 3089-3095.

LANGFORD,G.; COHEN,M. (1969): Strain hardening of iron by severe plastic deformation. Trans. ASM 62, 623.

LEE,W.B.; CHAN,K.C. (1991): A criterion for the prediction of shear band angles in f.c.c. metals. Acta Metall. 39(3), 411-417.

LEFFERS,T.; JUUL JENSEN,D. (1991): The relation between texture and microstructure in rolled f.c.c. materials. Text. Microstr. 14-18, 933-952.

LESLIE,W.C. (1972): Iron and its dilute substitutional solid solutions. Met. Trans. 3, 5-26.

LLOYD,D.J.; KENNY,D. (1982): The large strain deformation of some aluminium alloys. Met. Trans., A 13, 1445-1452.

LLOYD,D.J.; MCLAUGHLAN,B.D.; SANG,H. (1977): The stress-strain behavior of aluminium alloys at large strains. Scripta Metall. 11, 297-300.

LYTTON,J.L.; MEYERS,C.L.; TIETZ,T.E. (1962): The effect of elastic and plastic strain on the tensile flow stress recovery of aluminium. Trans. Metall. Soc. AIME 224, 1250-1258.

MAJOR,B. (1992): Texture, microstructure, and stored energy inhomogeneity in cold

rolled commercial purity aluminium and copper. Mat. Sc. Techn. 8(6), 510-515.

MAURICE,C.; DRIVER,J.H. (1993): High temperature plane strain compression of cube oriented aluminum crystals. Acta Metall. 41(6), 1653-1664.

MCGREGOR TEGART,W.J. (1967): Elements of mechanical metallurgy. 2nd ed. The McMillan company, New York.

MECKING,H.; GRINBERG,A. (1979): Discussion on the development of a stage of steady-state flow at large strains. In: Proceedings of the 5th International Conference on the Strength of Metals and Alloys, Aachen, Germany. Vol. 1. (Eds: HAASEN,P.; GEROLD,V.; KOSTORZ,G.) Pergamon Press, Oxford, 289-294.

MECKING,H.; KOCKS,U.F. (1981): Kinetics of flow and strain hardening. Acta Metall. 29, 1865-1875.

MECKING,H.; NICKLAS,B.; ZARUBOVA,N.; KOCKS,U.F. (1986): A "universal" temperature scale for plastic flow. Acta Metall. 34(3), 527-535.

MORII,K.; NAKAYAMA,Y. (1985): shear bands and microstructure of Al single crystals during rolling. Scripta Metall. 19, 185-188.

MORII,K.; TERADA,H.; NAKAYAMA,Y. (1986): Shear band formation in Al-2 Wt% Cu single crystals containing theta precipitates. Trans. Jap. Inst. Metals 27(10), 769-774.

NABARRO,F.R.N. (1967): Theory of crystal dislocations. Oxford University Press, Oxford.

NABARRO,F.R.N. (1989): Work hardening and dynamic recovery of f.c.c. metals in multiple glide. Acta Metall. 37(6), 1521-1546.

NABARRO,F.R.N.; BASINSKI,Z.S.; HOLT,D.B. (1964): The plasticity of pure single crystals. Adv. Phys. 13, 193.

NAKAYAMA,Y.; MORII,K. (1987): Microstructure and shear band formation in rolled single crystals of Al-Mg alloy. Acta Metall. 35(7), 1747-1755.

NEUHAUSER,H AND SCHWINK,C (1993): Solid solution hardening. In: Materials Science and Technogy, a comprehensive treatment (Eds: CAHN,RW; HAASEN,P; KRAMER,EJ). Vol. 6: Plastic deformation and fracture (Vol. ed.: MUGHRABI,H) VCH editions, Weinheim, Germany.

NIX,W.D.; GIBELING,J.C.; HUGHES,D.A. (1985): Time-dependant deformation of metals. Met. Trans., A 16, 2215.

NOURBAKHSH,S.; SONG,Q. (1989): Shear band formation in heavily cold rolled 70-30 brass. Met. Trans., A 20, 1267-1275.

NOURBAKHSH,S.; VUJIC,D. (1986): High strain plane strain deformation of 70-30 brass in a channel die. Acta Metall. 34(6), 1083-1090.

ORLANS-JOLIET,B.; DRIVER,J.H.; MONTHEILLET,F. (1990): Plane-strain compression of silicon-iron single crystals. Acta Metall. 38(4), 581-594.

PANCHANADEESWARAN,S.; DOHERTY,R.D. (1993): Direct observation of orientation changes by channel-die compression in polycrystalline aluminium - use of split sample. Scripta Metall. 28, 213-218.

POOLE,W.J. (1993): The Deformation of Copper-Tungsten Composites. Ph.D., McMaster University, Hamilton, Ontario.

PRINZ,F.B.; ARGON,A.S. (1984): The evolution of plastic resistance in large strain plastic flow of single phase subgrain forming metals. Acta Metall. 37(7), 1021-1028.

RACK,H.J.; COHEN,M. (1970): Strain hardening of Iron-Titanium alloys at very large strains. Mat. Sc. Eng. 6, 320-326.

RAO,K.P.; DORAIVELU,S.M.; GOPINATHAN,V. (1982): Flow curves and deformation of materials at different temperatures and strain rates. J. Mech. Work. Techn 6, 63-88.

RANDLE,V. (1992): Microtexture determination and its applications. The Institute of materials, London

ROLLETT,A.D. (1988): Strain Hardening at large strains in aluminium alloys. Ph.D., Los Alamos National Laboratory.

SCHOEK,G.; SEEGER,A. (1955): in : Defects in crystalline solids. Physical Society, London.

SHEN,Y.-L. (1993): Comment on "a criterion for the prediction of shear band angles in f.c.c. metals". Scripta Metall. 28, 145-146.

SUTTON,PM (1953): The variation of the elastic constants of crystalline aluminium with temperature between 63K and 773K. Phys. Rev. 91(4), 816-821

TAKESHITA,T.; KOCKS,U.F.; WENK,H.-R. (1989): Strain path dependance of texture development in aluminium. Acta Metall. 37(10), 2595-2611.

TAYLOR,G.I. (1938): Plastic strain in metals. J. Inst. Metals 62, 307-324.

TIETZ,T.E.; MEYERS,C.L.; LYTTON,J.L. (1962): Recovery of tensile flow stress of aluminium and Al-1% Mg alloy. Trans. Metall. Soc. AIME 224, 339-347.

TRUSZKOWSKI,W.; KROL,J.; MAJOR,B. (1982): On penetration of shear texture into the rolled aluminium and copper. Met. Trans., A 13(4), 665-669.

VAN HOUTTE,P.; AERNOUDT,E. (1976): Considerations on the crystal and the strain

symmetry in the calculation of deformation textures with the Taylor theory. Mat. Sc. Eng. 23, 11-22.

VOCE,E. (1948): The relationship between stress and strain for homogeneous deformation. J. Inst. Metals 74, 537-562.

YEUNG,W.Y. (1987): Shear band angles in f.c.c. metals. Scripta Metall. 21, 869-872.

YEUNG,W.Y.; DUGGAN,B.J. (1987): Shear band angles in rolled f.c.c. metals. Acta Metall. 35(2), 541-548.